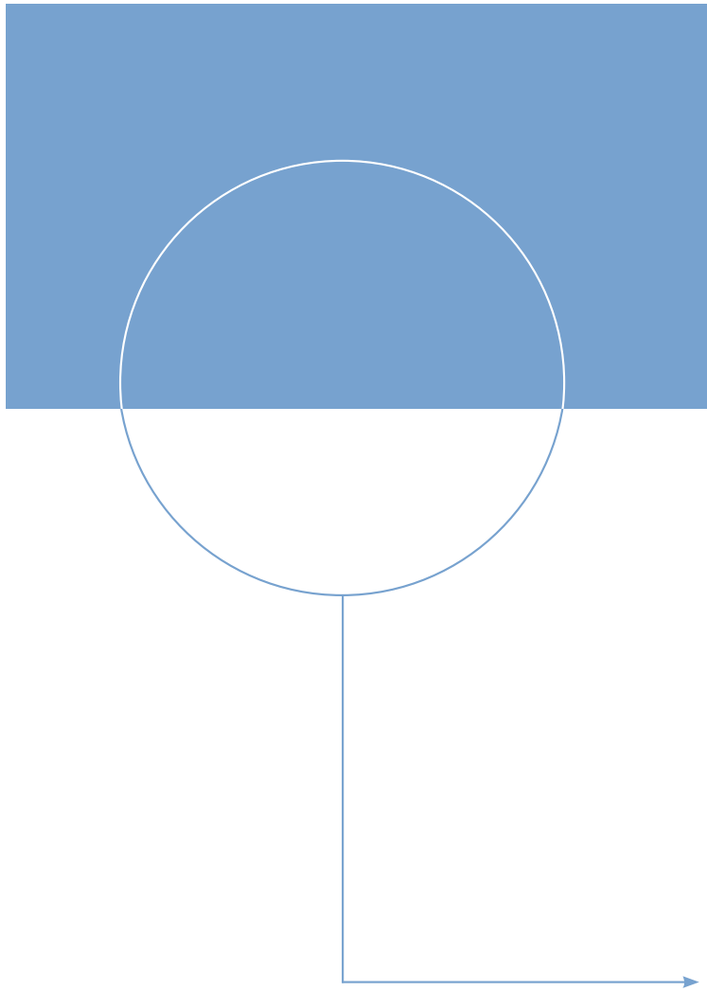

Master's thesis

2020

Yucong Ma

**NTNU**
Norwegian University of
Science and Technology
Faculty of Engineering
Department of Marine Technology

Yucong Ma

# Fishtailing behaviour of single point moored floating wind turbines

June 2020

NTNU
Norwegian University of
Science and Technology

NTNU
Norwegian University of
Science and Technology

NTNU
Norwegian University of
Science and Technology

# Fishtailing behaviour of single point moored floating wind turbines

Yucong Ma

Master of Science in Maritime Engineering
Submission date: June 2020
Supervisor: Erin Bachynski
Co-supervisor: Hans Liwång

Norwegian University of Science and Technology
Department of Marine Technology

**NTNU Trondheim**
**Norwegian University of Science and Technology**
*Department of Marine Technology – Group of Marine Structures*

# PROJECT THESIS IN MARINE TECHNOLOGY

## SPRING 2020

## FOR

## STUD.TECHN. Yucong Ma

Fishtailing behavior of single-point moored floating wind turbines
Koblet ustabilitet i svai og gir av flyttende vindturbiner med én forankringslinje

**Background:**
The offshore wind industry is moving toward deeper water, farther from land, where floating wind turbines (FWTs) become more economical than bottom-fixed turbines. The costs of FWTs still far exceed their bottom-fixed counterparts, and researchers are actively searching for opportunities for cost reduction. Several floating wind turbine platforms with single point mooring systems have been proposed: this type of system may be less expensive, especially in shallow water. There are, however, some questions which remain regarding the behavior of such systems in yaw. Fishtailing behavior has been observed in aero-hydro-servo-elastic simulations of certain systems. A simpler model of such platforms should be developed to better understand the behavior and to try to propose design or control system modifications which can lead to more stable yaw behavior.

**Assignment:**
The following tasks should be addressed in the project work:

1. Literature review regarding floating offshore wind turbine concepts and dynamic modelling, especially the aerodynamics of yawed wind turbines and fishtailing of single point moored systems.

2. Re-visit results from the project work, especially those which appear surprising. Examine angles of attack on the wind turbine with yaw misalignment, and repeat simulations in FAST if necessary to understand the results.

3. Extend results from the project work with simulations of the operating turbine near cut-out (SIMA or FAST).

4. Continue to improve the simplified model, for example by comparing the dynamic aerodynamic loads in SIMA with the quasi-static model in matlab, and by examining different definitions of the equations of motion and the mooring line force. Attempt to develop a linearized model.

5. Examine parametric changes in the design (distance to fairlead, line length, and barge dimensions) to establish stability criteria and identify more optimal designs.

6. Report and conclude on the investigation.

The work scope could be larger than anticipated. Subject to approval from the supervisor, topics may be deleted from the list above or reduced in extent.

In the project, the candidate shall present his personal contribution to the resolution of problem within the scope of the project work.

Theories and conclusions should be based on mathematical derivations and/or logic reasoning identifying the various steps in the deduction.

The candidate should utilize the existing possibilities for obtaining relevant literature.

The project report should be organized in a rational manner to give a clear exposition of results, assessments, and conclusions. The text should be brief and to the point, with a clear language. Telegraphic language should be avoided.

The project report shall contain the following elements: A text defining the scope, preface, list of contents, main body of the project report, conclusions with recommendations for further work, list of symbols and acronyms, reference and (optional) appendices. All figures, tables and equations shall be numerated.

The supervisor may require that the candidate, in an early stage of the work, present a written plan for the completion of the work. The plan should include a budget for the use of computer and laboratory resources that will be charged to the department. Overruns shall be reported to the supervisor.

The original contribution of the candidate and material taken from other sources shall be clearly defined. Work from other sources shall be properly referenced using an acknowledged referencing system.

Erin Bachynski
Supervisor

Deadline: 06.06.2020

# Abstract

The demand for clean energy is growing rapidly and the offshore wind industry is moving from shallow water to an intermediate depth. When the water is deep enough, the floating wind turbines are more feasible than the bottom-fixed wind turbines. However, the cost of floating structures is still far beyond the price of bottom-fixed supporting structures. Researchers proposed a single-point moored floating wind turbine concept aiming to reduce the installation cost by using a simpler platform and reduce the number of mooring lines. As the concept still has many challenges to solve, this thesis studied the fishtailing behaviour of the single-point moored floating wind turbines.

In order to have a better understanding of the fishtailing behaviour of the single-point moored turbine, literature research is conducted about wind turbine concepts and sideways motions of single-point moored systems. Based on the existing barge-based floating wind turbines, a $50m \times 50m \times 10m$ box-shaped barge model is built in GeniE and its hydrodynamic results are gotten from HydroD. The barge model is then put into SIMA and assembled with a DTU 10MW RWT. SIMA analysis can provide accurate results but it is extremely time-consuming when the design needs to be frequently changed. Thus, a quasi-static force linearised model is developed to provide a reasonable estimation of the fishtailing behaviour with a reduced computation cost. The 6-DOF problem is simplified to be a linear 3-DOF model with the surge, sway, and yaw motions considered. Static yaw misalignment aerodynamic loads are obtained from SIMA on a fixed turbine and some of the studies are compared with the OpenFAST result. These aerodynamic loads are taken as position-dependent excitation force input in the simplified model.

The study of fishtailing behaviour is carried at a 30m/s high wind speed and at a 25m/s cut-out wind speed. When a relatively long catenary mooring line is used, chaotic motion shows up for the barge at high wind speed and a long-period fishtailing is observed when the turbine is operating at cut-out. The initial studies are carried out on a turbine with a 75m tower-fairlead distance and a 125m long mooring line. The initial design fishtailing behaviour is studied by using the linearised model and SIMA. The results show that the linearised model can have a good estimation of the fishtailing period of a parked turbine by using an estimated artificial stiffness. Meanwhile, it has reasonable prediction on the stable position of an operating turbine. The linearised model is also used to find the stable yaw misalignment and some of the simulations are repeated in SIMA for comparison. A stable region is defined near cut-out wind speed to find out the bifurcation point of the operating turbine fishtailing behaviour at cut-out wind speed.

Based on the simplified model and the SIMA results, a more optimal model is proposed to reduce the fishtailing motion amplitude and to operate at a smaller yaw misalignment. The tower-fairlead distance of the design is 100m and its mooring line length is 200m. The dynamic motions and aerodynamic loads are compared with the initial design. Finally, study findings are concluded and recommendations for future work are proposed.

# Preface

This project thesis is carried out as the master's thesis in the Nordic Master in Maritime Engineering joint programme. The completion of this master thesis is a part of graduation requirement of obtaining the masters degree at both Norwegian University of Science and Technology(NTNU) and KTH Royal Institute of Technology. The main supervisor is Professor Erin Bachynski from department of Marine Technology, NTNU. Dr. Hans Liwång from KTH Centre for Naval Architecture is the co-supervisor. Professor Armin Troesch and Professor Matthew Collette are also involved in the process from University of Michigan.

I would like to express my sincere thanks to my professors, family, and friends for their countless support during this strange time. I would especially like to thank professor Erin Bachynski for her countless support during this uncertain time. Homeworking and distant meetings are different from normal life, but her understanding and patient help offered me confidence during the completion of the thesis. I would also like to express my appreciation to Professor Armin Troesch and Professor Matthew Collette who joined the discussion through video and offered me help on the development of the simple model. Thanks to them for answering my questions no matter how trivial it is and patiently explain things due to my awkward language skills. Finally, I would like to offer a thousand thanks to all of my friends and family members who gave me faith and let me feel not lonely during the social distancing time.

Trondheim, June 20,2020

Yucong Ma

# Table of Contents

# List of Tables

# List of Figures

# Abbreviations

## Symbol

| | |
|---|---|
| $m_a$ | Air mass |
| $A_d$ | Turbine disk area |
| $\rho_a$ | Air density |
| $v_w$ | Wind speed |
| $\phi$ | Fluid velocity potential |
| $\underline{u}$ | Fluid velocity scalar |
| $C_L$ | Lift coefficient |
| $C_D$ | Drag coefficient |
| $C_M$ | Pitch moment coefficient |
| $L_a$ | Lift force |
| $D_a$ | Drag force |
| $M_a$ | Pitch moment |
| $u_i$ | Inflow direction |
| $c$ | Chord length |
| $A_c$ | Blade cross-section area |
| $T$ | Thrust of 1D rotor disk |
| $v_i$ | Inlet velocity of 1D actuator rotor model |
| $v_o$ | Outflow velocity of 1D actuator rotor model |
| $A_i$ | Inflow control area |
| $A_o$ | Outflow control area |
| $\dot{m}$ | Mass flow rate |
| $v_a$ | Flow velocity before disk |
| $v_b$ | Flow velocity after disk |
| $p_i$ | Inflow pressure |
| $p_o$ | Outflow pressure |
| $p_a$ | Pressure before disk |
| $p_b$ | Pressure after disk |
| $A_D$ | Rotor disk area |
| $P$ | Power extracted by rotor |
| $\omega$ | Angular velocity imparted to free stream |

## Symbol

| | |
|---|---|
| $\Omega$ | Wind turbine angular velocity |
| $r$ | Annulus diameter |
| $dr$ | Annulus thickness |
| $a'$ | Anglar induction factor |
| $\lambda$ | Tip speed ratio |
| $\lambda_r$ | Local speed ratio |
| $R$ | Rotor diameter |
| $Q$ | Torque |
| $dQ$ | Torque of incremental element |
| $\underline{g}$ | body accelerations |
| $\underline{\underline{I}}$ | inertial matrix |
| $\underline{\underline{A}}$ | Added mass matrix |
| $\underline{\underline{B}}$ | Damping matrix |
| $\underline{\underline{C}}$ | Artificial stiffness matrix |
| $\underline{u}$ | Wind turbine motion vector |
| $\underline{\dot{u}}$ | Wind turbine velocity vector |
| $\underline{\ddot{u}}$ | Wind turbine acceleration vector |
| $\underline{F}^{ext}$ | External force vector |
| $F_m$ | Hawser tension |
| $L_m$ | Hawser length |
| $w$ | Hawser weight per meter |
| $E$ | Young's modulus of mooring line |
| $\alpha$ | Wind turbine yaw angle |
| $F_{xl}$ | Aerodynamic thrust force |
| $F_{yl}$ | Aerodynamic side-way force |
| $M_l$ | Aerodynamic yaw moment |
| $\underline{F^{ae}}$ | Aerodynamic force vector |
| $F_x$ | Aerodynamic x direction force in global coordinate system |
| $F_y$ | Aerodynamic y direction force in global coordinate system |
| $M_{ae}$ | Aerodynamic moment around z-axis in global coordinate system |
| $\underline{F^m}$ | Mooring force vector |
| $F_{xm}$ | Mooring line x direction force in global coordinate system |
| $F_{ym}$ | Mooring line y direction force in global coordinate system |
| $M_{mor}$ | Moment provided by mooring line |

## Acronym

| | |
|---|---|
| FWTs | Floating wind turbines |
| TLP | Tension Leg Platforms |
| CoG | Centre of Gravity |
| CoB | Centre of Buoyancy |
| SIMA | Simulation Workbench for Marine Operations, software |
| AoA | Angle of Attack |
| CFD | Computational Fluid Dynamics |
| BEM | Blade Element/Moment |
| GDW | Generalised Dynamic Wake |
| BL | Beddoes-Leishman model |
| 1D | One-dimensional |
| TSR | Tip Speed Ratio |
| LST | Local Speed Ratio |
| RWT | Reference Wind Turbine |
| NS | Navier-Stokes |
| SPM | Single Point Mooring |
| RK4 | Fourth-order Runge-Kutta method |
| PI | proportional-integral |
| PID | proportional-integral-derivative |
| DLF | Dynamic Load Factor |

Chapter 1

# Introduction

## 1.1 Background

### 1.1.1 Wind Energy

The world has been facing the growing threats of the energy crisis and global warming over the past decades. To reduce carbon emissions and bring more energy options, renewable energy has become increasingly important. Among all possible solutions, wind energy is particularly attractive because of its low cost, reliability, and zero-emissions during operation.

But still, there are challenges and limitations in the development of wind turbine technology. The first limitation is related to wind speed. The kinetic energy contained in wind is expressed in Eq.(1.1), it shows that wind energy $E_w$ is proportional to the captured area $A_d$, air density $\rho_a$ and cubed wind speed $v_w$. Thus, it is important to install wind turbines at suitable geographic locations with higher annual wind speed and stead wind fields with less turbulence. In this case, people change their scope from inland to offshore, which has more suitable wind conditions and vast space.

$$E_w = \frac{1}{2} A_d \rho_a v_w^3 \tag{1.1}$$

Moreover, wind turbines are made bigger and bigger nowadays, which has raised challenges to the transportation of huge components, as it has strict requirements for both the roads and vehicles. On the contrary, ships could be more suitable for wind turbine transportation and assemble. Owing to the reasons above, the ocean is considered as a good option to place the wind turbines.

### 1.1.2 Offshore Wind Turbines

The substructures supporting the tower and turbine can be simply classified into fixed and floating types. The choice is generally determined by operating water depth. Most of the constructed offshore wind turbines are based on fixed monopile foundations in water depth from 0 to 30m. Using a jacket or tripod foundation can make wind turbines to an intermediate water depth[1]. As shown in Figure 1.1, the average capacity for each wind turbine goes up by 16 per cent every year after 2014. The turbine capacity in 2019 reached 8MW, 1MW larger than the previous year[2].

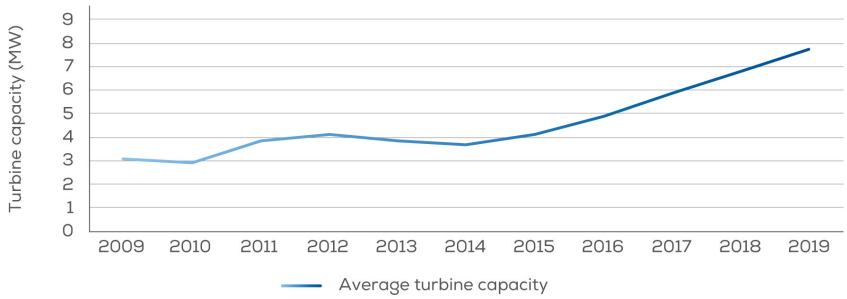


**Figure 1.1:** Average newly installed offshore wind turbine capacity since 2009[2]

Since 2008, a huge boost can be witnessedb in annual installed offshore wind turbine capacity. The accumulated capacity exceeded 17500MW in 2018 and reached 22.1GW by the end of 2019 as illustrated in Figure 1.2. Moreover, Germany, the UK and Denmark are among the countries with most installations and most of the wind farms are located close to the coast with water shallower than 30 meters.

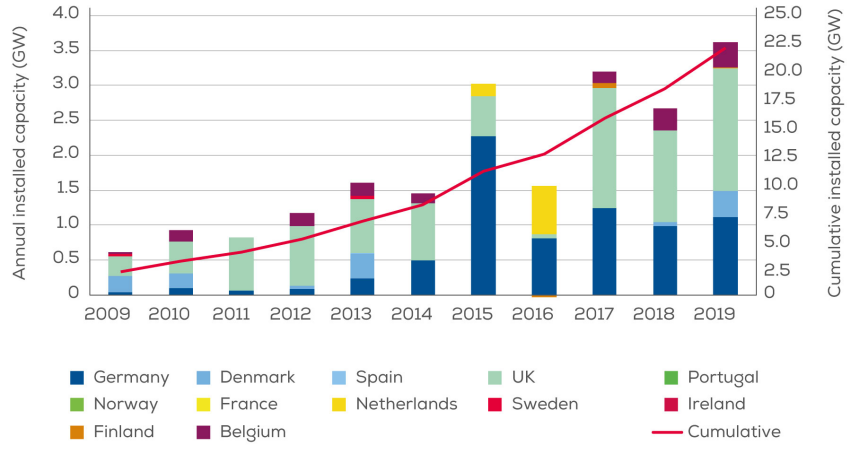


**Figure 1.2:** Annual offshore wind capacity installed in Europe[2]

To move the turbines to deeper water and make them larger and larger(as wind kinetic energy has a linear relation with turbine area $A_d$ according to Eq.(1.1)), floating wind turbines(FWT) could be used. Although the initial concept of FWTs was carried out in the year of 1972[3], it was restricted by the technology at the time and the concept itself did not draw much public attention. It was then brought up again after 1990 and became more realistic thanks to the development of technology related to offshore structures. In 2009, the first FWT was installed and operated in Norway[4]. The 2.3MW spar type turbine was developed by Equinor and its experience was further used in the first offshore floating wind farm Hywind constructed in Scotland in 2017[5].

### 1.1.3 FWT Substructure

A floating supporting structure can be broken down into four different systems: platform, mooring, anchoring and electrical cable. Among the four systems, floating platform, mooring line and anchor keep the entire structure stable when facing the wind, wave and current forces[1]. By looking at different concepts of keeping stability, FWTs can be classified into three groups[6]:

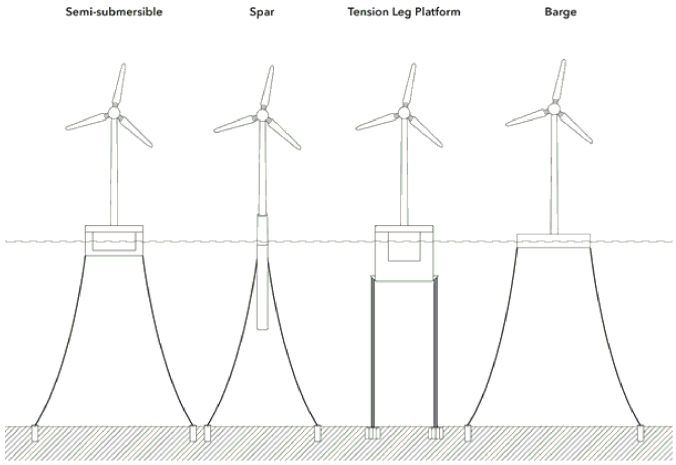


**Figure 1.3:** Different floater types[7]

- **Buoyancy stabilised platforms:** Buoyancy stabilised platforms use hydrostatic force to provide stability. Like a ship, the platform is floating owing to the Archimedes' principle. Hydrostatic pressure can be summed up as a force at the CoB pointing upward This type of FWTs tends to have a relatively large waterplane area. A change in the centre of buoyancy due to pitch or yaw motion can generate a restoring moment, making the platform return to an upright position. This kind of floater is generally designed as a semi-submersible platform, similar to those which are widely used in the offshore oil and gas industry. The barge substructure studied in this report also belongs to this category.

- **Mooring stabilised platforms:** Mooring stabilised platforms use their mooring system to provide stability. For these FWTs, unlike the previous type which has a balance between buoyancy and gravity, the buoyancy is larger than gravity for the TLP-type FWTs. Instead, they use the pretension of tension legs to reduce the motion and ensure stability.
- **Ballast stabilised platforms:** Spar platforms are the major type of FWTs using ballast to provide stability. These turbines are installed on a long cylinder substructure and its CoG is significantly beneath the sea surface and lower than CoB. The restoring moment is provided by the horizontal distance between two centres when the platform has a pitch or roll motion.

## 1.2 Barge-based FWT

The FWT concept discussed here is a novel single-point moored FWT. Similar to the semi-submersible FWTs, this kind of turbine relies on buoyancy to provide stability. The main advantages of this concept are listed[8]:

- Reduced floating structure manufacture cost thanks to the simple shape.
- Less expensive mooring system.
- Yaw bearing is not necessary.
- Single-point mooring system doesn't require any structures installed on the sea bed.
- Turbine can be constructed at the port and delivered to operation area.
- Can be located at places with deep water.
- Can be moved to avoid severe sea states or a typhoon.

A single-point moored FWT was proposed by Barber Wind[9]. A 1.6MW design was proposed and the turbine is mounted on a box shape barge.

There are also barge-based FWT designs with multiple mooring lines. These turbines look similar to the barge type turbine in Figure 1.3. EolMed project carried out a semi-submersible barge design. The 6MW turbine is based on a $53m \times 53m$ concrete barge with 6 anchor lines[10]. Similarly, Ideol designed a barge-based turbine. The first 2MW turbine is installed in France and another 3MW turbine was installed in Japan[11]. Both the EolMed project and the Ideol barges used moonpool in the design to provide additional damping and reduce the motions.

## 1.3 Fishtailing

### 1.3.1 Problem Description

Fishtailing is an uncontrolled side-ways movement that occurs most frequently on a land vehicle when its rear wheels lose traction. This behaviour happens to cars or lorries when they are trying to turn or have heavy braking on low friction surfaces(ice-covered road for instance) at a high speed.

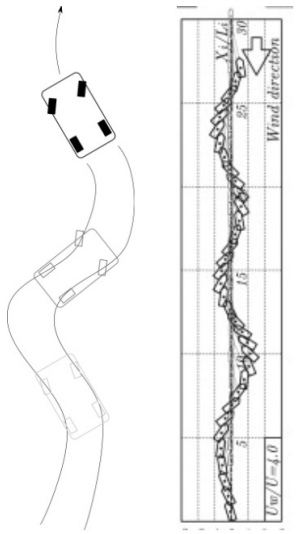


**Figure 1.4:** Fishtailing trajectory of a car and a ship[12, 13]

In marine operation, this behaviour may show up on a ship or other ocean structures under a certain scenario. Figure 1.4 gives an example of the trajectory of a fishtailing car and a fishtailing ship. Fishtailing for ships may happen during a towing operation, the ship is towed by a tug with a hawser tied at its bow and it was supposed to travel in a straight path. However, with combined effect of the hull shape, wind, wave, distribution of mass and fairlead position, the towed vessel initiated a side-to-side motion while the tug is moving straight forward.

Apart from towing operation, it also occurs on single-point mooring systems facing the current, which is a similar dynamic problem. Depending on the geometry of the vessel as well as the relevant speed between the vessel and water flow, then it may end up with three different circumstances: a symmetrical equilibrium position, an asymmetrical equilibrium position or a coupled oscillation behaviour between sway and yaw, this oscillation is called fishtailing. Figure 1.5 is an illustration of a single point moored vessel in the current.

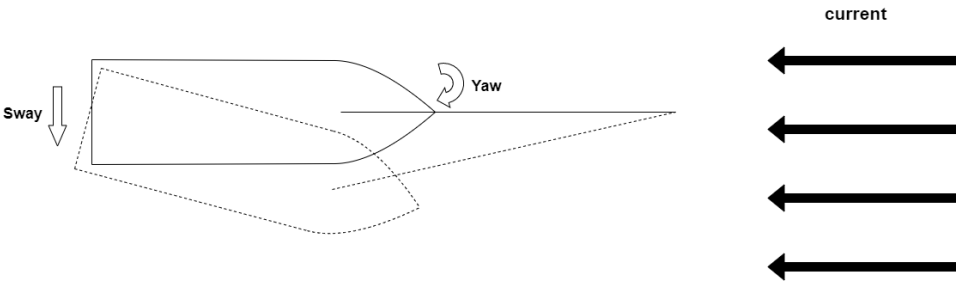


**Figure 1.5:** Single-point moored vessel in current

### 1.3.2 Literature Review

Research on the topic started long before on ships. In the 1980s, Bernitsas et al[14, 15] developed a nonlinear time-dependent mathematical model to study the stability criteria of a tanker towed by a nonlinear elastic rope. The research shows that the Routh-Hurwitz stability criterion can be critical in ship towing. Papoulias[16] conducted a parametric analysis of the SPM system and studied the significance of pitchfork, saddle-node and Hopf bifurcations to the system response. It shows that the system would oscillate under the action of time-independent external excitation. The study determined the stability boundaries and the occurrence of oscillating behaviour is observed, including chaotic responses. Lee [17] studied a similar nonlinear barge towing problem by first transforming the equations of motion into a 6-DOF state-space equation and then linearising the governing equation by using the Taylor series. The paper investigated the effect of length and material of mooring line basing on eigenvalue analysis.

Fang et al[18] developed a 6-DOF nonlinear hydrodynamic model to simulate ship towing in random waves. The model used hydrodynamic derivatives and coefficients to predict manoeuvring motion of the towed ship and RK4 method was used as the numerical integration method. The study investigated the optimal point of towing and provided suggested length for the towing line. Yasukawa et al[19] also developed a 6-DOF manoeuvring model to study the course stability of the ship towing system. Hydrodynamic coefficients were obtained through basin experiments and the hawser was developed using the 2D lumped-mass method. The study found out that a longer towing line has a positive impact on the stability for the investigated case and discussed the effect of the rudder. The wind effect was taken into account in further study[13] and the stability region was given with respect to heading angle, towline length and wind speed. Sinibaldi[20] modelled the problem as a 4-DOF dynamic system and found out that fishtailing behaviour can lead to major roll motion which results in a significant load on the towing line.

Another investigated towing operation scenario is for disabled vessels in an emergency situation. This kind of operation is usually carried out without a detailed plan in a limited time. Besides, the weather condition and sea state may sometimes be severe. Varyani et al[21] investigated a towed disabled tanker in wind only condition. The research focused

on course stability and trajectories of the operation. Wind speed, tow point and towline length were considered as control parameters. The author first looked into a fixed tug with a weathervaning vessel(assume bad weather with operation stopped) and then extended the study to the moving vessels. This study concluded the time domain result, trajectory and stability region of the investigated cases.

As for fishtailing behaviour in the SPM system, Leite et al[22] proposed 3 degrees of freedom heuristic hydrodynamic model to calculate the forces in horizontal direction acting on a VLCC with a turret mooring system. The tanker weathervanes in a uniform current, the effects of wind and waves are neglected. The model uses the ship's main dimensions and three hydrodynamic coefficients, and bifurcation analysis was carried out. The result of the tanker model was validated by experiments in yaw only condition as the turret is considered fixed above the water surface. This quasi-explicit model was further extended by taking yaw velocity into consideration and adding additional terms obtained from cross-flow theory[23]. The extended work checked fishtailing behaviour of different load case of an FPSO and the results are also confirmed by experiments. Further study was carried on an SPM system with a rigid hawser. The research investigated the condition for fishtailing for a VLCC model in ballasted condition. The result shows that the oscillation happens for a relatively high current velocity and some Froude effects included in the previous study can be neglected[24].

When the wind turbine is having a huge periodic side-ways motion, the aerodynamic forces are different from the situation when it is operating upwind. Kragh[25] conducted a study about yaw misalignment aerodynamics on an NREL 5MW reference wind turbine and tested two types of wind shear–power law and linear wind shears. The researchers noticed an alleviation on loads with certain yaw misalignment. The yaw angle with minimised blade load varies with wind speed and the wind load can be reduced by over 70% by introducing a yaw misalignment of approximately $-30°$.

## 1.4 Scope

A novel barge-based single-point moored wind turbine has been proposed[26]. Its aim is to design a platform with a lower cost of energy by reducing the installation cost. This kind of FWTs can be assembled at shipyards and then towed to wind farm, which can avoid the use of crane vessels. Meanwhile, its simpler shape can reduce the manufacture cost of the floater and mooring system, further to reduce the manufacture cost.

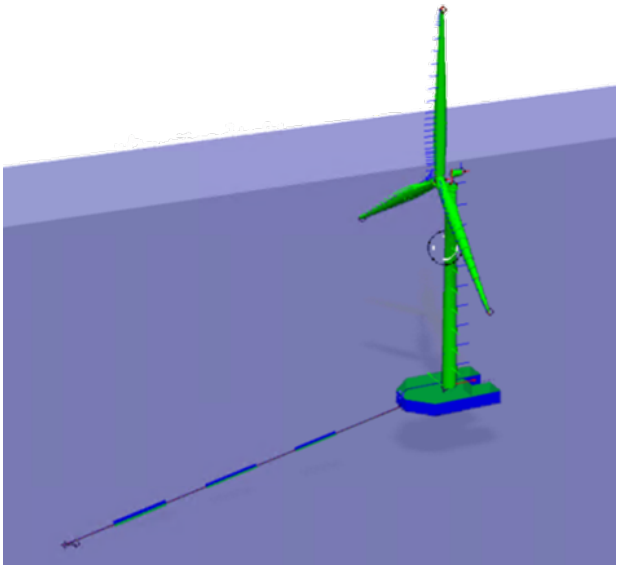

**Figure 1.6:** Single point moored FOWT novel design[27]

According to a previous study[27] on a single-point moored FWT( as shown in Figure 1.6), severe fishtailing behaviour can be observed from aero-hydro-servo-elastic simulations of a particular single-point moored FWT system. To have a better understanding of the phenomenon, this thesis carries out a preliminary design of single-point moored FWT and performs integrated analysis to understand the problem by using multiple software. Time-domain simulation was first carried out in SIMA and then the results were validated in OpenFAST. This report covers the following contents:

- An introduction to the background and development of offshore energy. Definition of the problem. Literature review related to floating offshore wind turbines and fishtailing behaviour.
- List and introduction of applied theories.
- Preliminary design of a barge, including hydrostatic stability assessment and hydrodynamic coefficients calculation using potential flow theory.

- Numerical integrated analysis on a parked turbine in extreme wind conditions and operating turbine near cut-out wind speed. Parameter studies were carried out to find stability limits of operating FWTs.
- Quasi-static load model for the parked turbine combined with a 3-DOF dynamic analysis model in extreme wind conditions
- Recommendation about a more optimal design basing on the findings.
- Conclude the studies and suggest future works.

Chapter 2

# Theory

This chapter introduces the theories used in the software and programmes to investigate the fishtailing behaviour of the single point moored FWTs. Potential flow theory is used by both SIMA and OpenFAST to calculate the dynamic motion of the floater. As for a parked wind turbine, airfoil aerodynamic can be applied to calculate the overall wind forces act on the turbine blade. When the turbine is operating, wind turbine control theory, BEM theory and various corrections are used in RIFLEX and in FAST. The SPM system uses a suction anchor together with an elastic catenary mooring line to ensure the turbines can move in a certain area and weathervane with the wind. Rigid body dynamics is used to build the 3-DOF model.

## 2.1 Potential Flow Theory

When solving the fluid motions, the potential flow theory is a method widely used. Comparing with using CFD to find a numerical solution for Navier-Stokes equations, the potential flow theory sometimes can be more practical as a result of shorter calculation time. Both SIMA and OpenFAST have used this method to calculate the forces and dynamic response for FWTs substructure[28].

Water is generally considered incompressible when solving hydrodynamic problems. Another major assumption for potential flow theory is that shear forces in the fluid are neglected, refering to the inviscid fluid. With these assumptions, Euler equations can be obtained from Navier-Stokes equations. Moreover, the flow is considered irrotational. These assumptions make the results of the potential flow theory sometimes unrealistic. For instance, it can not give an accurate estimation of ships' roll damping[29].

Potential flow theory describes the velocity field as the gradient of a scalar function. For irrotational flow, the equation is $\nabla \times \underline{u} = 0$ and $\underline{u} = \nabla\phi$. $\phi$ is the velocity potential and $\underline{u}$ is a vector consisting of the water particle velocity in three directions. Velocity potential

is a function of time and space $\Phi = \phi(x, y, z, t)$, so that the velocity components can be expressed as functions of space and time[30].

The governing equation of this problem is called Laplace equation. In the Cartesian coordinates, it can be written as:

$$\nabla\Phi = \underline{u} = \frac{\partial\Phi}{\partial x}\vec{i} + \frac{\partial\Phi}{\partial y}\vec{j} + \frac{\partial\Phi}{\partial z}\vec{k} \tag{2.1}$$

$$\nabla^2\Phi = \frac{\partial^2\Phi}{\partial x^2} + \frac{\partial^2\Phi}{\partial y^2} + \frac{\partial^2\Phi}{\partial z^2} = 0 \tag{2.2}$$

The Bernoulli equation is one of the most important and commonly used equations in fluid mechanics, it assumes frictionless flow without work/heat transfer. The equation is derived from Navier-Stokes equations together with the continuity equation. Still, assume that the fluid is inviscid and incompressible, and flow is irrotational.

$$\frac{\partial\underline{u}}{\partial t} + \underline{u}\cdot\nabla\underline{u} = -\frac{1}{\rho}\nabla p + \underline{g} \tag{2.3}$$

$$\nabla\cdot\underline{u} = 0 \tag{2.4}$$

In the equations above, $\underline{g}$ stands for body accelerations acting on the continuum, such as gravity or inertial accelerations. The Bernoulli equation is:

$$\frac{\partial\Phi}{\partial t} + \frac{1}{2}\nabla\phi\cdot\nabla\phi + gz = -\frac{1}{\rho}p \tag{2.5}$$

Reorder Eq.(2.5) to get the more standard form of Bernoulli equation:

$$p = -\rho\frac{\partial\phi}{\partial t} - \frac{\rho}{2}\nabla\phi\cdot\nabla\phi - \rho gz + \rho C(t) \tag{2.6}$$

From the above equation, it can be seen that once the velocity potential is known, the velocity and pressure can be solved.

## 2.2 Airfoil Aerodynamics

In extreme wind conditions, a wind turbine will stop rotating and have its blades at the feathered position. In this case, aerodynamics for an operating wind turbine is no longer appropriate. Thus, it makes no sense to use blade element/momentum theory. Instead, as wind turbine blades are relatively long comparing to their length, strip theory can provide a good estimation for aerodynamic loads acting a parked turbine.

Figure 2.1 shows the aerodynamic forces acting on an airfoil element if the flow comes with a certain angle of attack(AoA). These forces include a lift force normal to the income wind direction, a drag force inline with inflow and a pitching moment pointing from positive lift force direction to inflow direction[31].

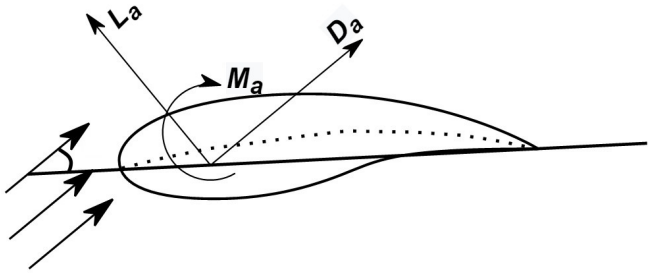


**Figure 2.1:** Loads on an airfoil element[31]

In a 2D airfoil cross-section, the dashed line is called **mean camber line**, which is between the upper and lower surface of the airfoil. The black straight line is **chord line**, and it connects the leading edge in the front and trailing edge at the end. The **camber** is the distance between the mean camber line and the chord while the thickness is the distance between the upper and lower surface. The **angle of attack** is the angle between inflow direction and chord line. The **span** of blade represents its total length.

Lift force($L_a$) is the force perpendicular to wind direction, and a non-dimensional lift coefficient is defined as:

$$C_L = \frac{L_a}{0.5\rho_a u_i^2 A_c} \tag{2.7}$$

Drag force($D_a$) is parallel to the inflow direction, and similarly, the drag coefficient can be expressed as:

$$C_D = \frac{D_a}{0.5\rho_a u_i^2 A_c} \tag{2.8}$$

Pitch moment($M_a$) is positively defined pointing from lift force to drag force and pitch moment coefficient is expressed as:

$$C_M = \frac{M_a}{0.5\rho_a u_i^2 A_c c} \tag{2.9}$$

In the above equations, $\rho_a$ is the air density, $u_i$ represents the inflow speed, $A_c$ stands for the blade area and $c$ is chord length.

Lift coefficient, drag coefficient and pitch coefficient are expressed with respect to the angle of attack in Figure 2.2. These data are generally measured by experiments or calculated with mathematical methods. When the inflow angle equals to zero, the aerodynamic forces on the airfoil are relatively small. With the increase of angle of attack, all forces go up to a different extent. Lift force will start dropping after the stall angle. Drag coefficient keeps increasing with the angle of attack and the increasing speed keeps growing. Generally, it will arrive at a peak value at $\pm 90$ degrees.

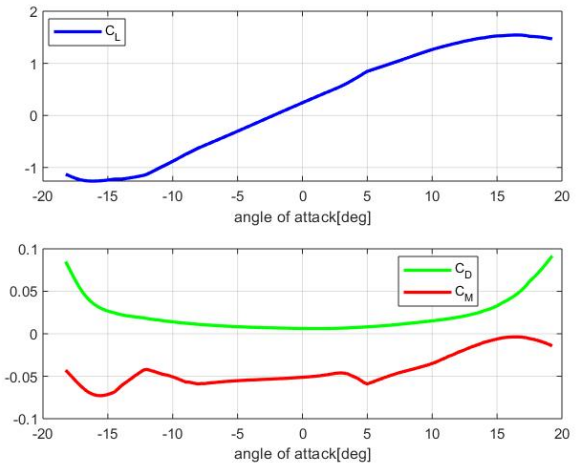


**Figure 2.2:** Airfoil characteristic for NACA 2414

## 2.3 Operating Wind Turbine Aerodynamics

The main purpose of a floating wind turbine is the same with a bottom fixed wind turbine, that is to extract kinetic energy from the incoming wind to generate electricity by the rotor. Even though the applied principles and mechanisms are in general the same, a floater has larger motions compared with an onshore fixed tower due to the flexibility of the mooring system as well as combined effect from wave, wind and current. These motions can influence the aerodynamics of the rotor and the blades[1]. Comparing with the existing types of FWTs, a barge-based single point moored floating wind turbine has fewer constraints on its motions, which means it is even more flexible. This might result in an undesirable movement or stable state for the turbine.

There are two most general aerodynamic models for wind turbines. The first one is the Blade Element/Moment (BEM) method, used together with corrections for tip loss, hub loss, dynamic stall and dynamic wake. Another way is the Generalised Dynamic Wake (GDW) method, which is an acceleration potential method and originally developed for helicopters[32, 33].

Different software uses different methods to do the simulation. Both GDW and BEM can be used in OpenFAST while SIMA uses BEM approach for aerodynamic calculation. The methods used for the single-point moored FWT is same as the methods listed in Table 2.1. Prandtl correction is used for tip loss and hub loss in both cases. Also, either SIMA or FAST considers the tower shadow effect by potential flow theory. One difference of the dynamic correction is SIMA-BEM considered dynamic wake effect while it is not included in FAST-BEM. Also, Stig Oye model is used in SIMA and Beddoes-Leishman(BL) dynamic stall model is used in OpenFAST for dynamic stall correction.

**Table 2.1:** Comparison of implemented aerodynamic methods[34, 35]

| | SIMA | FAST |
|---|---|---|
| Aerodynamic theory | BEM | |
| Tip loss | Prandtl | |
| Hub loss | Prandtl | |
| Dynamic stall | Oye | BL |
| Dynamic wake | Oye | not implemented |
| Skewed inflow correction | Glauert | Pitt & Ptters |
| Tower shadow | Potential flow | |

In the following section, blade element/momentum theory and the implied corrections are introduced.

### 2.3.1 1D Momentum Theory

To start with, the power and thrust of an ideal rotor turbine need to be determined by looking at a 1D actuator disk model(Figure 2.3). The following assumptions are made in the model[36]:

- The flow will not cross the upper and lower boundaries.
- The flow only travels through left and right boundaries(Corresponding to inflow and outflow).
- Homogeneous, incompressible steady flow.
- No friction drag.
- Infinite number of blades with uniform thrust.
- The wake is not rotating.
- Pressure jump at the rotor disk with continuous velocity across rotor disk. Pressure equal to ambient pressure at far away flow field.

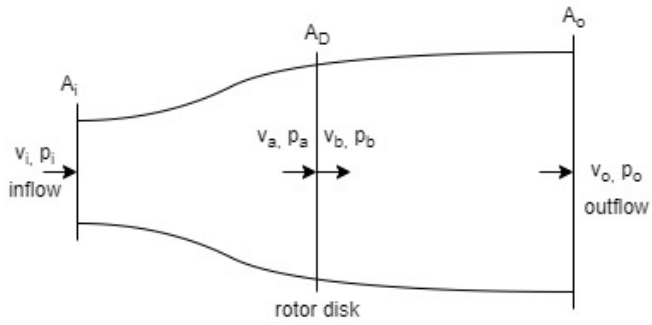


**Figure 2.3:** One-dimensional disk rotor model[31]

With the conservation of momentum, thrust force can be obtained from the momentum difference between inflow and outflow. Then introduce conservation of mass through the control volume. Thrust can be expressed as the product of mass flow rate and velocity difference.

$$T = v_i(\underbrace{A_i \rho_a v_i}_{\dot{m}}) - v_o(\underbrace{A_o \rho_a v_o}_{\dot{m}}) \tag{2.10}$$

$$= \dot{m}(v_i - v_o) \tag{2.11}$$

Then apply Bernoulli's equation and calculate the pressure discontinuity before and after the rotor disk. Pressure drop across the disk is:

$$p_a - p_b = \frac{1}{2}\rho_a v_i^2 - \frac{1}{2}\rho_a v_o^2 \tag{2.12}$$

Use the pressure drop to express thrust at disk $A_D$:

$$T = \frac{1}{2}\rho_a A_D (v_i^2 - v_o^2) \tag{2.13}$$

From (2.11), (2.13), and conservation of mass knowing that

$$\dot{m} = \rho_a A_D v_a = \rho_a A_D v_b \tag{2.14}$$

Relations of velocities can be found.

$$v_a = \frac{1}{2}(v_i + v_o) \tag{2.15}$$

Here introduce a new variable called axial induction factor:

$$a = \frac{v_i - v_a}{v_i} \tag{2.16}$$

Then both $v_o$ and $v_a$ can be expressed by inlet velocity and axial induction factor. When $a = \frac{1}{3}$, a maximum power can be extracted, which is known as the Betz limit with a power coefficient $C_P = \frac{16}{27}$.

$$C_p = \frac{P}{\frac{1}{2}\rho_a v_i^3 A_D} \tag{2.17}$$

### 2.3.2 Ideal Turbine with Wake Rotation

The previous section ignored the fact that the wake is rotating. As the turbine need to give kinetic energy to the wake, the Betz limit could not be reached in reality[31]. Introduce $\omega$ to represent angular velocity imparted to free stream and define the wind turbine angular velocity as $\Omega$.

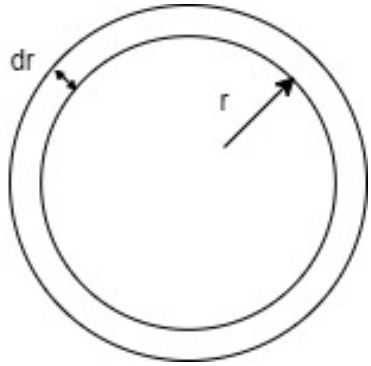


**Figure 2.4:** Disk rotor model slice[31]

Pressures are marked in Figure 2.3 and Figure 2.4 is the front view of the actuator disk rotor model. It can be noticed that pressure difference across the blade can be expressed as

$$p_b - p_a = \rho_a \left(\Omega + \frac{1}{2}\omega\right) \omega r^2 \tag{2.18}$$

Then integrate over the annulus:

$$dT = \left(\rho_a \left(\Omega + \frac{1}{2}\omega\right) \omega r^2\right) 2\pi r dr \tag{2.19}$$

Similarly, introduce the angular induction factor $a'$:

$$a' = \frac{\omega}{2\Omega} \tag{2.20}$$

Then with the change of angular momentum in the wake, the torque on the annulus can also be expressed. Replace the velocity component with the result from 1D momentum theory, torque is expressed as:

$$dQ = 4a'(1-a)\rho_a v_i \Omega r^2 \pi r dr \tag{2.21}$$

Then introduce tip speed ratio(TSR) and local speed ratio(LSR):

$$\lambda = \frac{\Omega R}{v_0} \tag{2.22}$$

$$\lambda_r = \frac{\lambda r}{R} \tag{2.23}$$

Together with the calculated torque of a single incremental element, the power from incremental element can be expressed. Then integrate it through the full rotor, for a given TSR, power coefficient is

$$C_P = \frac{8}{\lambda^2} \int_0^{\lambda} a'(1-a)\lambda_r^3 d\lambda_r \tag{2.24}$$

As a result, the maximum $C_P$ for ideal horizontal axis wind turbine with wake rotation is a function of TSR.The relation is shown in Figure 2.5.

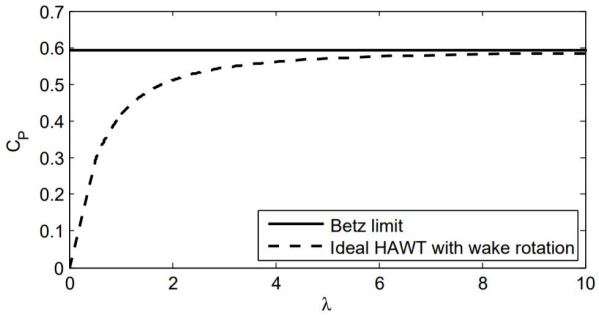


**Figure 2.5:** Power coefficient for ideal turbine with wake rotation[31]

### 2.3.3 Prandtl Correction

At the tip of the blade, air would flow from the lower to the upper side around the tip as a result of the pressure gradient. This is known as the tip loss of the blade. Due to this effect, aerodynamic forces at the tip blade are less than it elsewhere. One of the assumptions made in the BEM theory is an infinite number of blades, which is different from a real wind turbine. The Prandtl correction needs to be made. Correction factor on the aerodynamic forces owing to the finite number of blades is written as:

$$F = \frac{2}{\pi} cos^{-1} \left[ exp\left( -\frac{B(1-r/R)}{2rsin(\Phi)/R} \right) \right] \tag{2.25}$$

### 2.3.4 Glauert Correction

Apart from the finite number of blades and tip loss effect, another limitation of the BEM theory is the invalid estimation of the thrust when the induction factor $a$ is greater than 0.4. Thus the theory doesn't reflect the reality when the turbine is operating at a high tip speed ratios(during low wind speed), which is the case when it enters the turbulent wake state $a > 0.5$[37]. When the incoming wind speed is low, considerable difference of velocity shows up inside and outside the control area, which makes some of the flow in the far wake after the disk move upstream. This phenomenon violets the assumptions made in BEM theory.

In 1926, Glauert used experimental data based on helicopter rotors to develop a rotor thrust coefficient correction for large induced velocities[39]. Even though the model was initially developed to correct the thrust coefficient for the entire rotor, it is also used to correct individual blade in BEM theory.

After Glauert's experiment, other researchers have also done various improvements in the correction. The major consideration is the effect of tip-loss. When the losses close to blade tips are high, the induced velocities are large, which can generate a turbulent wake around the tips. Wilson and Walker have done correction in 1984, the result and comparison with

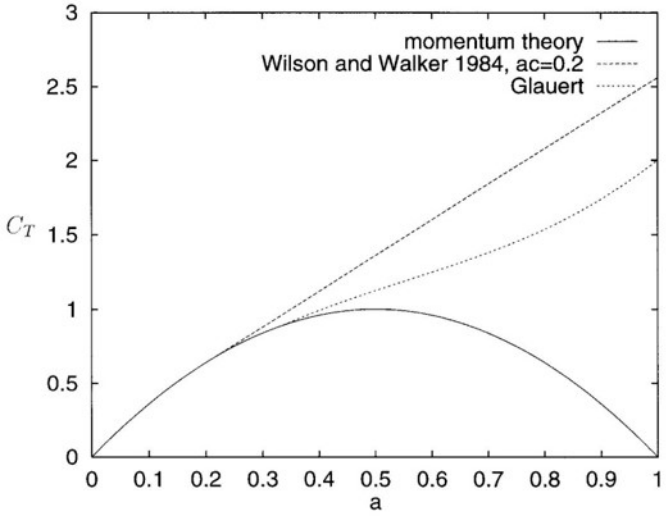


**Figure 2.6:** Thrust coefficient with respect to induction factor[38]

the original theory are shown in Figure 2.6.

## 2.4 Catenary Mooring Line

Faltinsen's book[40] gives a really good explanation for elastic and inelastic catenary mooring lines. To start with, assuming a structure is moored in calm sea, the vertical axis is defined as z-axis and the horizontal axis is defined as x-axis. As is shown in Figure 2.7, mooring line lays at the seabed close to the anchor position and then extends to the barge with a large radius of curvature.

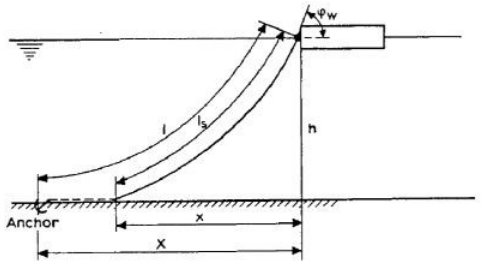


**Figure 2.7:** Moored Barge[41]

Figure 2.8 is an illustration of a mooring line element. $D$ and $F$ acting on the body represent a tangential and normal direction force. w is defined as the unit mass of the line inside the water and A is the cross-section area for the cable. E is Young's modulus for the material and T is the tension. Equilibrium of forces in Figure 2.8 can be expressed as:

$$dT - \rho g A dz = [w \sin\phi - F(1 + \frac{T}{AE})]ds \tag{2.26}$$

$$Td\phi - \rho g A z d\phi = [w \cos\phi + D(1 + \frac{T}{AE})]ds \tag{2.27}$$

The two equations above are nonlinear and impossible to solve explicitly. Still, for many

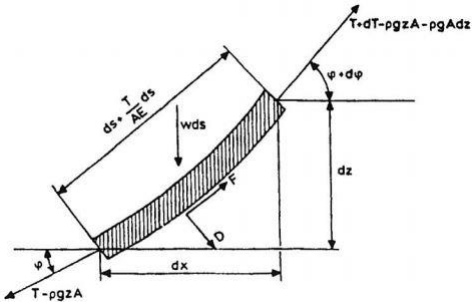


**Figure 2.8:** Mooring Line Element[41]

cases, neglecting the effect of current force F and D could be a good option. Also, assume that the line is inelastic and has constant weight distribution.

Skipping the process, the vertical force component of T can be expressed as:

$$T_z = ws \tag{2.28}$$

Consider the case in Figure 2.7 and try to find the minimum length of the mooring line $l_{min}$. The floating part length of mooring line $l_s$ can be expressed as:

$$l_s = \frac{T_H}{w} \sinh\left(\frac{xw}{T_H}\right) \tag{2.29}$$

$T_H$ is the horizontal drag force of the mooring line. Water depth $h$ can then be calculated as:

$$h = a\left[\cosh\left(\frac{xw}{T_H}\right) - 1\right] \tag{2.30}$$

The maximum tension in the cable line can be written as:

$$T_{max} = T_H + wh \tag{2.31}$$

Minimum length of the cable is given as:

$$l_{min} = h\sqrt{2\frac{T_{max}}{wh} - 1} \tag{2.32}$$

Horizontal distance between anchor and fairlead position $X$ is:

$$X = l - l_s + x \tag{2.33}$$

Relation between $X$ and $T_H$ is:

$$X = l - h\sqrt{1 + 2\frac{w}{hT_H}} + \frac{T_H}{w}\cosh^{-1}\left(1 + \frac{hw}{T_H}\right) \tag{2.34}$$

When the chain is elastic, extensional stiffness $EA$ needs to be taken into consideration. In this case, horizontal stiffness could be expressed as:

$$T_H = \frac{T_z^2 - \left(\frac{w^2 l_s^2}{2AE}\right)^2}{2\left(wh - \frac{w^2 l_s^2}{2AE}\right)} \tag{2.35}$$

Horizontal distance of the floating part of elastic cable is:

$$x = \frac{T_H}{w}\log\left(\frac{\sqrt{T_H^2 + T_z^2} + T_z}{T_H w}\right) + \frac{T_H}{AE} l_s \tag{2.36}$$

## 2.5 Wind Turbine Control Theory

This section provides an overview of the control system related to wind turbines. Burton et al[42] and Manwell[36] both give a general introduction about wind turbine controllers in their books. The main function of a wind turbine control system is to let the turbine operate in a safe and productive way. A well-designed system can reduce the cost of energy, provide steady energy output and ensure a consistent dynamic response with respect to the unresting change of the weather condition. There are two types of control systems used in wind turbines: supervisory control and operational control. Both theories are discussed later.

### 2.5.1 Control System Components

Figure 2.9 illustrates the flowchart of a wind turbine control system. This system consists of five different components: sensor, controller, power amplifier, actuator and processor. The sensors collect environment data and monitor the state of the turbine, then deliver the feedback to the controller. The controller is a system consists of hardware and software, it processes the feedback from the sensors, calculate the error and generates the output signal. A power amplifier can provide extra power to the actuator for control action when the signal from the controller is not enough. The output signals generated by the controller is then delivered to actuators that changes the system's operation. Finally, the process will change the output, which is consistently monitored by the sensors.

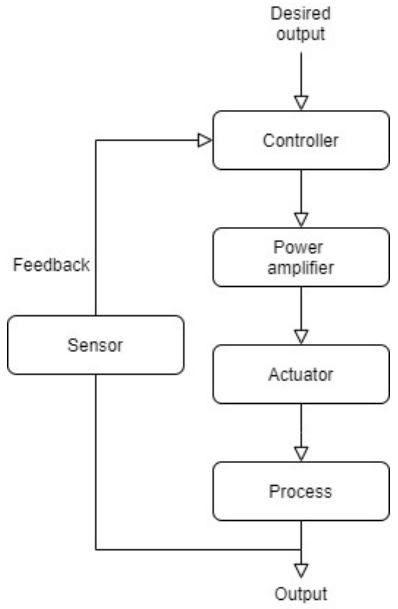


**Figure 2.9:** Wind turbine control system components[36]

### 2.5.2 Supervisory Control

Supervisory control oversees the overall operation of the wind turbines. It can detect the problems and activate the safety system. The turbines operate automatically and supervisory control can bring the turbines from one predefined operating state to another. The operational states includes[36]:

- Standby
- Start-up
- Power production
- Shut-down
- Freewheeling
- Emergency shutdown due to faults

The tasks for the supervisory control system includes monitoring of the operating conditions for the wind turbines. If any of the values exceed the preset limit, the system also needs to take appropriate actions, a shift between operating states.

### 2.5.3 Operational Control

The operational control is also called closed-loop control, the controller is generally a reprogrammed software system to automatically modify the turbine's state of operation. The operational controller can make the turbine's operation follow the predefined curves and characteristics. Following are some examples of operational control application on wind turbines[36]:

- Blade pitch control: To obtain a steady power output or rotational speed around a desired set point.
- Generator torque control: To regulate the rotational speed for a variable-speed wind turbine.
- Yaw control: A yaw controller can ensure the wind turbine facing the wind and avoid the yaw misalignment.

The demanded response time varies with tasks. Some control loops require a fast response. These controllers need to be designed carefully to keep the output values consistent with the pre-defined operating curves. Whereas some other controllers are less demanding for the response time, yaw controller for instance.

### 2.5.4 Wind Turbine Power Control

#### Stall-Regulated Wind Turbine

A stall-regulated wind turbine is a wind turbine with its blades designed with a fixed pitch angle to stall in high winds. This kind of turbine does not have pitch actuators. Many old wind turbines use stall control as the design is mechanically less complicated. This kind of control method is rarely used nowadays or on a large commercial wind turbine but the simple mechanical arrangement is an advantage for small turbines.

As the blades are designed to operate at high wind speeds, it is desired that the turbine operates close to the stall. However, a lower aerodynamic efficiency is resulted when the speed is below rated. A stall controlled turbine has gradually changing twisted blades, this can avoid an abrupt stall when critical wind speed is reached.

#### Pitch-Regulated Wind Turbine

Many of today's commercial large wind turbines are pitch controlled. It's more mechanically complicated but has more advantages than its drawbacks. For this type of turbines, aerodynamic loads can simply be affected by a changed pitch angle.

An operating wind turbine has different stages. When below rated wind speed, the generator output can not reach the rated power, thus, it should maximise the power it extracts from the wind. This means the blade pitch doesn't need to be changed a lot in low winds. Figure 2.11 shows the critical characteristics of an NREL 5MW turbine, of which DTU 10MW RWT is a direct upscale. From the figure, when the wind speed is lower than rated wind speed, the blade pitch remains to be 0. In the same region, the aerodynamic loads are also lower. Both thrust, torque, and power go up as a function of wind speed in this region.

When the wind speed surpasses rated, pitch control can provide an effective influence on the generator torque and power output so that the design limits won't be exceeded. Generator power and rotor torque remain at the rated value when the wind speed is higher than rated, while thrust drops from its peak value at rated. This requires a consistent change of blade pitch with respect to wind speed, also, the response needs to be rapid enough to satisfy the changing wind condition.

When the wind exceeds the cut-out speed, turbine blades would either pitch to feather position or stall position(depends on how the turbine is designed). Pitching to feather position is more demanding for pitching activity and flexibility. On the other hand, pitching to stall position is fewer demanding to pitch angle but has higher thrust force but less fatigue loads. Another problem with pitching to stall is that the lift coefficient decreases with an increasing AoA and further cause negative aerodynamic damping, which result in instability of blade bending. DTU 10MW RWT is a pitch to feather position when the turbine is at a shut-down state.

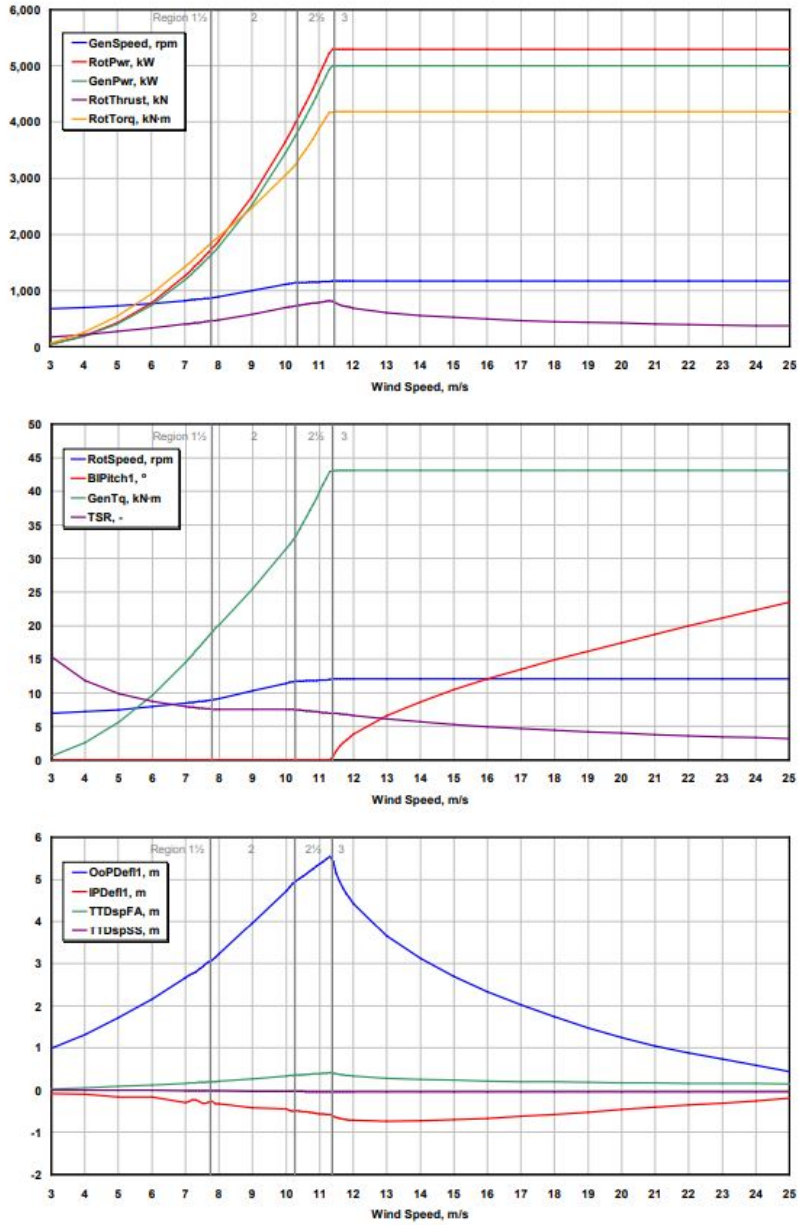


**Figure 2.10:** NREL 5MW characteristics with respect to wind speed[43]

### 2.5.5 Blade-Pitch Control

When the wind speed surpasses the rated, critical curves look like region 3 in Figure 2.11. In this region, the blade-pitch control system dominants. It adjusts the power output and generator torque. As introduced, the blade-pitch controller uses close loop control method. Either an NREL 5MW RWT or a DTU 10MW RWT is built based on gain-scheduled proportional-integral control. Whereas the pitch controller DTU 10MW is set to be a PID controller, and the derivative term coefficient is zero[44]. The controller compares the speed error between the filtered generator speed and the rated generator speed and then makes corrections.

The blade-pitch control is considered as a 1-DOF problem. Even though the aerodynamic forces are directly related to pitch angle, the aim of building such a controller is to regulate the generator shaft speed. Thus, this degree of freedom is set to be the rotation of the shaft rather than the blade pitch. A blade-pitch control system follows the baseline below[43]:

To begin with, it is helpful to list the equation of motion of the shaft rotational degree of freedom.

$$T_{aer} - N_{gea}T_{gen} = \left(I_{rot} + N_{gea}^2 I_{gen}\right) \frac{d}{dt}\left(\Omega_0 + \Delta\Omega\right) = I_{driv}\Delta\dot{\Omega} \tag{2.37}$$

Here $\Omega_0$ is the rated speed of the low-speed shaft and $\Delta\Omega$ is its perturbation. $T_{aer}$ is the aerodynamic torque of the low speed shaft connected to the disk, $T_{gen}$ is the generator shaft torque. $N_{gea}$ represents the gear box ratio between the shafts. $I_{rot}, I_{gen}$ and $I_{driv}$ stand for the inertia of rotor, generator and drivetrain respectively.

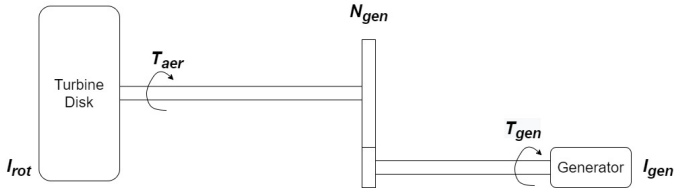


**Figure 2.11:** Wind turbine drivetrain free-body diagram

When the wind speed is above rated, the generator torque and power output remain unchanged, which means $T_{gen}$ is a constant value and is proportional to the rated power $P_0$.

$$T_{gen}\left(N_{gea}\Omega\right) = \frac{P_0}{N_{gea}\Omega} \tag{2.38}$$

Introduce a small variation of aerodynamic torque to the initial state. Then the aerodynamic torque acting on the turbine disk can be expressed as:

$$T_{aer}(\theta) = \frac{P(\theta, \Omega_0)}{\Omega_0} \tag{2.39}$$

Here $\theta$ is called the full-span rotor-collective blade-pitch angle and $P$ is the mechanical power. Then extract the 1st order Taylor theory expansion of the aerodynamic torque and generator torque. The blade-pitch perturbation $\Delta\Omega$ of the PID control equation is written as:

$$\Delta\theta = K_P N_{gea}\Delta\Omega + K_I \int_0^t N_{gea}\Delta\Omega dt + K_D N_{gea}\Delta\dot{\Omega} \tag{2.40}$$

In the above equation, $K_P, K_I$, and $K_D$ are non-negative coefficients, respectively denoting the proportional, integral, and derivative gains. The right side of the equation is thus divided into proportional term, integral term, and derivative term.

## 2.6 Rigid Body Dynamics

This section follows the course compendium of TMR4182 Marine Dynamics[29] and Benacquista's book[45], giving a description of dynamic behaviour of rigid body with a single degree of freedom. A single DOF system can be extended to a multiple DOF system by extending the numbers and coefficients into vector and matrix form, but the basic idea doesn't change.

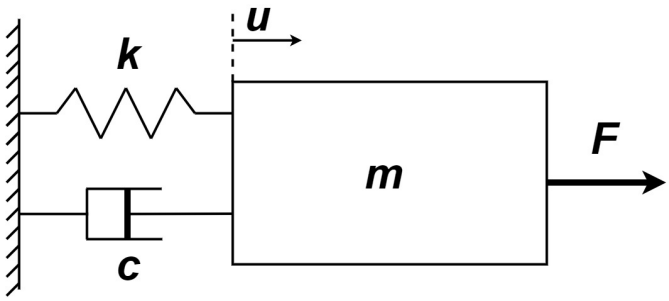


**Figure 2.12:** Single DOF dynamic system

Figure 2.12 shows a single degree of freedom system. An object with mass $m$ is able to move in the horizontal direction, its motion is influenced by an external force $F$, a damper providing linear damping with damping coefficient $c$, and a spring with stiffness $k$.

According to Newton's second law, the acceleration of the object is proportional to the sum of external forces. Thus, there is an equilibrium between inertia force, damping force, restoring force and excitation force. From Figure 2.12, positive velocity and force pointing to right. Then the equation of motion can be written as:

$$m\ddot{u} + c\dot{u} + ku = F \tag{2.41}$$

When the external force F equals 0 and damping coefficient c equals 0, the oscillation will take place without external influence. With a non-zero initial displacement away from the equilibrium position a free oscillation starts. The natural frequency $\omega_0$ of the system is defined as:

$$\omega_0 = \sqrt{\frac{k}{m}} \tag{2.42}$$

Where the unit is rad/s.

When the system is damped ($c \neq 0$), there will be three possible consequences, depending on the significance of damping. When solving the equation of motion, it can be seen that two solutions of the 2nd order ODE can be found. The solutions depend on the damping coefficient $c$. When the homogeneous equation has two results coincide, critical damping is:

$$c = c_{cr} = 2m\omega_0 = 2\sqrt{mk} \tag{2.43}$$

To compare the exact damping with critical damping, introduce damping ratio $\xi$, a non-dimensional coefficient.

$$\xi = \frac{c}{c_{cr}} = \frac{c}{2\sqrt{mk}} \tag{2.44}$$

When $\xi > 1$, the damping is supercritical, and if $\xi < 1$, the damping is sub-critical. Different levels of damping lead to different time histories of the motion. Figure 2.13 presents how the time histories of a 1-DOF system with damping over, equal, and under critical damping generally look alike. The motion damps out in the shortest time with critical damping.

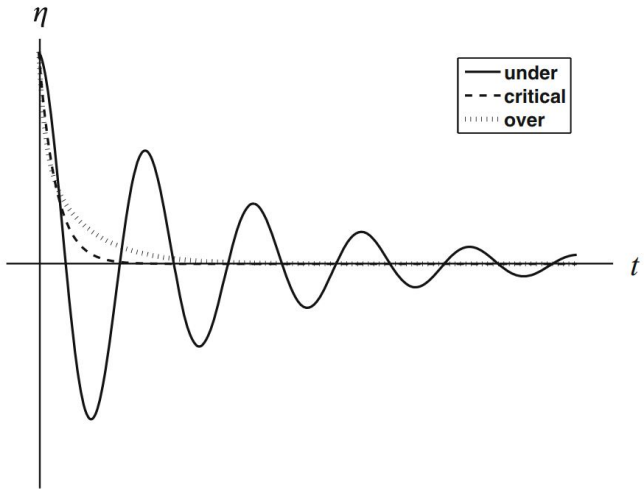


**Figure 2.13:** Time histories for different damping

As for the forced oscillation, with simple harmonic loads, the response amplitude will be influenced by load amplitude, excitation frequency as a function of the system's natural frequency and damping of the system.

Introduce the concept of Dynamic load factor(DLF), which is defined as the ratio between the dynamic and static response. This ratio represents the dynamic amplification or reduced motion of the system due to changed damping or load frequency. The ratio can be gotten from:

$$DLF = \left| \frac{u_{dyn}}{u_{sta}} \right| = \frac{1}{[(1-\beta^2)^2 + (2\zeta\beta)^2)]^{\frac{1}{2}}} \tag{2.45}$$

where $\beta$ is the ratio between load frequency and undamped natural frequency, called frequency ratio. $\xi$ is the damping ratio.

Figure 2.14 shows how DLF looks like as a function of external force frequency with different damping ratio. It can be seen that the DLF approaches 1 when the load frequency

is low enough. When it is considerable high, the dynamic response will drop to 0. The response is the highest when the excitation frequency is close to the natural frequency, and the dynamic response at resonance is the highest. Also, the dynamic response amplitude can be reduced by a higher damping ratio.

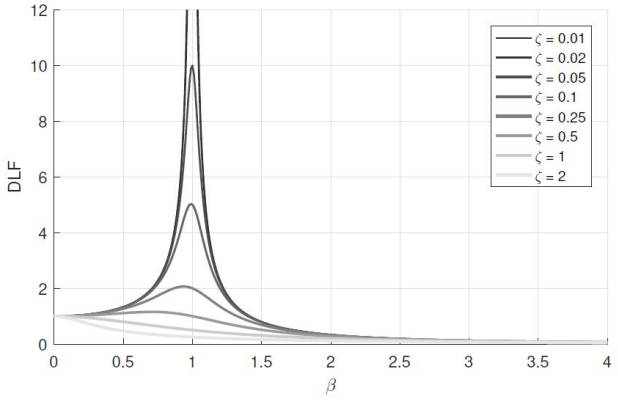


**Figure 2.14:** DLF as a function of frequency ratio for given damping ratio[29]

## 2.7 Stability

A stable state is a state at which the system is not easily changed or moved. This means, with a small disturbance, the system may start with oscillation and finally rest at a position. In the fishtailing problem of ships, the ships may end up with 2 kinds of stable states or an unstable state. Figure 2.15 illustrates three different potential behaviours of a single-point moored vessel. It may stay at a symmetric stable position facing the current or an asymmetric stable position with a certain sway offset and yaw angle. Otherwise, it may show a fishtailing oscillation behaviour, which is an unstable state.

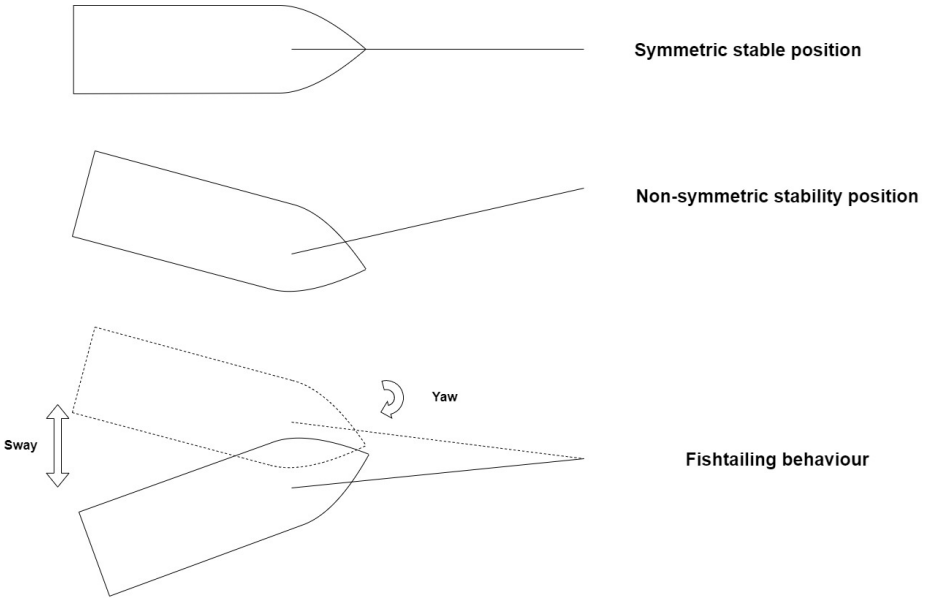


**Figure 2.15:** Different state of a SPM ship

Chapter 3

# Preliminary Design

## 3.1 Coordinate System

The same coordinate system is used in SIMA, OpenFAST and the linearised model to keep the consistency of the variables. As for the global coordinate system, the origin is set to be at the still water surface and locates at the initial position of the wind turbine tower. The positive x-direction is pointing backwards from the wind turbine, which is the same direction as wind propagation. Thus, both the fairlead and the anchor are located at the negative side of the x-axis. Also, right-hand rule is applied thus the z-axis is pointing upward, align with the tower column. The initial position of the wind turbine local coordinate system locates at the origin of global coordinate system and moves together with the wind turbine. The x-axis of the local coordinate system is perpendicular to the turbine disk and pointing backwards The direction of other axis follows the right-hand rule.

## 3.2 Wind Turbine Model

The development of wind turbines is introduced in Chapter 1.1.2. Up-scaling the turbine size is one of the most efficient ways to reduce the cost of energy when designing an offshore FWT, which has significant substructure investment compared with an onshore wind turbine. Owing to this, a bigger turbine can reduce the number of installations and further reduce the energy cost. Thus, a 10MW wind turbine can be a good model for the single-point moored floating wind turbine study.

DTU 10-MW reference wind turbine model[46] is an upscale of NREL 5MW RWT and was proposed by the Technical University of Denmark in 2013, and it is the most commonly used 10MW reference turbine for offshore wind turbine study. The main geometry, mass and operation data are shown in Table 3.1. In this thesis, cut-out wind speed and two extreme wind speeds are particularly interesting to look at. A DTU 10MW RWT model is shown in Figure 3.2.

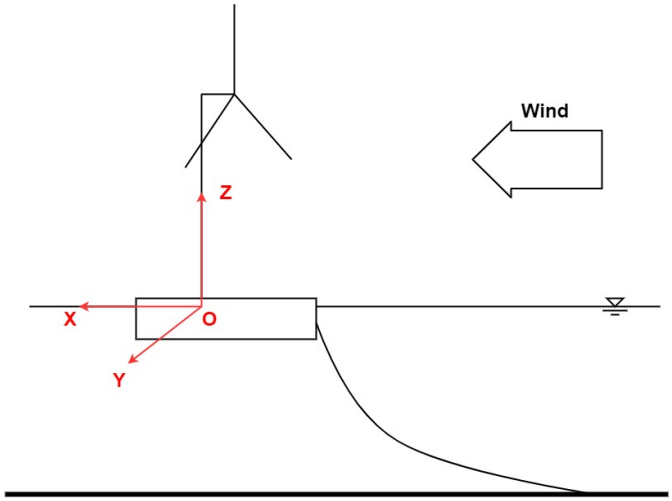


**Figure 3.1:** Coordinate System

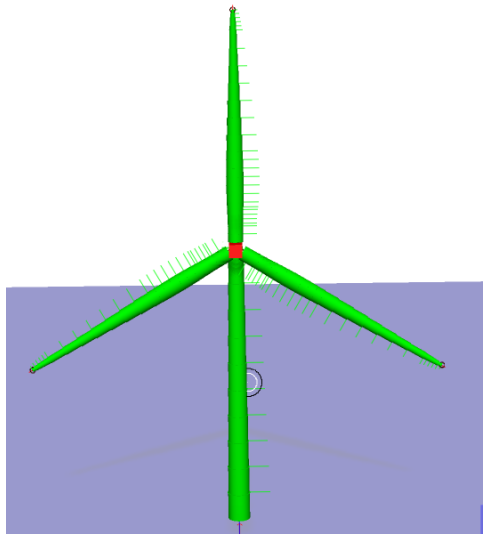

**Figure 3.2:** DTU 10MW RWT

Simulations are carried out on an operating turbine near cut-out wind speed and high wind above rated to examine the aerodynamic forces and fishtailing behaviour for operating and parked turbines. With an operating turbine at rated wind speed, BEM theory is used and the blade controller is activated. However, when the turbine is parked, the blades are set to be 90 degrees feathered and induction calculation is turned off.

**Table 3.1:** Wind Turbine Data[46]

| Description | Value | Description | Value |
|---|---|---|---|
| Rating | 10MW | Cut-in Rotor Speed | 6RPM |
| Blade Number | 3 blades | Rated Rotor Speed | 9.6RPM |
| Rotor Orientation | Clockwise, Upwind | Control | Variable speed<br>Collective pitch |
| Centre of Mass | (-0.3m, 0m, 85.5m) | Rated Thrust | 1500kN |
| Rotor Diameter | 17.83m | Blade Mass | 41t |
| Hub Diameter | 5.6m | Rotor Mass(Blades Inc.) | 229t |
| Cut-in Wind Speed | 4m/s | Nacelle Mass | 446t |
| Rated Wind Speed | 11.4m/s | Tower Mass | 605t |
| Cut-out Wind Speed | 25m/s | Total Mass | 1305t |
| Rated Tip Speed | 90m/s | Maximum Thrust | 1500kN |
| Rotor Diameter | 178.3m | Hub Diameter | 5.6m |
| Hub Height | 119m | Tower Height | 115.63m |

## 3.3 Barge Model

### 3.3.1 Preliminary Design

The first step of the study is to design a preliminary floater model as the supporting structure of the wind turbine. Although the floater does not need to be detailed as it aims to study the fishtailing behaviour. The initial design must fulfil the following two basic requirements for any structures floating in the sea:

- The floater must have sufficient buoyancy to support turbine tower.
- The floater must ensure enough restoring force to keep the hydrostatic stability of the FWT.

To start with, a box-shaped barge is used as a preliminary design. The projection of the barge to XOY plane is a square and its shape is a rectangle when looking from side or front. The finite element model of the barge is built in GeniE, and then it is put into WADAM to calculate added mass, damping matrix, restoring force and wave transfer function.

**Table 3.2:** Barge Input

| Description | Value |
|---|---|
| Depth | 10m |
| Length | 50m |
| Width | 50m |
| Unloaded draught | 6.49m |
| Operating draught | 7.00m |
| Operating freeboard | 3m |
| Barge mass | 16633t |
| Total mass | 17938t |
| Mesh Size | 2m |
| COG of free floating barge without WT | (0m,0m,-4.58m) |
| COG of the assembled FWT | (0m,0m,1.80m) |

Design values of the barge and assembled floating wind turbine are shown in Table 3.2. Depth, length and width stand for its geometry in Z, X and Y direction. The unloaded condition means the wind turbine is not yet installed on the barge and operating condition represent the integrated mass model of the FWT. The wind turbine is located at the centre of the barge, and the centre of gravity of the total structure is found at 1.8m above the waterline.

### 3.3.2 Hydrostatic Stability

The FE model built in GeniE is then put into HydroD to calculate hydrostatic and hydrodynamic parameters, and hydrostatic data is listed in Table 3.3. From the table, it can be seen that heave-heave restoring coefficient $C_{33}$, pitch-pitch restoring coefficient $C_{55}$ and roll-roll restoring coefficient $C_{44}$ are considerable and positive, which means the barge can float at an upright position above water.

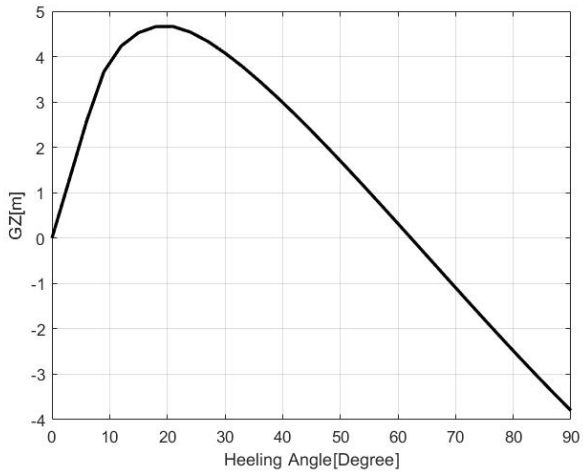


**Figure 3.3:** GZ curve of the Single-point moored floating wind turbine

For a barge type of floater, the DNV standard[47] makes the requirement for the intact stability as: the area under the righting moment curve from 0 degree inclination to the smaller angle between the downflooding angle and the second intercept angle should be equal to or be larger than 140% of the area of wind heeling moment under in the same area. Here the downflooding angle is the angle when the edge of the barge deck is submerged. The second intercept is the point where the righting moment is surpassed by wind heeling moment for the second time and it's also the point after which the FWT capsizes.

The metacentre position and GZ curve of a floater can be calculated once the floater's geometry, CoG position, and mass are defined. Figure 3.3 shows the hydrostatic restoring lever as a function of heeling angle. The metacentre height is the slope of GZ curve at around upright position, and it's calculated as 0.5m. Highest righting moment is provided at 20 degrees and the positive righting lever is up to 63 degrees.

**Table 3.3:** Hydro Static Data

| Parameter | Value | Unit |
|---|---|---|
| Waterplane area Displacement | 1.75E4 | $[m]$ |
| Mass displacement | 1.79E7 | $[kg]$ |
| Centre of buoyancy | (0,0,-3.5) | $[m]$ |
| Trans.& long. metacentric height | 0.5 | $[m]$ |
| $C_{33}$ | 2.513E7 | $[kg/s^2]$ |
| $C_{44}$,$C_{55}$ | 4.3E9 | $[kg * m/s^2]$ |

### 3.3.3 Hydrodynamic Properties

Damping and added mass of an ocean structure can be calculated from radiation problem and is generally expressed as a function of wave frequency. Both SIMA and OpenFAST requires the WAMIT hydrodynamic results as an input of the floating structure. Either the linear damping or the added mass for a given wave frequency can be expressed as a 6 by 6 matrix. In a linear damping matrix, row 1 to 6 and column 1 to 6 represent surge, sway, heave, roll, pitch and yaw term respectively. Coupling terms are relatively small and can be neglected. Unit of element (1,1),(2,2) and (3,3) is $Ns/m$, and unit of element (4,4), (5,5) and (6,6) is $Nsm$.

The added mass coefficient is also gained from radiation problem. In the following matrix, Wadam data of infinite wave length is used and negligible values are set to 0. Therefore, the added mass matrix looks like the following:

$$\underline{\underline{A}}= \begin{bmatrix} 5660896kg & 0 & 0 & 0 & 37810450kg \cdot m & 0 \\ 0 & 5660891kg & 0 & -37810450kg \cdot m & 0 & 0 \\ 0 & 0 & 84311631kg & 0 & 0 & 0 \\ 0 & -37381750kg \cdot m & 0 & 4343745000kg \cdot m^2 & 0 & 0 \\ 37381750kg \cdot m & 0 & 0 & 0 & 4343745000kg \cdot m^2 & 0 \\ 0 & 0 & 0 & 0 & 0 & 1307374687kg \cdot m^2 \end{bmatrix} \tag{3.1}$$

SIMA calculates the retardation function can be expressed as a $6 \times 6$ matrix, and for the barge, the damping matrix is given below:

$$\underline{\underline{B}} = \begin{bmatrix} 32051 & 0.0 & 0.0 & 0.0 & 0.0 & 0.0 \\ 0.0 & 20128 & 0.0 & 0.0 & 0.0 & 0.0 \\ 0.0 & 0.0 & 16389 & 0.0 & 0.0 & 0.0 \\ 0.0 & 0.0 & 0.0 & 7.5433e+05 & 0.0 & 0.0 \\ 0.0 & 0.0 & 0.0 & 0.0 & 2.4395e+06 & 0.0 \\ 0.0 & 0.0 & 0.0 & 0.0 & 0.0 & 3.506e+06 \end{bmatrix} \tag{3.2}$$

When taking WADAM result as an input to SIMA and OpenFAST, it is notable that OpenFAST requires an infinite frequency and zero frequency result, which can be modified in the WADAM output file. Negligible small frequency and considerable large frequency can be approximated as zero and infinite.

## 3.4 Scenario

### 3.4.1 Wind

Offshore wind turbines are subject to the simultaneous effects of wind, wave and current. However, this thesis considers a wind-only condition to investigate the fishtailing behaviour of the barge-based single-point moored floating wind turbine.

In general, aerodynamic forces tend to be larger for higher wind speed and the fishtailing behaviour was first observed in aero-hydro-servo-elastic simulations for a certain system

under extreme wind condition. Thus, simulations are carried out first in a high wind above cut-out wind speed on the parked wind turbine to get the amplitude and period of the coupled sway and yaw motion. The study is then extended to an operating turbine near cut-out wind speed to find out the stability margin and stable region with respect to different fairlead position and length of the mooring line. In the simulations, constant wind is used.

### 3.4.2 Water Depth

Compared to spar type wind turbines, semi-submersible wind turbines, and TLP type wind turbines, the barges have a smaller depth and therefore are more suitable for shallow or intermediate-depth water. Compared with other FWTs, the mooring line of a barge type turbine is much shorter, which means that the mooring cost is reduced. However, it also means that this kind of FWTs is not suitable for deep ocean. This study considered and carried out researches on a wind turbine operating in 100m deep water.

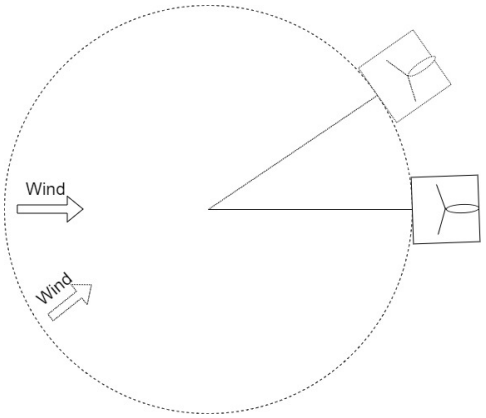


**Figure 3.4:** Single-point moored weathervaning barge type floating wind turbine

**Table 3.4:** Mooring line configuration

| Parameter | Value | Unit |
|---|---|---|
| Mass per metre | 155 | $[kg/m]$ |
| Axial stiffness | 3.84e8 | $[N]$ |
| Normal drag coefficient | 3.1 | [-] |
| Tangential drag coefficient | 3.0 | [-] |
| Normal added mass coefficient | 1.0 | [-] |
| Tangential added mass coefficient | 0.5 | [-] |

## 3.5 Mooring Line

The main function of the mooring system is to keep the station and to control the motion of the ocean structure. It can provide significant damping and restoring force to reduce the offset during marine operations. In this system, a single catenary mooring line is used to limit the movement of the barge and it allows the barge to move within a certain region and weathervanes.

The stiffness of the chain type catenary mooring line comes from its tension and weight in the water. The critical parameters of the mooring line is listed in Table 3.4. The selection of hydrodynamic coefficients follows the results of the experiments conducted by Lyons in 1997[48].

Chapter 4

# Fixed Turbine Yaw Misalignment Aerodynamics

This chapter presents the aerodynamic forces on a fixed turbine with various yaw angles. The simulation was done on both a parked turbine under extreme weather condition and an operating turbine at the cut-out wind speed.

Horizontal axis wind turbines are designed to operate against the wind. Almost all of this kind of wind turbines use the yaw mechanism to keep the turbine disk consistently perpendicular to the wind propagation direction. The sensors monitor the azimuth angle, and measure the wind speed and direction. Then the feedback will be delivered to the controller which calculates the yaw error between desired yaw angle and current azimuth position and then generates the output signal. Based on the output signal, the mechanism will turn the turbine to the upwind position. One reason for using the SPM system concept is to reduce the manufacturing cost by building a less complicated turbine structure without the yaw mechanism. The FWTs with multiple mooring lines have more restricted motion and the yaw angle is actively controlled, whereas the SPM turbine weathervanes passively. Thus, for the latter type of turbine, the disk plane may not be perpendicular to the wind, which will lead to a yaw misalignment during the operation.

## 4.1 Parked Turbine Yaw Misalignment Aerodynamics

The yaw motion is consistently changing during the fishtailing behaviour. Feathered blades generally have smaller thrust, side-ways aerodynamic force and aerodynamic moment. However, when the yaw displacement is considerable, aerodynamic forces acting on the feathered turbine blades will also increase dramatically. The coordinate system is introduced in Chapter 3.1. The aerodynamic thrust force is parallel to the local x-axis. The positive aerodynamic side-ways force(or lift force) is pointing in the positive local y-direction. Positive aerodynamic moment follows the right-hand rule pointing from local x-axis to local y-axis.

Loads introduced by wind are the excitation force of wind turbine fishtailing behaviour. These forces can be thought as a function of wind turbine angle in the simplified model, although in general, the surge, sway and yaw velocity also matter. The forces are also considered steady after reaching a stable state. Parked turbine aerodynamic forces are considered as the integral of aerodynamic loads acting on the wind turbine blade airfoil. These loads only change with the angle of attack when the wind field remains the same. Thus, parked turbine aerodynamic loads are independent of its translation position. This means the only variable aerodynamic forces depend on is the yaw angle. Static aerodynamic loads at different yaw angles are recorded and used as the wind force input in the linearised model.

Figure 4.1 shows the static wind thrust force on a parked turbine in 30m/s wind, while Figure 4.2 shows the side-ways force under the same scenario. It can be seen that the turbine shaft has the lowest side-ways force and a relatively small thrust when it is at upwind position. With certain inflow angle, the forces become tremendous and significant deflection happens on the blades. To avoid the influence of blade deflection and to get static aerodynamic forces, the blades are considered as rigid slender structures by adding extra stiffness. As defined in the coordinate system, a positive wind inflow angle corresponds to a negative yaw motion, thus the simulations were carried out with a changing inflow direction with a fixed turbine and then reversed to match the corresponding yaw motions. The time-domain simulations are done in RIFLEX, a built-in programme inside SIMA used to analyse slender structures, and in OpenFAST. According to the manual[49], OpenFAST has different coordinate set up with SIMA thus the results are transformed to make sure the coherence.

The upwind thrust force is 40kN and it rapidly decreases with an increasing absolute yaw angle. Zero thrust force happens around $\pm 10^{\circ}$ and still declines with yaw misalignment. The absolute maximum thrust is observed at around $\pm 40^{\circ}$. FAST and RIFLEX show different results for $-40^{\circ}$ yaw motion but have good coincidence at $40^{\circ}$ yaw position. The maximum aerodynamic force is $-120kN$ with positive yaw motion and $-80kN$ to $-110kN$ with negative yaw motion, pulling the turbine forward. When the turbine turns further, the wind thrust increases. Finally, it reaches $-20kN$ and $20kN$ with negative and positive $90^{\circ}$ yaw motion respectively. In these states, the wind is blowing from one side to the other parallel with the turbine disk.

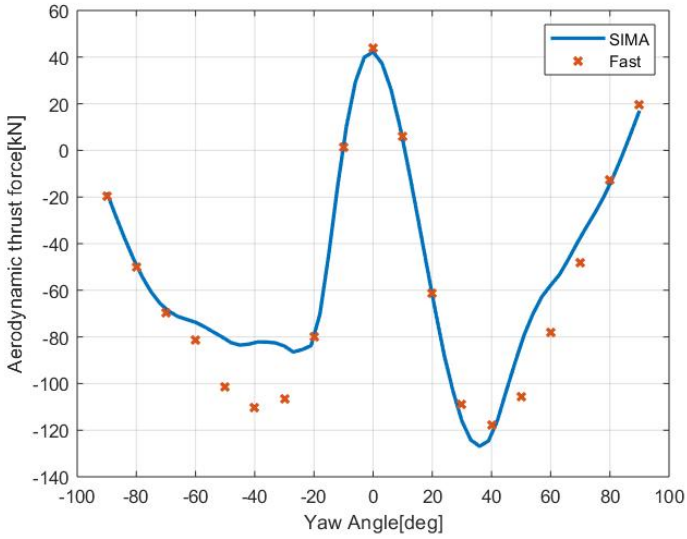


**Figure 4.1:** Parked turbine aerodynamic thrust as a function of yaw angle

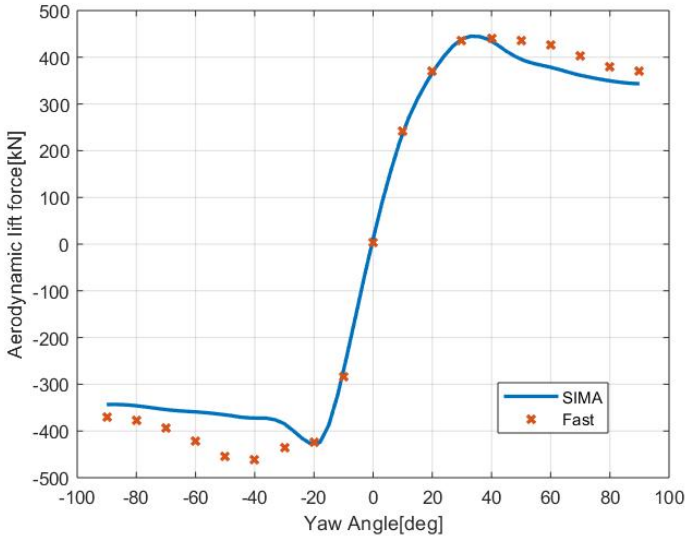


**Figure 4.2:** Parked turbine aerodynamic side-ways force as a function of yaw angle

The static wind-produced side-ways force on a parked wind turbine is presented in Figure 4.2. A good agreement is reached between OpenFAST and RIFLEX with an absolute yaw angle under 20°. With a high angle of attack, FAST gets a higher side-ways force than SIMA but the difference is relatively small. The minimum absolute value of side-

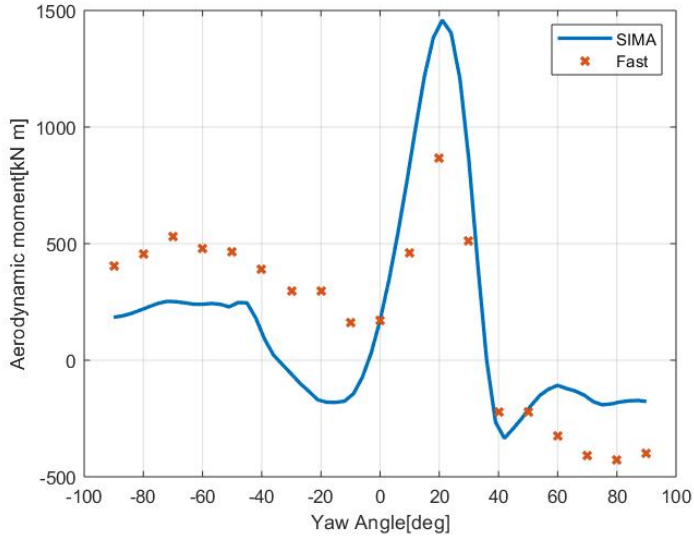


**Figure 4.3:** Parked turbine aerodynamic moment as a function of yaw angle

ways force is observed at upwind position, this small aerodynamic force is the result of a small AOA of the blades. The highest side-ways force also happens around $\pm 40^\circ$ according to the OpenFAST result, however, the maxima in RIFLEX happen at $+36^\circ$ and $-21^\circ$ respectively. The maximum static result for aerodynamic side-ways force is around $450kN$.

Results of the aerodynamic moment around z-axis are shown in 4.3. The trend of the moment as a function of yaw angle is similar among the two software, but the values are different. The peak yaw moment shows up at 20 degrees in both cases but FAST predicts the maximum to be $866kN \cdot m$ while a much larger $1458kN \cdot m$ aerodynamic moment is predicted by RIFLEX. Another interesting feather to be mentioned is that while thrust force is reflectional symmetric and side-ways force is central symmetric, the aerodynamic moment is not symmetric about the upwind position.

## 4.2 Operating Turbine Yaw Misalignment Aerodynamics

Severe fishtailing behaviour is observed on a parked turbine as a result of tremendous sideways force. When the turbine is operating, wind kinetic energy is captured to generate electricity. This transformation of energy can be considered as a huge damping in the dynamic system.

The wind speed is set to 25m/s at rated and yaw angles between $\pm 81°$ are tested. As discussed in the starting of this chapter, when the wind speed is below cut-out, the turbine might operate at a stable position with certain yaw misalignment. Thus it would be useful to look at operating states and aerodynamic loads in this situation. As shown in Figure 4.4, at 25m/s wind speed, if the yaw misalignment is between $\pm 72°$, the turbine can reach a 10MW rated power output. The blade pitch angle varies with the yaw misalignment as the blade controller is used to obtain a steady 10MW generator output. At high wind speeds, rated power is easy to reach. However, as wind speed presented in Figure 4.5, a rapid drop of wind can be seen with high yaw angle. This means when the wind is not high enough, the energy captured by the turbine may be lower than 10MW even though the wind speed is above rated. Although the study shows that a yaw misalignment may cause a load alleviation, the reduced energy production is a drawback.

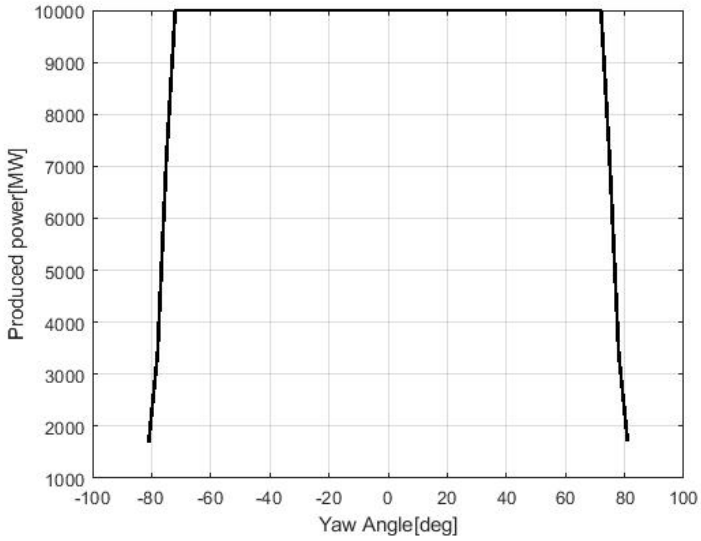


**Figure 4.4:** Turbine power output as a function of yaw misalignment at cut-out wind speed

A time-domain fixed turbine aerodynamic load case from SIMA and OpenFAST are presented in Appendix A, SIMA and FAST agree on the aerodynamic thrust but have a different results on the side-ways force. It suggests that the aerodynamic forces are oscillating with a period of 2.08s, which is the turbine's 3P period. To obtain the static force result, the mean value of the steady-state is used. As shown in Figure 4.6, the aerodynamic thrust force for an operating turbine is highly symmetric about 0 yaw angle. Highest 1363kN thrust force can be observed at $\pm 72^\circ$ and the force is quite low when the yaw misalignment is within $\pm 40^\circ$. Lowest thrust force is around $\pm 30^\circ$ and the value is 520kN.

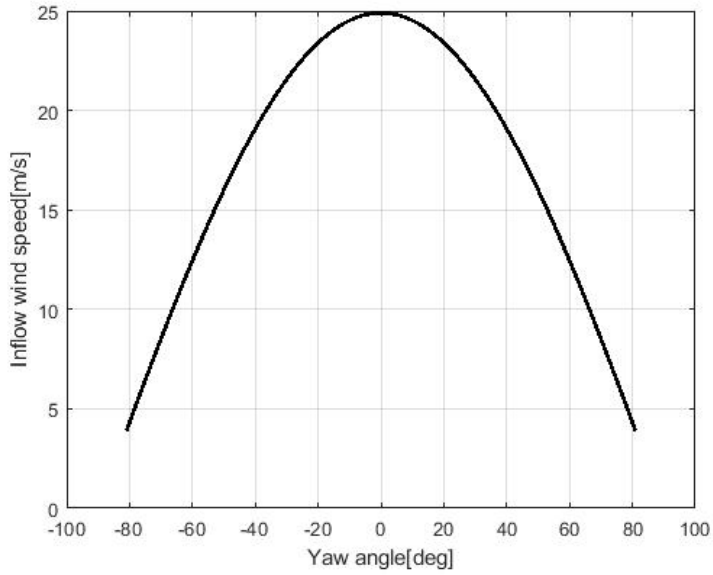


**Figure 4.5:** Wind speed in x direction shaft system

The side-ways wind force and moment around z-axis are both symmetric about a certain point as shown in Figure 4.7 and Figure 4.8. The side-ways force reaches zero at $-1.5^\circ$. The maximum side-ways aerodynamic force to negative y-direction appears at $33^\circ$ and the load is $-143kN$. The maximum side-ways force to positive y-direction is found at a positive yaw angle with the same amplitude. The positive force is slightly higher, which is about $156kN$. When the absolute yaw motion exceeds $33^\circ$, the side-ways load drops.

When the yaw position is between $\pm 60^\circ$, the aerodynamic moment tends to exaggerate the yaw misalignment. When a turbine is installed on a fixed bottom structure or a floating structure with constrained motion, the mooring system can provide a balancing force to the opposite direction to turn the turbine to the upwind position. At the upwind position, the wind turbine suffers a $-3039kN \cdot m$ yaw moment. This force reaches maximum at $-33^\circ$ and the maximum positive yaw moment happens at $33^\circ$ but the amplitude of external moment is slightly lower. Zero yaw moment happens at $6^\circ$.

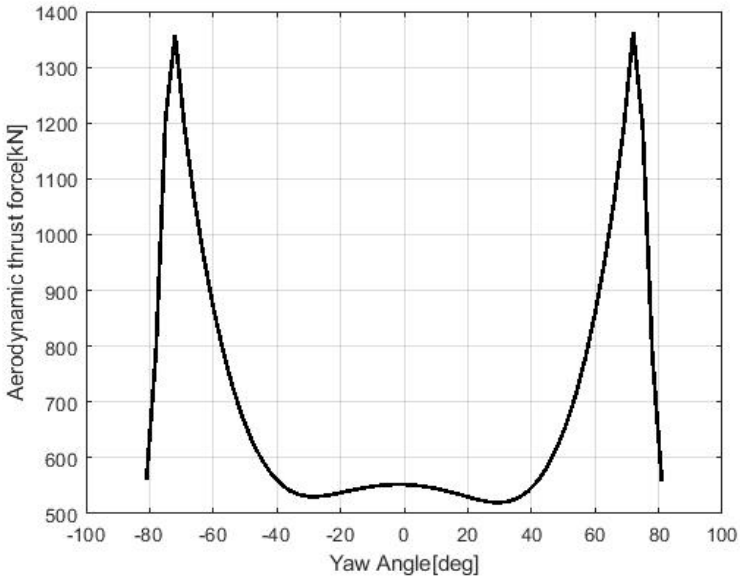


**Figure 4.6:** Aerodynamic thrust force as a function of yaw misalignment at cut-out wind speed

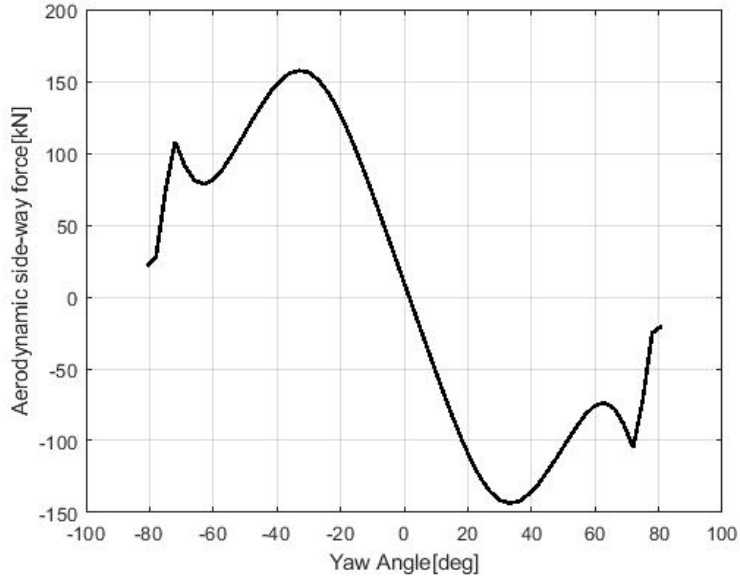


**Figure 4.7:** Aerodynamic side-ways force as a function of yaw misalignment at cut-out wind speed

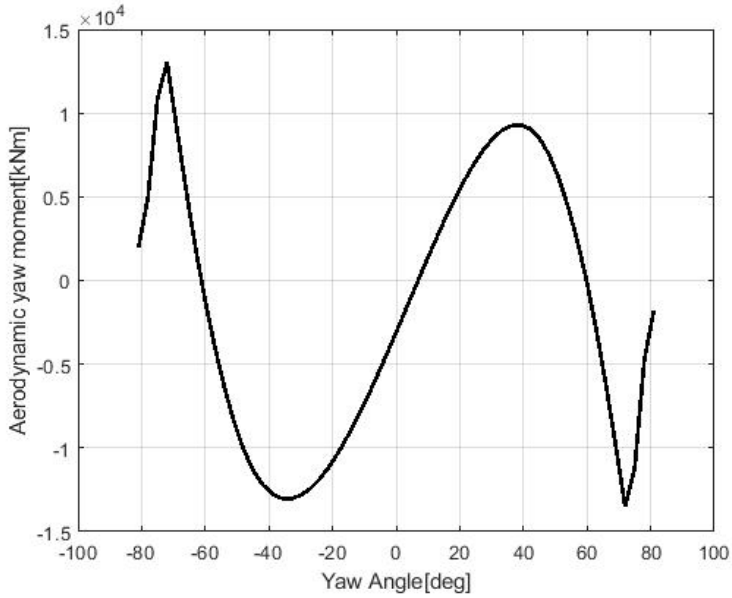


**Figure 4.8:** Aerodynamic yaw moment as a function of yaw misalignment at cut-out wind speed

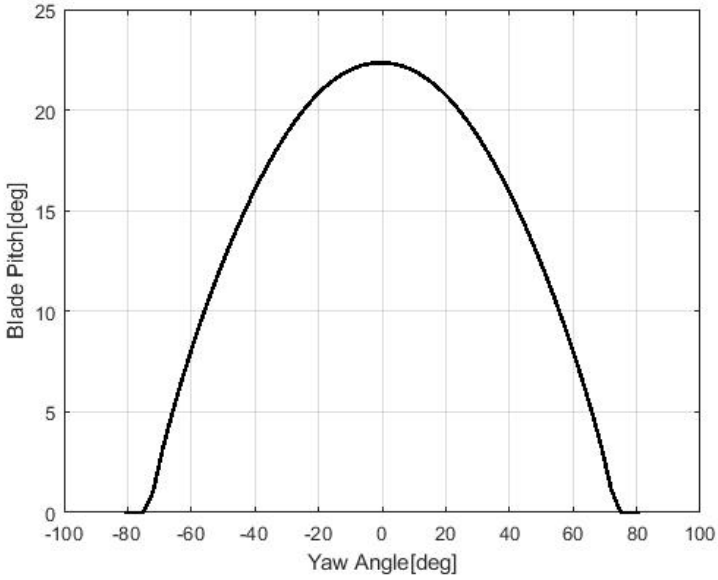


**Figure 4.9:** Blade pitch angle as a function of yaw misalignment

Kragh's study about wind turbine yaw misalignment is shown in the literature review. The results shows that the wind load can be reduced significantly by introducing a yaw misalignment of approximately $-30°$. Compared with the findings, a load reduction is found in thrust force at -30 degree yaw angle; however, the side-ways force increases with a growing of yaw angle and the change in aerodynamic load is not significant for a DTU 10MW RWT. The total aerodynamic loads on the turbine shaft system are relatively low when the absolute yaw misalignment is smaller than $30°$.

An interesting exponential growth shows up in the thrust force when the yaw misalignment exceeds $30°$. To explain this, the steady blade pitch angle as a function of yaw motion is presented in Figure 4.9. When the way misalignment increases, the side-ways wind becomes faster and faster and the blade pitch angle decreases. As a result, the relative angle between inflow direction and blade airfoil angle matches the AOA with significant lift force, whose direction is perpendicular to the turbine disk plane.

Chapter 5

# Dynamic Model

This chapter introduces the set-up of the SIMA model and a more simple linearised model. Compared with other offshore wind turbine concepts, single-point moored floating wind turbines have much larger motions and are more time-consuming to reach a steady state when running time-domain simulations. Thus, a simplified model allows quick changes in critical design parameters and saves more calculation time.

## 5.1 Linear Model

### 5.1.1 Mooring Line

In the simplified model, the anchor position is put at the same plane with wind turbine floater, which means that the anchor is floating at the sea surface and the floater is tied by a hawser. The hawser is considered to be elastic, with the effect of gravity also considered. The tension of the hawser is related to the distance between fairlead and anchor. This can be expressed by using an elastic catenary equation[50]:

$$L_{dis} = \frac{F_m L_m}{EA} + 2\frac{F_m}{w}\sinh^{-1}\left(\frac{wL_m}{2F_m}\right) \tag{5.1}$$

Here $L_{dis}$ is the distance between the fairlead and anchor position and $L_m$ is the hawser length without external force. $w$ is the weight per metre of the hawser. $F_m$ is the tension of the mooring line. E is Young's modulus and A is the hawser's cross-section area. They together become the stiffness of the mooring system. Design parameters are listed in Chapter 3.5. The mooring line tension as a function of dimensionless deformation is shown in a semi-logarithmic graph Figure 5.1. When the distance is smaller than mooring line length, the mooring force is contributed by the hawser's weight. When the line is extended, the main contribution comes from the elastic trench, which is proportional to the extended length of $\Delta L_m = L_{dis} - L_m$.

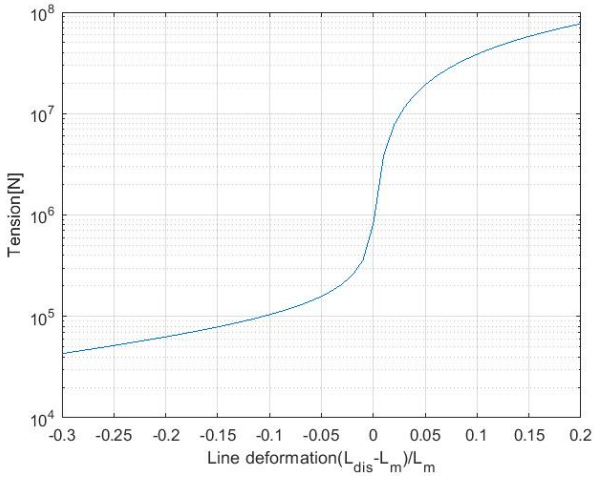


**Figure 5.1:** Mooring line tension

### 5.1.2 Equations of Motion

The equation of motion for a typical linear system contains the mass term, linear damping term, restoring term, and external force term. For this fishtailing problem, the equations of motion are expressed in vector form as:

$$(\underline{\underline{I}} + \underline{\underline{A}})\ddot{\underline{u}} + \underline{\underline{B}}\dot{\underline{u}} + \underline{\underline{C}}\underline{u} = \underline{F}^{ext} \tag{5.2}$$

For the fishtailing behaviour of a surface floating offshore wind turbine, the floater is moving on the sea surface. Thus, it is reasonable to neglect the vertical motions. To simplify this problem, the 6 degrees of freedom are reduced to be three: only motions in the horizontal plane are taken into consideration. The wind turbine's surge motion in the x-direction, sway motion in the y-direction, and yaw motion in XOY plane are taken as the 3 DOF. The other variables can be expressed as a function of the three degrees of freedom and other constants.

#### Inertia term

Due to the symmetry of the barge, the mass matrix and added mass matrix are both diagonal. Mass matrix takes the floating wind turbine's mass and moment of inertia around z-axis. The added mass of a marine structure is calculated by solving the radiation problem, in this model is obtained by HydroD. Added mass varies with frequency and is expressed as a function of income wave frequency. For a fishtailing problem, the period of oscillation is long. Thus, zero-frequency added mass is chosen and shown as Eq.5.5.

$$\underline{\underline{I}} = \begin{bmatrix} 1.79 \times 10^7 & 0 & 0 \\ 0 & 1.79 \times 10^7 & 0 \\ 0 & 0 & 2.80 \times 10^9 \end{bmatrix} \tag{5.3}$$

$$\underline{\underline{A}} = \begin{bmatrix} 5.67 \times 10^6 & 0 & 0 \\ 0 & 5.67 \times 10^6 & 0 \\ 0 & 0 & 1.31 \times 10^9 \end{bmatrix} \tag{5.4}$$

The added mass component is around 40% of mass matrix.

**Damping term**

Linear damping also comes from the radiation problem and is gotten as a function of generated wave frequency. In the thesis, 12% of the critical frequency is used in the calculation:

$$\underline{\underline{B}} = \begin{bmatrix} 1.4411 \times 10^6 & 0 & 0 \\ 0 & 5.83 \times 10^4 & 0 \\ 0 & 0 & 9.47 \times 10^6 \end{bmatrix} \tag{5.5}$$

The potential damping at zero wave period is relatively small, and this is a challenge for limiting the sway and yaw motion of the fishtailing problem. In Appendix B, initial design fishtailing motions with different levels of damping are presented. To compare with, the appendix includes the result of initial design at cut-out wind speed with a 5% critical damping, 10% of critical damping, 15% of critical damping, and zero-period potential damping from HydroD.

**External forces**

External forces applied to the barge and wind turbine include the aerodynamic forces and mooring line force. The fixed wind turbine static aerodynamic loads obtained from SIMA simulation are used as aerodynamic loads input.

Figure 5.2 shows the set-up of the simplified two-dimensional model, symbols of different distances used in the calculation are listed in the figure. The centre of gravity is located at the turbine tower position and this is also the origin of the global coordinate system.

As the wind forces do not change with the translation position of the turbine, it can be taken as a variable only depending on the yaw motion $\alpha$. The aerodynamic forces are expressed as a $3 \times 1$ vector:

$$\underline{F^{ae}} = \begin{bmatrix} F_{xl} \\ F_{yl} \\ M_l \end{bmatrix} = \begin{bmatrix} F_x \\ F_y \\ M \end{bmatrix} \tag{5.6}$$

As shown above, $F_{xl}, F_{yl}, M_l$ stand for wind forces in X, Y direction and aero-moment around Z-axis in wind turbine coordinate system. The motion of the wind turbine is described in the global coordinate system. The external force acting on the system is shown in Figure 5.3. Coordinate transformation is needed. This can be done by using the following equations:

$$F_y = F_{yl} \cos\beta + F_{xl} \sin\beta \tag{5.7}$$

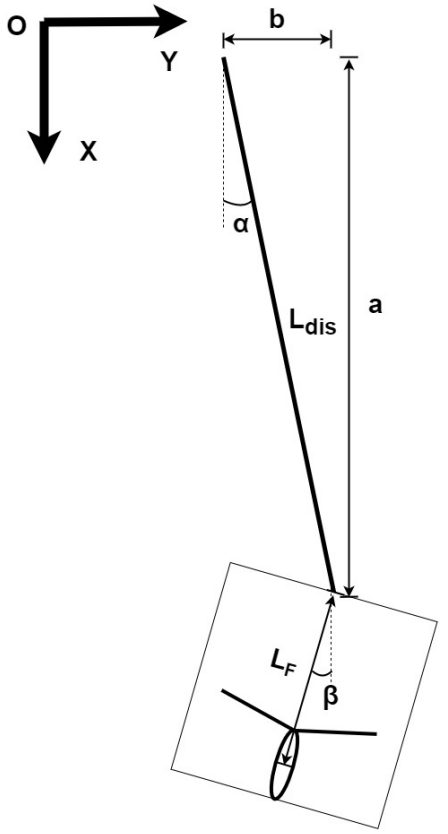


**Figure 5.2:** 3-DOF model set up

$$F_x = F_{xl} \cos\beta - F_{yl} \sin\beta \tag{5.8}$$

$$M_{ae} = M_l \tag{5.9}$$

As for the forces from the mooring line, if the hawser is considered as inelastic, then the problem only contains 2 degrees of freedom. When an elastic mooring line with the effect of hawser mass and elasticity considered, an extra degree of freedom is added.

The mooring line equation is described in Chapter 5.1.1. The distance between fairlead and anchor is expressed as

$$L_{dis} = \sqrt{a^2 + b^2} \tag{5.10}$$

Here, a and b are used to express the longitudinal and transverse distance between the fairlead and anchor. The angle between the mooring line and x-axis in the global coordinate system can be expressed as:

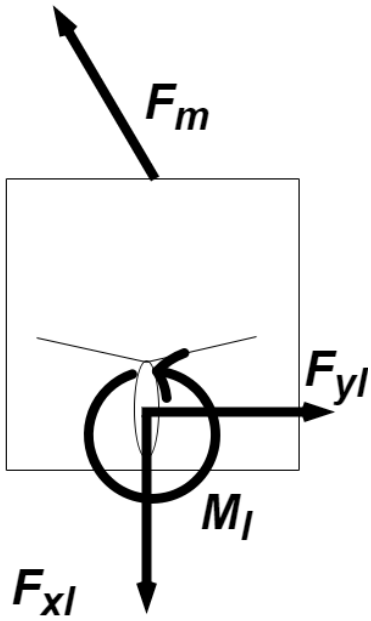


**Figure 5.3:** External forces acting on the FWT

$$\alpha = \arctan \frac{b}{a} \tag{5.11}$$

The mooring force comes from the tension of the hawser and acts at the fairlead position pointing to the anchor position. Moving the forces from the fairlead position to the centre of gravity of the wind turbine, the mooring force can be expressed as a $3 \times 1$ vector:

$$\underline{F^m} = \begin{bmatrix} F_{xm} \\ F_{ym} \\ M_{mor} \end{bmatrix}, \tag{5.12}$$

where

$$F_{xm} = -F_m \sin \alpha \tag{5.13}$$

$$F_{ym} = -F_m \cos \alpha \tag{5.14}$$

$$M_{mor} = -F_m L_F \sin(\beta - \alpha) \tag{5.15}$$

So far, the mooring line restoring force can be expressed as a function of $a$, $b$ and $\beta$. However, the defined three degrees of freedom are $x$, $y$ and $\beta$. This can be achieved by:

$$a = L_m + L_F + x - L_F \cos \beta \tag{5.16}$$

$$b = y - L_F \sin\beta \tag{5.17}$$

With all forces considered, the equation of motion can be expressed in the following form:

$$(\underline{\underline{I}} + \underline{\underline{A}})\underline{\ddot{u}} + \underline{\underline{B}}\underline{\dot{u}} = \underline{F^{ae}} + \underline{F^{m}} \tag{5.18}$$

Equivalence is reached between inertia term, damping term, mooring force and external forces. From the equations of motion, damping and inertial force are linear related to velocity and acceleration. From the above equation, all external forces in this problem are found as time-independent but as a function of its own position, $F^{ae} = f(\beta)$ and $F^{m} = g(x, y, \beta)$. This means the problem is different from a typical dynamic system with time-dependent excitation forces.

**Stiffness term**

The equations of motion for a linear system must contain restoring force term. The restoring coefficient vector is useful and necessary when predicting the natural period and conducting eigenvalue analysis of the system. In this problem, restoring forces include the side-ways force pointing at the symmetrical position, x-direction force pushing the turbine to its origin, and moment to turn the turbine to its upwind position.

An artificial stiffness is defined to linearise the problem and increase the stability of the numerical solution. To build up a linear system, restoring force resulted by small motions around the initial position is used to provide an estimation of the linear stiffness. The initial equation of motion is (5.18). A unit motion is then implied on the turbine, then the external force is obtained from the programme, this restoring term is defined as the elements in the artificial stiffness matrix. The artificial stiffness estimated from the small motion around the origin is shown in (5.19). The element at (1,1) is the surge-surge stiffness estimated from the slope of catenary mooring line equation around zero in Figure 5.1. Element (2,2) is the sway-sway stiffness estimated from the side-ways force caused by mooring line with a 5m sway motion. Similarly, the yaw-yaw stiffness is estimated from the external force of 3 degrees of yaw motion.

$$\underline{\underline{C}} = \begin{bmatrix} 4400 & 0 & 0 \\ 0 & 3600 & 0 \\ 0 & 0 & 5.4 \times 10^5 \end{bmatrix} \tag{5.19}$$

## 5.2 SIMA Model

The DTU 10MW RWT is used in this thesis and its main parameters are introduced in Chapter 3.2. It is assembled with a barge model and mooring line in SIMA. Integrated FWT SIMA model is shown as Figure 5.4.

In this model, the turbine tower is located at the centre of the barge, which is also defined as the system's centre of gravity location. The fairlead point is defined as a slave of barge location and in this way $L_m$ can be easily adjusted. The fairlead position may be on the barge or be put at the sea surface and is connected to the barge by a rigid imaginary beam. A rough design can provide a good estimation of the dynamic behaviour of the system. Once the desirable fairlead position is identified, detailed design can be conducted in the future study to achieve such an $L_F$. In the initial design, $L_F = 75m$. Anchor position is defined as a fixed supernode either floating above the water surface or moved to the seabed. In SIMA, the mooring line is first set as a rigid straight line and the anchor and fairlead point are the two endpoints of the line. Then the anchor is moved to its fixed position. When this process is done in SIMA, the anchor position needs to be carefully adjusted when doing the dynamic simulations. However, fixing the anchor position floating at the sea surface can save time for finding the suitable anchor position and $L_m$ can thus be defined as the horizontal distance between anchor and fairlead position. In the initial design, the length of the mooring line is set to be $L_m = 125m$.

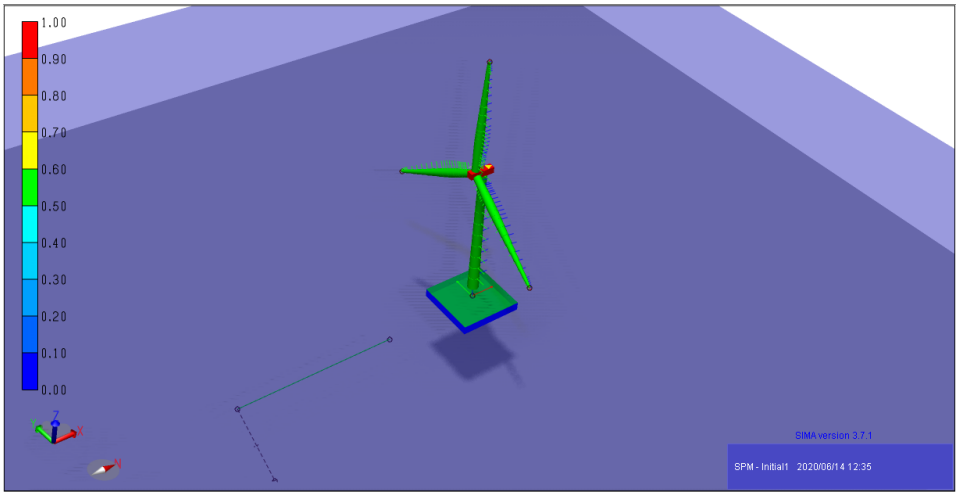


**Figure 5.4:** SIMA FWT model

Chapter 6

# Parked Turbine Dynamic Behaviour

This chapter shows the simulations performed on the parked turbines under an extreme wind condition of 30m/s. The main variables considered when studying the fishtailing behaviour are the mooring line length $L_m$ and the distance between fairlead position and turbine tower $L_F$. Different dynamic behaviour shows up as a result of changing mooring line length and fairlead-tower distance. The side-ways forces and aerodynamic moments on the parked turbines tend to be larger than the operating turbines. Chaotic dynamic motion is found from time-domain simulation with long mooring lines and fishtailing behaviour then shows up when its length is shortened. Different wind velocities above rated are discussed on a proposed initial design.

## 6.1 Chaotic Dynamic Behaviour

In the literature review the chaotic response on a single point moored tanker is metiond[16], this behaviour may also show up on the single-point moored FWTs. For those current existing FWTs which use catenary chains as mooring system, the mooring line length is fairly long. Thus, at the initial stage of design, a longer mooring line is also used in this study. As a result, when the length of the mooring system is long enough, the motion of the barge is unpredictable rather than periodic. The first simulation was done with a 250m long mooring line and the anchor is placed at (-250,0,-100).

Figure 6.1 shows the trajectory of the barge. From the figure, the turbine is moving from place to place in the restricted area, rather than a curve-shapeed fishtailing trajectory. The same result is shown with respect to time. Figure 6.2 and Figure 6.3 illustrates the surge and sway motion of the platform with a 250m catenary mooring line. The periods of sway and surge motion are not constant. The maximum sway motion is around 300m in both a positive direction and negative direction. The maximum surge motion is $-250m$ and surpasses the anchor position. When the surge motion is at its bottom, there is also a peak/bottom value in sway motion and the surge period still corresponds to half sway

period. As for yaw motion, unlike the periodic motion in fishtailing behaviour, the wind turbine turns around rapidly and the yaw motion exceeds $\pm 180°$.

From Figure 6.1, the distance between the anchor point and fairlead position is sometimes less than mooring line length. From the force diagram shown in the 2-dimensional model (Figure 5.3), the restoring yaw moment is provided by a mooring system. When the line is too long, it failed to provide this restoring force which keeps the turbine at the upwind position.

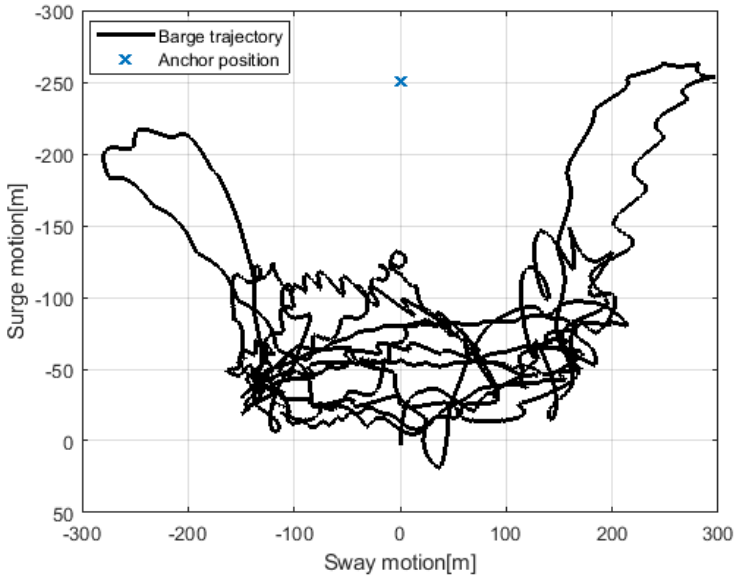


**Figure 6.1:** Platform trajectory with 250m long mooring line

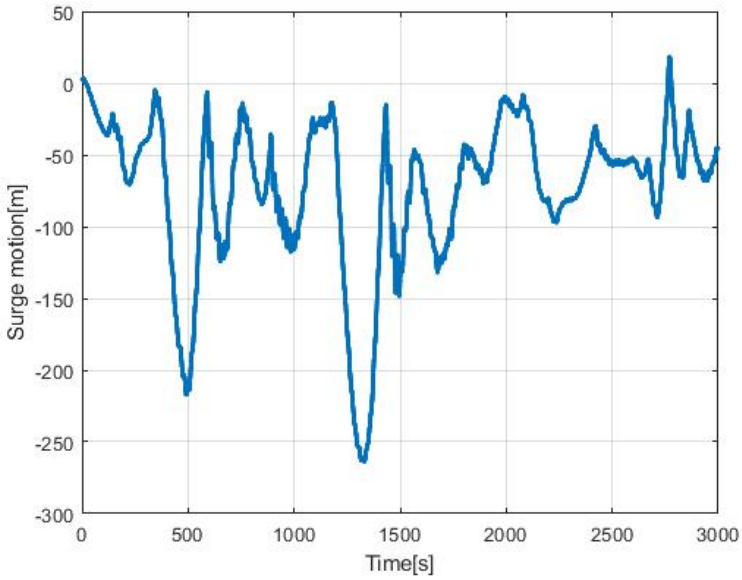


**Figure 6.2:** Platform surge motion with 250m long mooring line

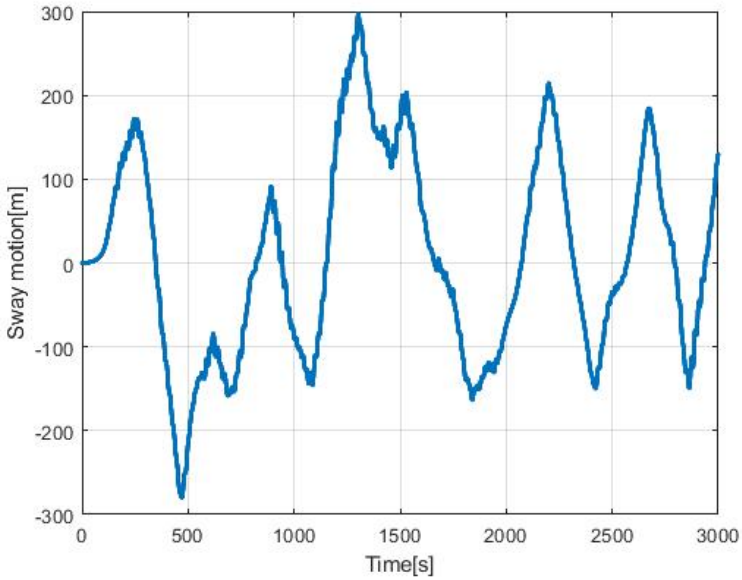


**Figure 6.3:** Platform sway motion with 250m long mooring line

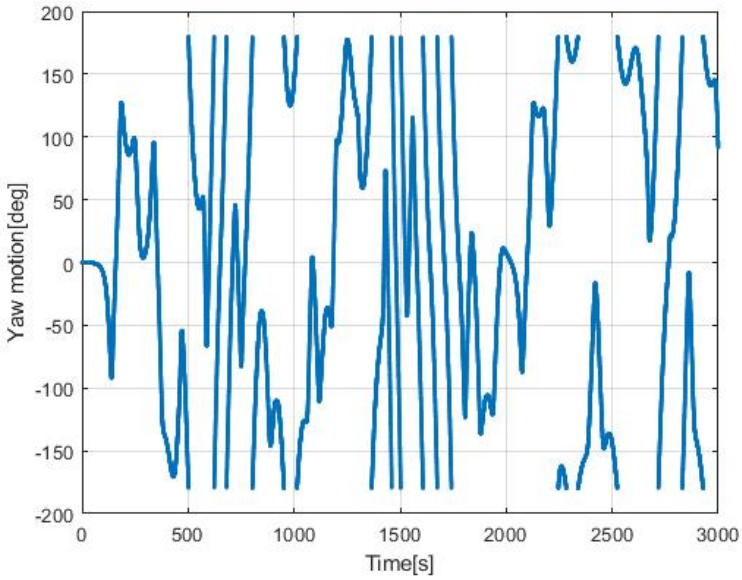


**Figure 6.4:** Platform yaw motion with 250m long mooring line

## 6.2 Initial Design Fishtailing Oscillation

When the mooring length becomes shorter and shorter, the side-ways oscillation behaviour starts showing up. In the initial design, the length of mooring line $L_m$ equals to 125m and distance between the turbine tower and fairlead $L_F$ equals to 75m. Anchor position is set at (-200m, 0m, -6m) and then moved to the seabed before dynamic simulation. The designed anchor position is set to be (-170m, 0m, -100m).

Compared with the situation when $L_m$ equals to 250m, the side-to-side motion for the initial design is more obvious. The platform's trajectory is shown in Figure 6.5. In the beginning, the wind turbine is parked at origin position (0, 0). Once the turbine is released, owing to the pretension of the mooring line, the turbine will first rapidly move forward and surpass the anchor position. Then it will be pushed back by the wind force. With a tightened mooring line, the platform is soon bounced back and travels to the right side of the domain. Then due to the wind force, it is pushed back gently. This time there won't be a sudden change in mooring line tension, the side-way oscillation starts. A single-point moored FWT needs more time to get out of the initial condition effect. For the fishtailing behaviour of the parked turbine, this effect disappears after the first cycle, after which the system reaches a steady state. From the trajectory, the motion shows as an arch shape. The surge motion amplitude is 80m and the distance between anchor position and tower position is around 160m.

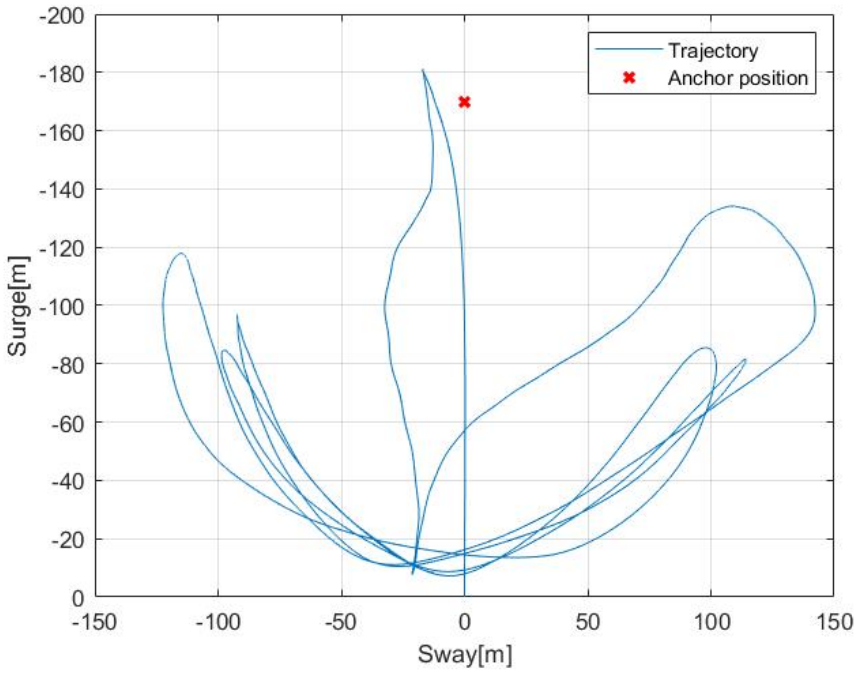


**Figure 6.5:** Platform Trajectory with 125m long mooring line

Sway and yaw motion time series for this parked turbine are shown in Figure 6.6 and Figure 6.7. The surge oscillation and yaw oscillation are in phase with each other and the period is around 520s. The blue line in the figure is the SIMA simulation result and the red line is the linearised model result. The initial condition takes 1000s to disappear in SIMA model, the amplitude of sway motion is 101.5s and the yaw amplitude is $85^\circ$ .

The aim for building the linearised model is to save the computation time and to provide some quick and rough estimation on the model's dynamic behaviour. The linear stiffness matrix for this specific case is provided in Chapter 5.1.2. The elements in stiffness matrix are obtained from small motions which are considered as 1st order Taylor expansion result of the restoring force. This matrix varies from case to case. The eigen period for the model is thus calculated to be $T_e = 549.90s$, which is quite close to the measured period from the linearised model. The results are obtained by solving the linearised equation of motion and the external force is expressed as a function of wind turbine tower position. Compared with the numerical time-domain simulation result, the linearised model is less complicated and the results have fewer features. It is a typical 3-DOF dynamic system which starts oscillation from the beginning. The motion amplifies in the first 600 seconds and reaches a steady-state due to the hydrodynamic damping. Comparing with SIMA simulation, the linearised model underestimates the motion amplitude but overestimates

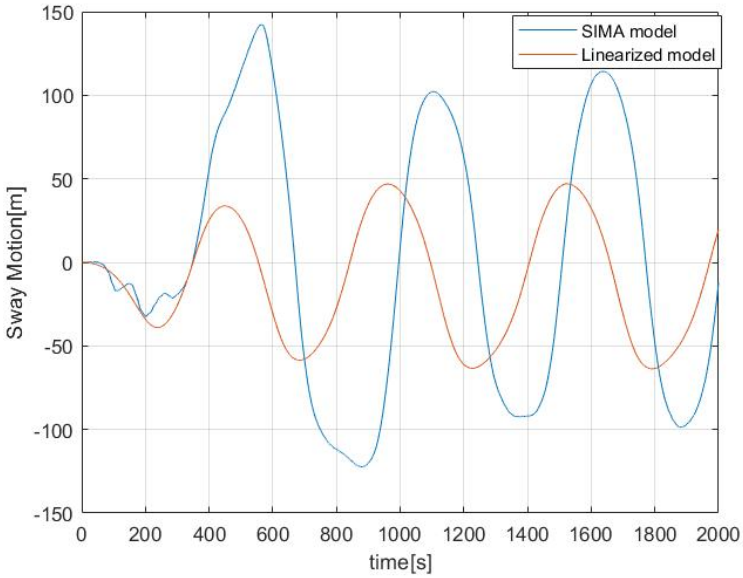


**Figure 6.6:** Sway motion for SIMA and linearised model, $L_m = 125m$

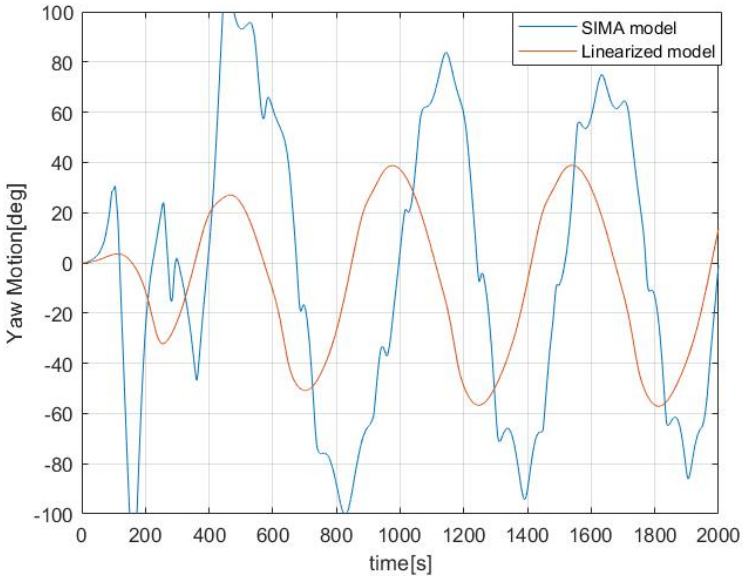


**Figure 6.7:** Yaw motion for SIMA and linearised model, $L_m = 125m$

the period. The error of the predicted period is around 8%. Result comparison between the two cases is shown in Table 6.1

**Table 6.1:** Initial design result summary

| | SIMA model | linearised model |
|---|---|---|
| Anchor position | Seabed | Surface |
| $L_m$[m] | 125 | 125 |
| Sway amplitude [m] | 101.5 | 54.85 |
| Mean sway motion [m] | -13 | -8 |
| Measured sway period [s] | 530.9 | 572 |
| Yaw amplitude [deg] | 89.54 | 47.69 |
| Mean yaw motion [deg] | -5.15 | -8.94 |
| Measured yaw period [s] | 515 | 552.9 |

## 6.3 Dynamic Aerodynamic Force Validation

### 6.3.1 Blade Deflection

The reason for parking the turbine in high wind is to avoid the tremendous aerodynamic forces by pitching the blades to 0° AoA. However, with a yaw misalignment, the blade foil angle of attack may increase to an undesirable position, which generates huge aerodynamic loads on the blade elements. The blades are assumed to be rigid when performing simulations on the fixed turbine in order to get a stable result. However, huge deflection can be observed at the blade tips either in-plane or out-of-plane. Figure 6.8 shows the blade tip out-of-plane deflection during the fishtailing. Severe deflection happens after 1600 seconds. The deflection amplitude exceeds 20m and the frequency for this blade vibration is 1Hz. The side-ways aerodynamic load is shown in Figure 6.9 as a result, the aerodynamic loads acting on the shaft system also vibrates at the same frequency. However, as the vibration frequency is quite high, if the load is integrated with respect to time, the integration of the fluctuation should be zero. As is shown in Figure 6.6 and Figure 6.7, this fluctuation does not show up in sway and yaw and the motions remain the same before and after 1600 seconds. This suggests that the elastic blade fluctuation does not make the SIMA result unreliable when looking at the dynamic motion of the platform fishtailing behaviour.

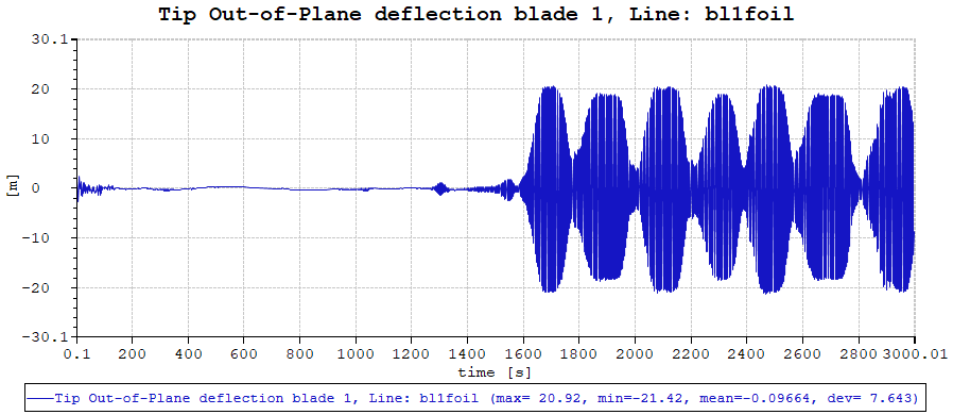


**Figure 6.8:** Blade 1 tip out-of-plane deflection

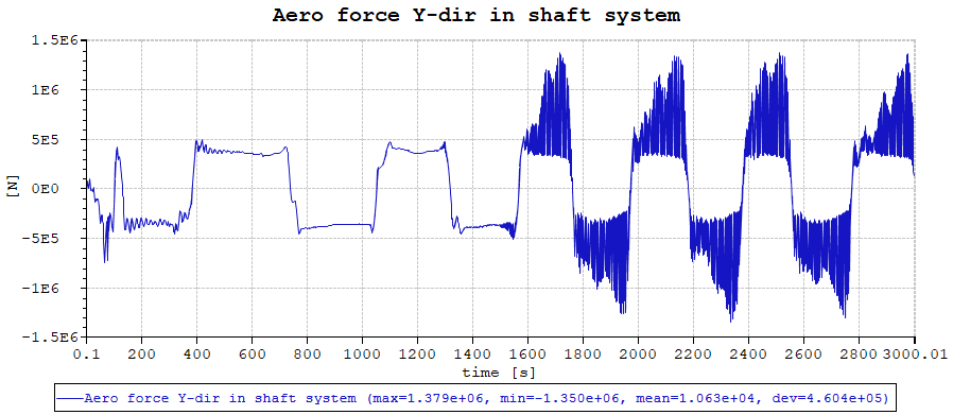


**Figure 6.9:** SIMA result for side-way aerodynamic load

### 6.3.2 Aerodynamic Load Validation

One major assumption for the linearised model is that the aerodynamic loads are considered to be quasi-static and only yaw-motion-dependent. In reality, the dynamic effect may not be negligible. This assumption may be questionable as with the platform moving in the domain, the dynamic loads may be quite different from the static result. For instance, the dynamic stall is an example of this kind of effect. To examine the quasi-static force input in the simple model, the dynamic aerodynamic loads in SIMA are compared with previous results. The fishtailing motion of platform with $L_F = 75m$ and $L_m = 125m$ has experienced the yaw misalignment between -120 deg to 125 deg. The aerodynamic forces are plotted as a function of yaw angle and the dynamic behaviour of wind forces can be captured. As each yaw angle will be experienced several times during the oscillation, the difference between each cycle can also be seen.

The comparison is shown from Figure 6.10 to Figure 6.12. The result of first 1000 seconds in the simulation is used to avoid the fluctuating loads happening after 1600 seconds and to make the figures more clear. There is a good consistency between dynamic result and static load in thrust, as presented in Figure 6.10. With 0 deg and 30 deg yaw misalignment, the dynamic thrust has a significant variation between different cycles. At 30 deg yaw misalignment, the dynamic result tends to be much larger than the static result. The maximum thrust force is $-1500kN$, around 2 times of the static value. When the turbine is exactly at the upwind position, the thrust force also varies a lot and may experience a sudden change in the first cycle due to the sudden motion caused by huge pretension of the mooring line. The shaft system detects a huge positive and negative x-direction force. However, due to the turbine motion, the relevant wind speed is quite different from 30m/s. Apart from this, the dynamic thrust is quite close to the static results in the other cycles.

Comparison of side-ways aerodynamic load is shown in Figure 6.11 and a better coherence can be found in side-ways force than in the thrust result. Major variation happens at $-30°$

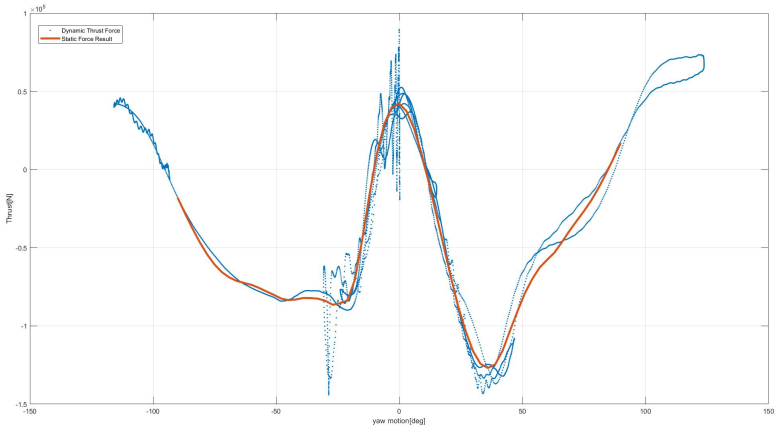


**Figure 6.10:** Comparison between static wind force result and dynamic aerodynamic load: Thrust

yaw motion and this is caused by the sudden forward surge motion due to line tension. This corresponds to 257s in Figure 6.7. In general, the red line static force result can be basically considered as the mean value of dynamic aerodynamic side-ways force at each yaw angle. For the thrust and side-ways loads, good consistency in trend and value can be found among the dynamic and static results.

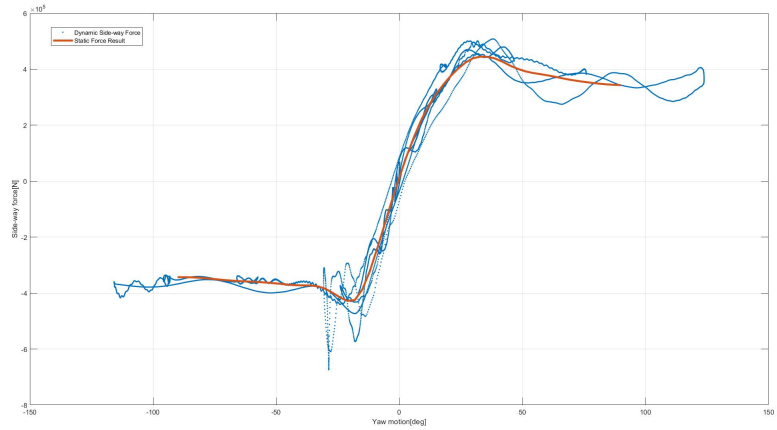


**Figure 6.11:** Comparison between static wind force result and dynamic aerodynamic load: Side-way force

The yaw moment from the dynamic result appears to be more random than the thrust and side-ways loads. The moment varies a lot between different cycles at the same yaw position. From Figure 6.12, maximum yaw moment can be seen at 23° yaw misalignment

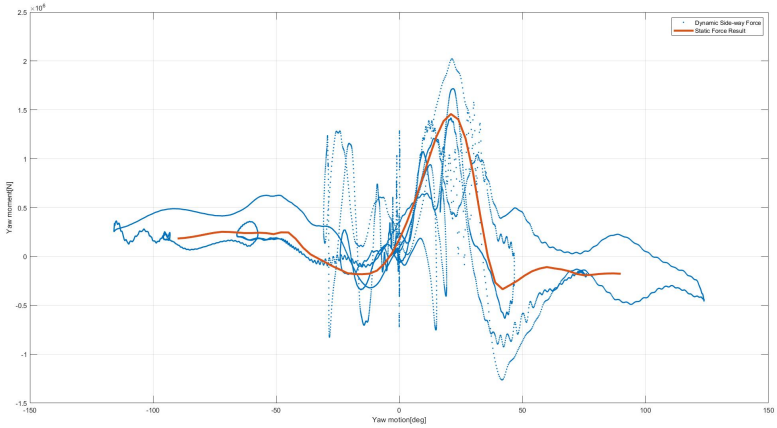


**Figure 6.12:** Comparison between static wind force result and dynamic aerodynamic load: Yaw moment

and the static moment is $1.46 \times 10^3 kNm$ while the dynamic result varies from $29.2 kNm$ to $2.02 \times 10^3 kNm$. The results show that dynamic effect is more significant on yaw moment than on the translation forces.

## 6.4 Various Speed Result

The previous simulation is carried out at a 30m/s wind speed to be compared with the linearised model result. In the severe sea state, the wind speed may exceed 30m/s. One limitation for the quasi-static force model is that when the wind speed needs to be changed, simulations on the fixed turbine need to be done again to obtain the desired static wind loads. If the design is completed, case study needs to be carried out on different wind speeds, it is faster to use SIMA to do the simulations by using condition set. To find out how the motions change with increasing wind speed, extra simulations are carried out on higher wind speed at 42m/s and 54m/s.

Figure 6.13 shows the time domain result of the surge motion. The surge motion curve shows a more sharp peak and a more blunt bottom as the turbine rapidly passes the origin and becomes slower when moving to the maximum surge position. The surge amplitude for high wind speed is smaller than the lower wind speed. Also, it can be noticed that the period for high wind is shorter. The initial condition is similar for all cases; however, it disappears in a shorter time for 54m/s case than 42m/s and 30m/s cases.

In the same case, the platform sway period presented in Figure 6.14 is two times of its surge period and in phase with the yaw period as shown in Figure 6.15. This means the floating wind turbine is at its 1st eigenmode and the platform yaws to the same direction with the sway motion. The 2nd eigenmode does not show up in any cases but can be expected as an opposite motion between sway and yaw. There is a slight decrease in all three motions when comparing the low wind cases with the high. An increasing wind speed makes the aerodynamic force amplitude to be larger, also, the mooring line hawser has larger tension to balance this increased force. This changes the linear restoring force and makes the system to be stiffer. As a result, higher wind speed causes a smaller fishtailing motion amplitude and higher natural frequency. From the results, the change in wind speed influence the period more than the motion amplitude. Measured results are summarised in Table 6.2.

**Table 6.2:** Fishtailing motion result summary

| Wind speed | 30m/s | 42m/s | 54m/s |
|---|---|---|---|
| Surge motion amplitude [m] | 71.62 | 68.63 | 61.03 |
| Surge period [s] | 270 | 160 | 120 |
| Sway motion amplitude [m] | 101.5 | 89.41 | 82.57 |
| Sway period [s] | 531 | 292 | 245 |
| Yaw motion amplitude [deg] | 89.54 | 82.81 | 88.59 |
| Yaw period [s] | 515 | 313 | 249 |

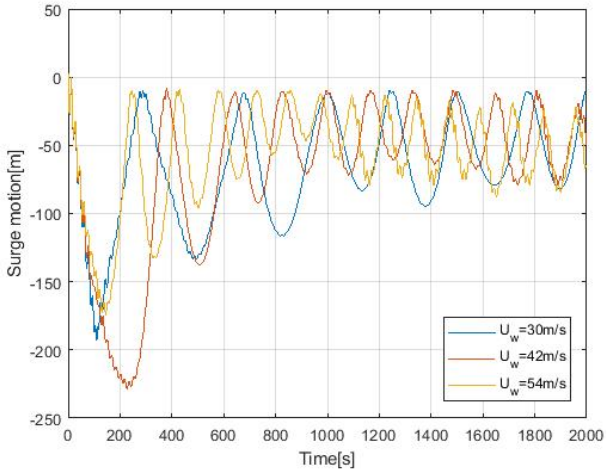


**Figure 6.13:** Platform surge motion of different wind speed

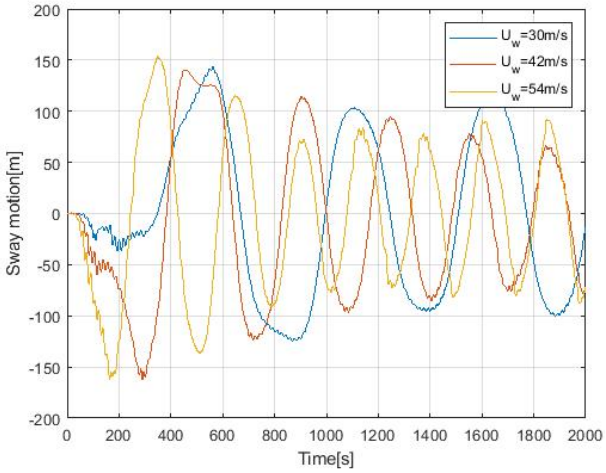


**Figure 6.14:** Platform sway motion of different wind speed

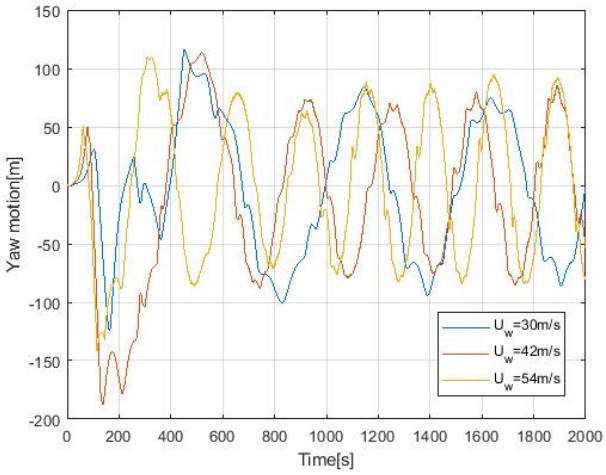


**Figure 6.15:** Platform yaw motion of different wind speed

Chapter 7

# Operating Turbine

In this chapter, the study was carried out on an operating turbine. As the turbine generally has more severe motion at higher wind speed, wind condition is set to be 25m/s at rated. Firstly, the fishtailing behaviour of an operating wind turbine is presented. The catenary mooring line length in the initial design is given based on the longest mooring line length with the ability to ensure the stability of the system. The dynamic motion of the initial design is presented and the results from the linearised model and SIMA model are compared. Based on the linearised model, the distance between fairlead and tower position $L_F$ can be easily changed. This model is used to predict stable yaw misalignment and the results are verified in SIMA. The stable region for a mooring-line-as-a-hawser model is presented(Figure 7.1).

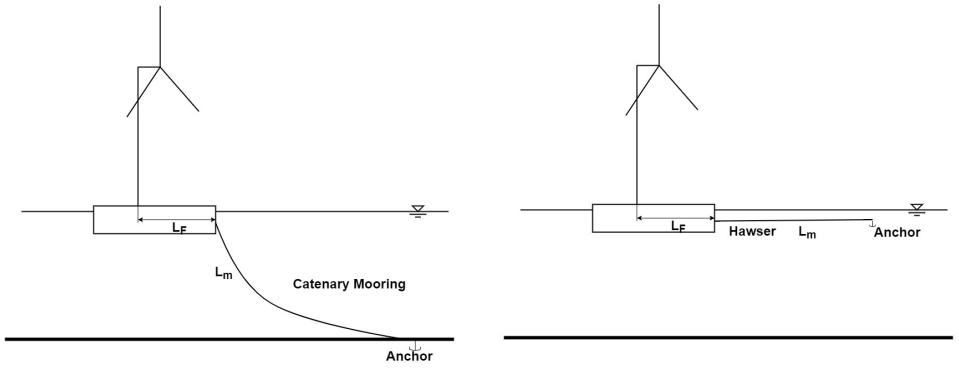


**Figure 7.1:** Catenary mooring line(left) and mooring-line-as-a-hawser(right)

## 7.1 Operating Turbine Fishtailing Behaviour

When the single-point moored floating wind turbine is parked, the energy that keeps the turbine moving comes from the wind kinetic energy. When the turbine is operating, wind kinetic energy is captured and transformed into electricity. This process provides huge damping to the system. When the mooring line is beyond a certain length, the system is still unstable and the dynamic motion shows up. A fishtailing behaviour of operating turbine is seen when the mooring line length is set as 225m. As Figure 7.2 shows, the wind turbine moves mainly in the region where the y-axis is negative. Also, compared with the results in Chapter 6.1, the initial surge motion is much smaller as the thrust force is more significant on an operating turbine when the blades are facing the wind.

Figure 7.3, Figure 7.4, and Figure 7.5 show the result of surge, sway and yaw respectively. The total motion of the platform is not symmetric about x-axis any more and the sway motion is mainly negative. As a result of the asymmetric motion, the periods also change. Surge motion time domain result has a flat peak and a sharp bottom and this can be verified from the asymmetric trajectory. The sway and yaw motion shows a more smooth periodic behaviour than a parked turbine. The steady motion of sway is between 30m and -190m and steady yaw is between $6^\circ$ and $-50^\circ$.

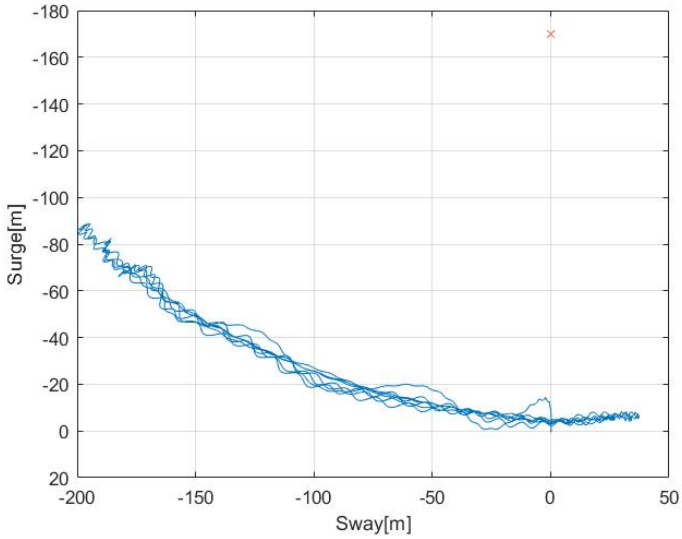


**Figure 7.2:** Fishtailing trajectory of FWT with 225m mooring line at cut-out wind speed

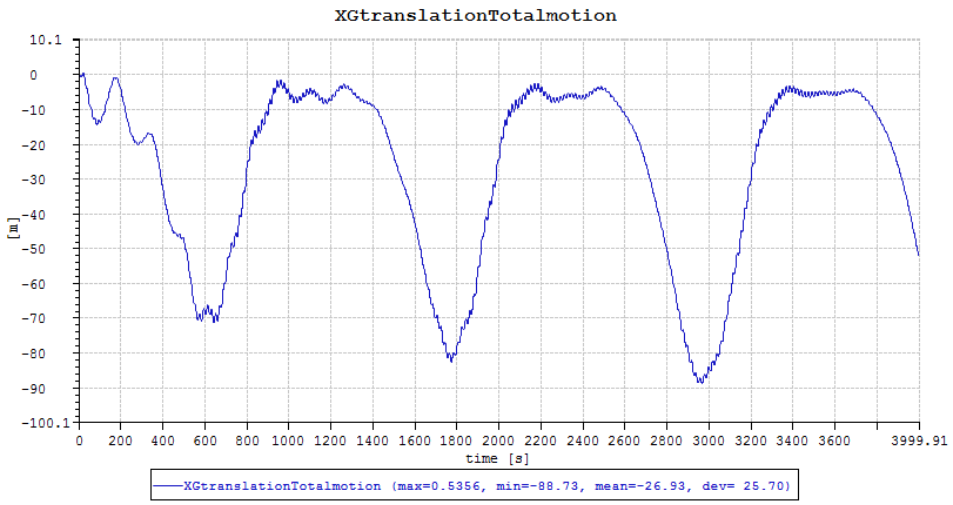


**Figure 7.3:** Surge motion of FWT with 225m mooring line at cut-out wind speed

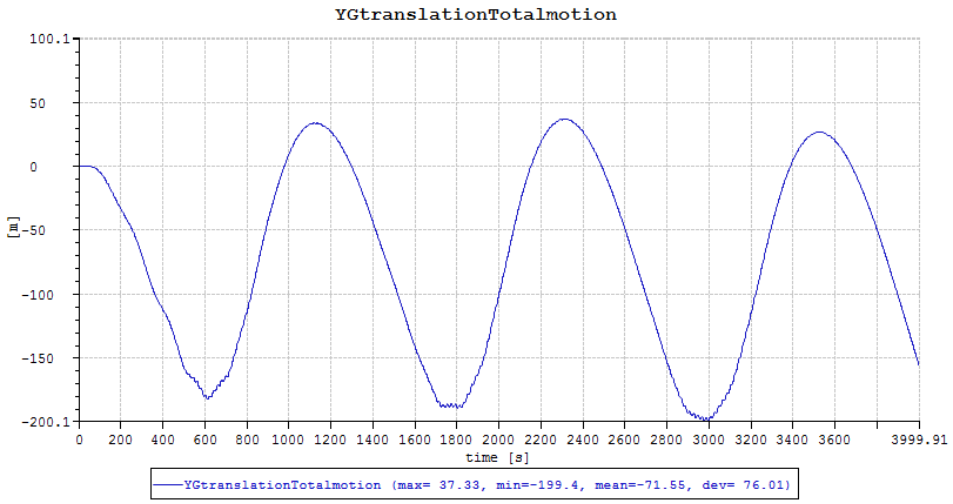


**Figure 7.4:** Sway motion of FWT with 225m mooring line at cut-out wind speed

For symmetric fishtailing oscillation, the surge period is half of the sway period. But for the asymmetric fishtailing behaviour, all of the three motions are in phase. The initial effect takes 600s to disappear after the barge is released. the steady period of the platform is 1200 seconds, which is much larger than a parked turbine. The change of period can be considered as a result of tremendous damping generated during turbine operation. As the wind is high, a steady power output of the turbine is 10MW. From the simulation result,

the blade pitch speed is much faster than the turbine yaw motion, so it is reasonable to assume that dynamic aerodynamic loads are the same with static results and to use the static forces as input into the simplified linearized model.

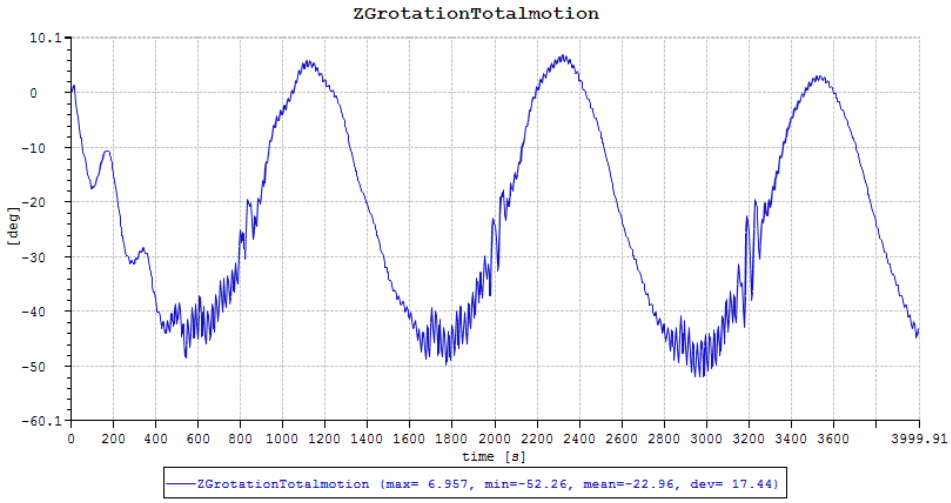


**Figure 7.5:** Yaw motion of FWT with 225m mooring line at cut-out wind speed

## 7.2 Initial Design Performance at Cut-Out Wind Speed

### 7.2.1 Model Setup

The initial design of the mooring line parameter of the single point-moored floating wind turbine is given by the minimum value to make the turbine to become stable at cut-out wind speed. The value is found to be 125m for 100m water depth. 5000s long SIMA simulation is carried out and the results of its dynamic motions are compared with estimation from the linearised model. In the model, the mooring system is a 125m long hawser floating at the sea surface, the set up of the system is same with Chapter 6.2 but wind speed is 25m/s at cut-out. The quasi-static force input data comes from the simulation result of the fixed turbine. Fixed turbine aerodynamic forces oscillate with 3p period(blade-passing period) and to get a static result, the mean value is taken basing on the time domain result.

### 7.2.2 Dynamic Motion

The below figures shows the time domain dynamic motion of the platform. From the results, one challenge with the single-point moored turbine simulation is its long transient period. Normally for a spar or semi-submersible platform, the position of the platform is kept by multiple mooring lines, the mooring stiffness is quite high and the turbine's motion is restricted by the mooring system and close to the initial position, Thus the initial effect will be damped out quite soon. Nevertheless, with one mooring line, the stable position of the turbine varies with the environment. The stable surge position is the place where mooring force in x-direction is equilibrium with aerodynamic thrust force. Depends on the mooring line pretension and wind loads, the stable position may far from the origin.

Figure 7.6 presents the turbine's surge motion. As a relatively short mooring line is used in the model, a tremendous pretension can be predicted. When the turbine is released, rapid forward motion is predicted in either the linear model and SIMA model, the maximum surge motion in linearised model in Matlab is -100m while the maximum surge due to the pretension is -150m in SIMA. Then the turbine is pushed backwards by the wind force and reached -20m in the x-direction at 600s. The linear model result shows some local oscillation, the period for these local oscillation matches with the yaw period of its yaw motion. Also, the linearised model damped much faster than SIMA finite element model and reached stable yaw position at 3000s while the SIMA barge is still surging slowly until the end. For both models, the stable surge motion is -50m.

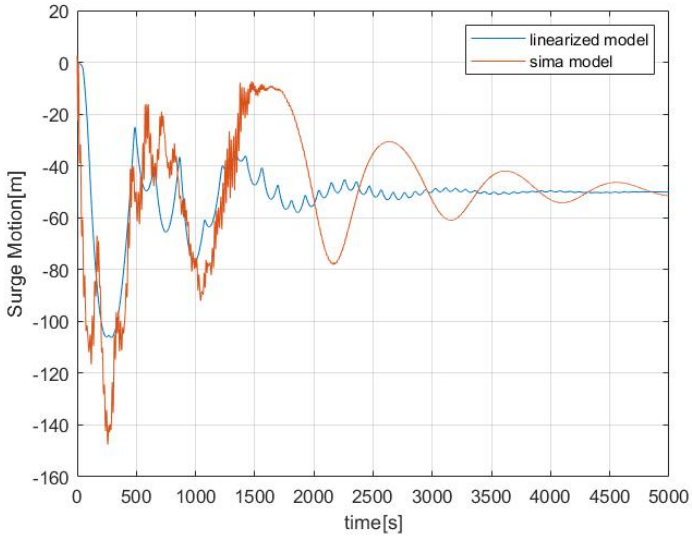


**Figure 7.6:** Platform surge motion with 125m mooring line at cut-out wind speed

The sway motion of the platform is shown in Figure 7.7. Same results are predicted in both models for the first 1100s. Due to the mooring line pretension, the maximum sway motions predicted to be -140m. The local oscillation behaviour also shows up for sway motion in the linearised model in the same period with its yaw motion. In both the Matlab linearised model and SIMA model, the sway motion has the same period with surge motion, and they are in phase. In the linearised model, the stable sway position is 130m, 15m larger than SIMA result. In the linearised model, the mooring line is considered as a hawser floating above the water, while the SIMA model anchor position is located at the bottom position (-170m,0,-100m).

Figure 7.8 is the yaw motion for the 125m mooring line result, the period of simple model yaw motion is much smaller compared with the SIMA model, this is because the stiffness in the linearised model in yaw is larger than the numerical result. This high yaw frequency caused the local sway and surge oscillation in Figure 7.7 and Figure 7.6. The yaw motion effect does not show up in the SIMA model as the three motions are in phase. This also means that the eigenmode for the 125m mooring line operating turbine case is the same as the previous cases. The two models both predicted the same stable yaw position slightly lower than -50 degree, this means even for the stable case, the wind turbine is not at the exactly upwind position.

Even though the dynamic behaviour is not perfectly represented in the simplified model, it can provide a reasonable estimation on translation stable point of the operating wind turbine and provide an accurate prediction on the stable yaw misalignment. Furthermore, the linear model can save significant calculation time comparing with a full-scale numerical

model in SIMA.

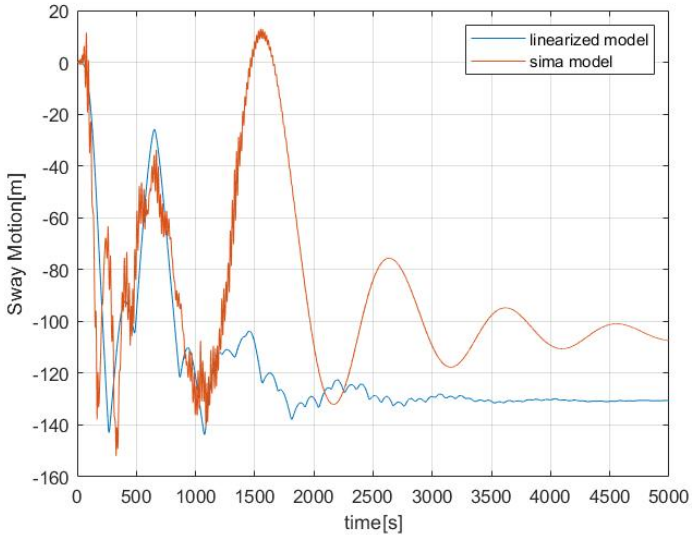


**Figure 7.7:** Platform sway of FWT with 125m mooring line at cut-out wind speed

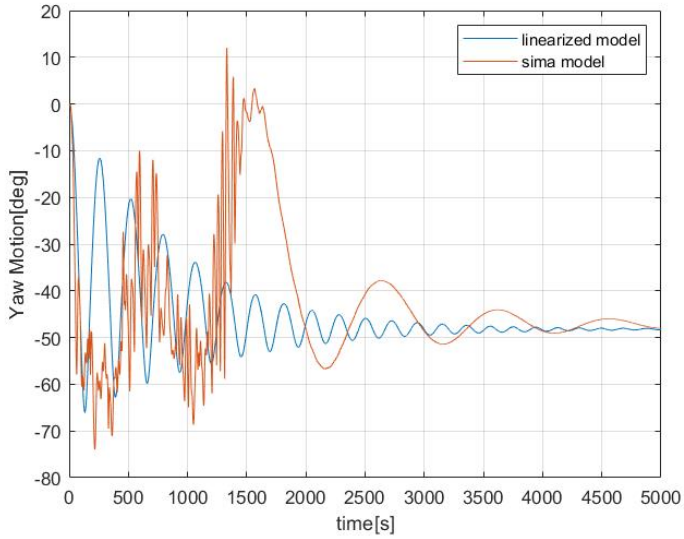


**Figure 7.8:** Platform yaw of FWT with 125m mooring line at cut-out wind speed

### 7.2.3 Operating Status

**Working Condition Hydrodynamic Stability**

The single-point moored floating wind turbine has a large extent of freedom and its dynamic motion is much more significant compared with other FWTs such as spar, semi-submersible and TLP type. The wind force is acting on the rotor blades and can be considered at 119 metres above tower base vertical position and the mooring line force is acting on 6 metres below the free water surface at the fairlead position. the total distance between the two forces is around 130m, a huge moment is generated due to the long lever. Moreover, the platform is moving in the ocean rather than stay at a certain position a severe coupling between different degrees of freedom might happen. Thus, the hydrostatic stability during the operating condition of the single point floating wind turbine is worth checking.

Hydrostatic stability of a barge with a parked turbine in no wind condition has been checked and its GZ curve is given in Figure 3.3. Hydrostatic stability of an operating turbine is shown in figures below. Figure 7.9 is the result for heave motion of the stable operating turbine with $L_F = 75m$ and $L_m = 125m$. Figure 7.10 and Figure 7.11 corresponds to the roll motion and pitch motion. As discussed in the previous section, at the first 1500 seconds, the result is strongly influenced by the pretension and the platform is moving at a significantly high speed. As a result, the heave motion fluctuates between -0.2m and -1.1m, the roll motion shows to be symmetric and maximum value happens to be 6 degrees. The maximum pitch motion happens at the same time with the maximum heave motion and the pitch angle exceed $11°$. These maxima happen when the platform has the highest surge motion and happen at the same time when the turbine stops moving forward and pulled back by the wind.

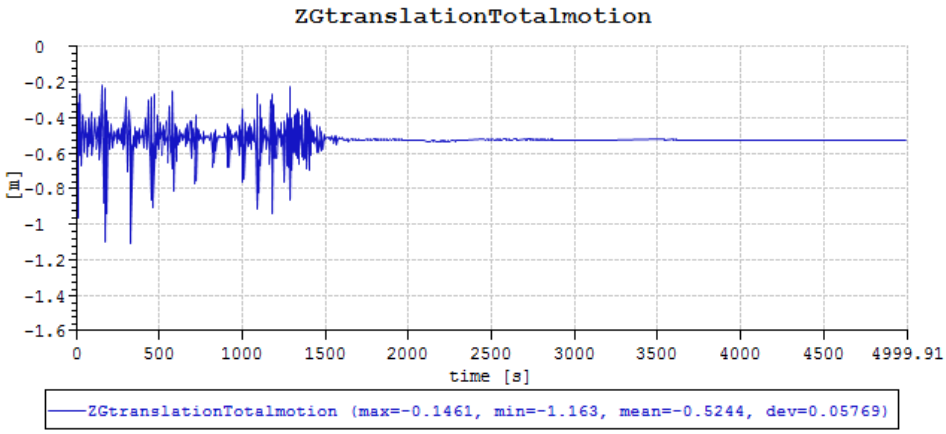


**Figure 7.9:** Platform heave of FWT with 125m mooring line at cut-out wind speed

As the barge is relatively large, enough restoring force is provided. The heave, roll and pitch motions are not largely effected by the dynamic fishtailing behaviour. The stable

heave motion is $-0.52m$ and the pitch and yaw motion ca be neglected. Some periodic behaviour of rolling can be seen as a result of side-way motion and forces but as the side to side slowly reduces, the roll motion also went to zero.

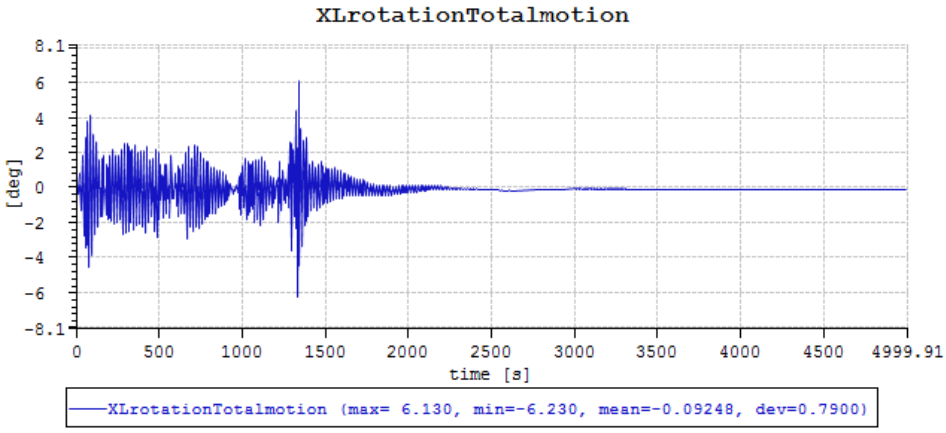


**Figure 7.10:** Platform roll of FWT with 125m mooring line at cut-out wind speed

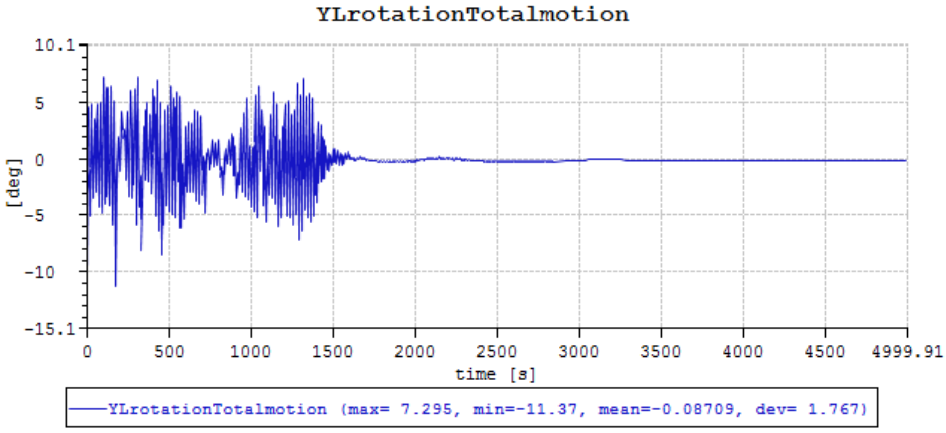


**Figure 7.11:** Platform pitch of FWT with 125m mooring line at cut-out wind speed

### Wind Turbine Rotor Output

In this case, the steady misalignment is proved to be around -50 degree, at this yaw angle, the aerodynamic moment and the restoring moment generated by the mooring line and side-ways aerodynamic force reached the equilibrium. The steady-state wind speed along shaft x-axis is 16.9m/s, which is above 11.4m/s rated but when a low wind happens, the equivalent wind speed along the local x-axis may below rated.

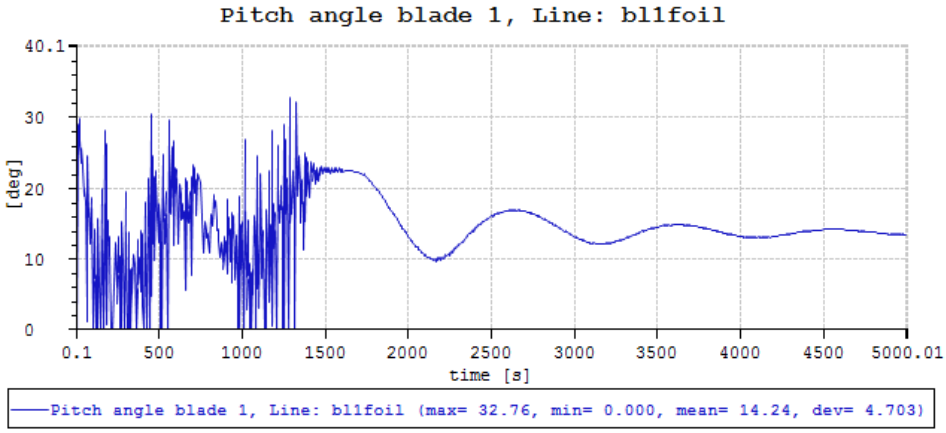


**Figure 7.12:** Blade pitch for $L_m = 125m$ case

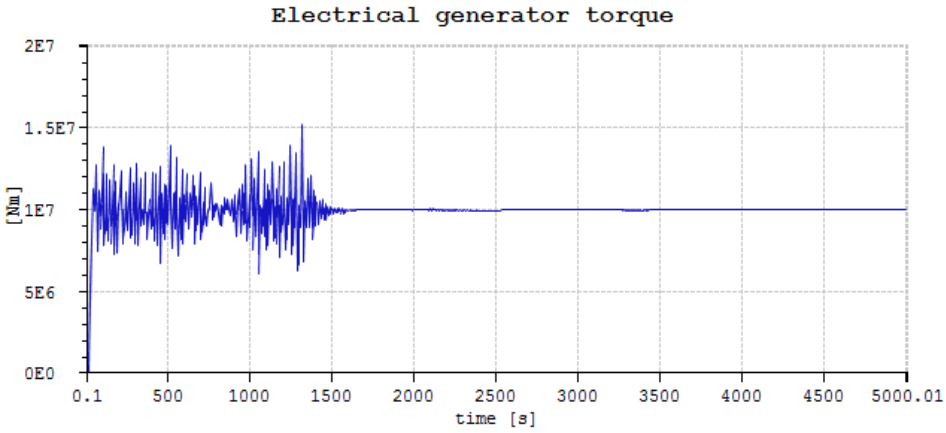


**Figure 7.13:** Generator torque of $L_m = 125m$ case

Figure 7.12 shows the change of pitch angle as a function of time. The pitch controller can provide real-time feedback and the blade pitch mechanism change the pitch angle depends on the inflow wind speed. It can be seen that the processor provides a timely update on the blade pitch angle and as a result, the dynamic aerodynamic wind force is similar to the static result on a fixed turbine. The pitch controller is designed to operate at an upwind

position and the yaw controller is used to balance the aerodynamic motion and turns the turbine facing the wind. Thus, if no yaw controller is installed, the pitch controller might be one of the reasons for generating the high yaw misalignment as the desired energy output is considered prior to aerodynamic moment when designing the pitch controller.

Although a high yaw misalignment is witnessed, the inflow wind speed is still higher than rated, thus the turbine will still operate with a rated torque and rated 10MW power output. Figure 7.14 and Figure 7.14 shows the torque and power of the initial design. When the initial effect disappears, the generator torque and power output remain unchanged.

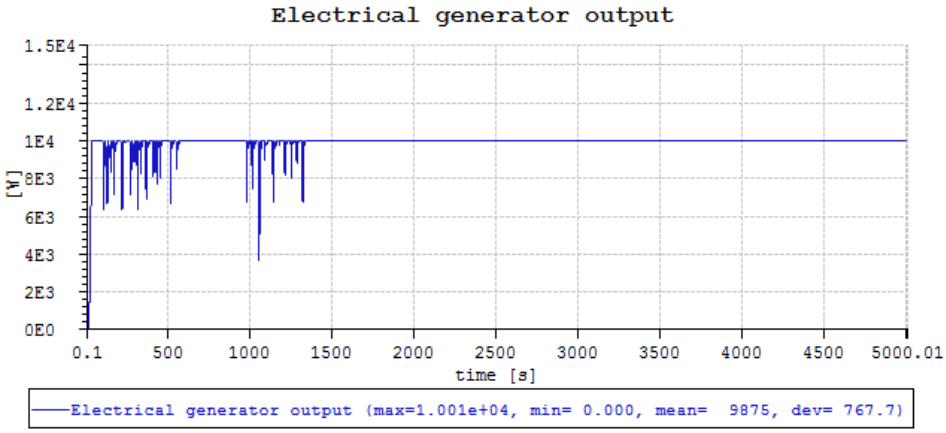


**Figure 7.14:** Generator torque of $L_m = 125m$ case

## 7.3 Stable Yaw Misalignment

Previous results show that the barge may either have a fishtailing steady-state or stable at an asymmetric position. The equilibrium point is found at a minus sway and yaw position and this is also the mean point oscillation is around. As the minimum mooring line length that guarantees the system to be stable is found, the yaw misalignment could also result in reduced equivalent wind speed and further cause a dropped turbine power output at the wind speed.

The stable yaw misalignment for $L_m = 125m$ and $L_F = 75m$ is at $-49°$. From the static result on a fixed turbine at cut-out wind speed, the upwind side-ways yaw misalignment force is almost negligible when the aerodynamic yaw moment is in the counterclockwise direction. Thus the turbine will start having a negative yaw motion when the turbine is turning, the aerodynamic side-way force increases and the righting lever also increases. The problem is dynamic when the platform is oscillating, when it reaches the equilibrium point, the righting moment should equal to the aerodynamic excitation moment. The external forces acting on the turbine are shown in Figure 5.3, by using the same symbols, static state yaw moment equilibrium should be expressed as:

$$M_l + F_{yl} L_F = 0 \tag{7.1}$$

SIMA simulations are carried out on various $L_m$ and $L_F$ to find the determinants of stable yaw misalignment. When setting up the mooring line in SIMA, anchor position and artificial stiffness of FWT structure need to be carefully selected to avoid errors during the dynamic calculation. To save the time spend in setting up the finite element model, the anchor position is moved to the free surface of the water and thus the mooring system can be considered as a hawser.

Figure 7.15 shows the yaw motion of the barge with 90m fairlead distance with different hawser length, the presented cases are all stable but the time consumption to reach the stable state is quite different. Another presented case in Figure 7.16 is the $L_F = 100m$ case, which is also stable and shows similar behaviour. From the figures, it can be seen that the shortest hawser length doesn't guarantee the highest damping and the shortest time for the initial condition effect to disappear is also not necessarily happens when using the shortest mooring line. From listed cases in the figures, the length of the mooring line does not affect the stable yaw misalignment. When the fairlead is 90m away from the tower, steady yaw motion is -29.6 degree. When $L_F = 100m$, the steady-state yaw offset is -21 degree.

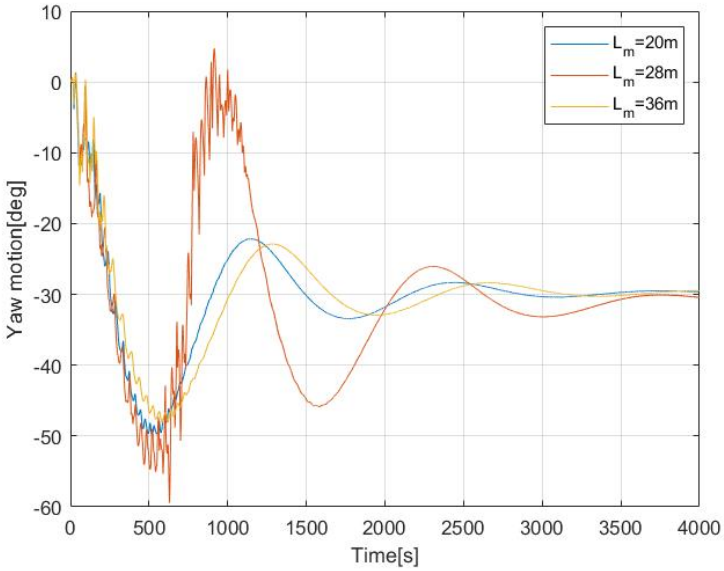


**Figure 7.15:** Yaw motion of $L_F = 90m$ with different mooring line length

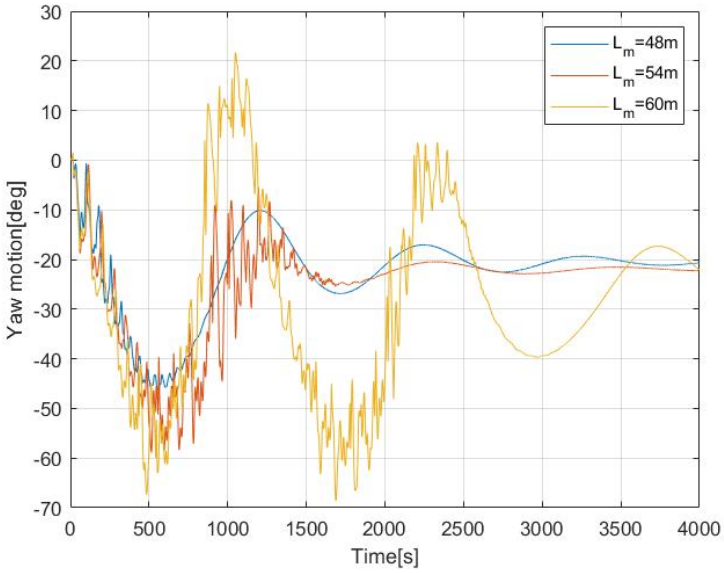


**Figure 7.16:** Yaw motion of $L_F = 100m$ with different mooring line length

Linearised model is used to estimate the steady yaw misalignment due to high computation

cost of SIMA. SIMA is later used for result validation. The findings are presented in Figure 7.17. The initial yaw misalignment with small $L_F$ is around -60 degree and the yaw angle decreases with an increasing restoring lever. The steady yaw angle starts changing rapidly when $L_F = 75m$ and drops from -50 degree to -10 degree at 100m. From then the cost of reducing yaw misalignment increases and the curve is flattened. The red crosses are some critical $L_F$ tested in SIMA and the two results have a high degree of agreement and share the same trend. Although there are still some differences between the simplified linear model and numerical model, the further optimal design can be carried out based on this reasonable estimation.

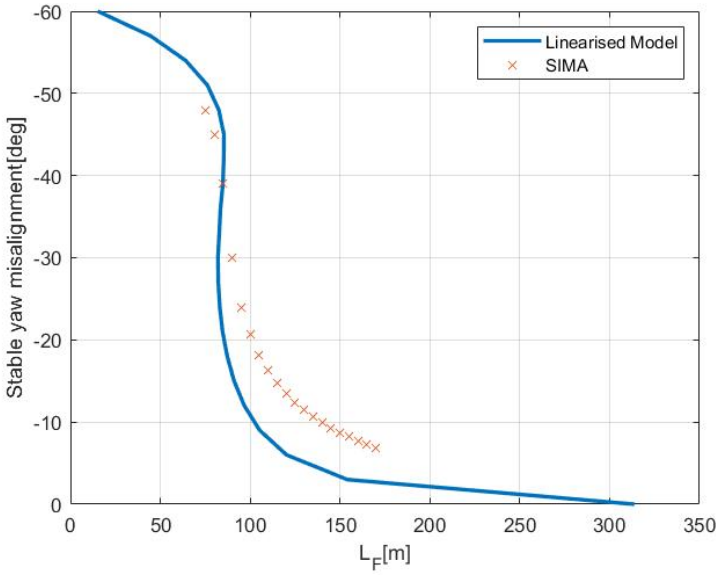


**Figure 7.17:** Steady yaw misalignment as a function of $L_F$

## 7.4 Stable Region

Simulations are done in SIMA to find the stability region of the floating wind turbine. The mooring system is considered as a hawser line and its length is the same with the initial distance between fairlead position and anchor position. Results for the tested cases are shown in Table 7.1 and the hawser length stands for the maximum possible hawser length to maintain the stability. When $L_F = 75m$ and $L_F = 80m$, the stable hawser length is within 10m, but when the fairlead distance reached 37m, the maximum stable length boosted from 7m to 37m. After that, the minimum $L_m$ grows linearly with the increasing the fairlead-tower distance.

**Table 7.1:** Operating turbine stable region

| Dist. from fairlead to tower[m] | Hawser length[m] | Stable yaw misalignment [deg] |
|---|---|---|
| 75 | 4 | -48 |
| 80 | 7 | -45 |
| 85 | 37 | -39 |
| 90 | 44 | -30 |
| 95 | 61 | -24 |
| 100 | 72 | -20 |

Chapter 8

# Optimal Design Recommendation

## 8.1 Selection of Values

The previous chapters have studied the dynamic motion of parked and operating turbines with various $L_m$ and $L_F$. For 100m deep water, the maximum mooring line length to make the turbine stable at cut-out wind speed is 125m. An anchor is normally designed to withstand horizontal drag force but can't resist high vertical force. A short mooring line may result in a high vertical force and high stress inside the chain component. Furthermore, when $L_F = 75m$, the stable yaw misalignment is found to be $-50°$, which means that the wind speed in the y-direction is even higher than x-direction. This considerable yaw misalignment may not only require a considerable high wind speed to let the power production to reach rated, but also will cause a huge thrust force. According to Figure 4.6, the thrust force is at a low level between $\pm 25°$, when the yaw angle exceeds $30°$, the aerodynamic thrust increases dramatically and reaches 700kN at $-50°$ yaw angle. Besides, BEM theory is not perfectly reliable when the inflow angle exceeds $30°$, thus, a more optimal design is needed.

Linearised model provides a good estimation on the yaw misalignment, as shown in Figure 7.17. From $L_F = 75m$, the stable angle drops quickly with the growing of $L_F$. The curve is flattened after 110m and increasing $L_F$ becomes an inefficient way of reducing yaw angle after 125m fairlead-tower distance. Thus, the fairlead-tower distance is chosen to be 100m in the updated model. As an increased $L_F$ is also beneficial for the stability, the length of mooring line is thus increased to 200m, the rest of mooring line parameters remain the same. The simplified linearised model is used to estimate the dynamic motion of the turbine at cut-out wind speed, the study is also conducted in SIMA at 30m/s wind speed and 25m/s at cut-out.

## 8.2 Dynamic Motions

Figure 8.1 shows the SIMA result of the optimised turbine fishtailing behaviour at the high wind. A huge forward surge motion can be seen in the first 500 seconds due to the pretension. The initial condition effect disappears after 1000s. Same as observed in the initial design, at the steady-state, the sway and yaw motion have the same frequency around 470s and in phase with each other. Also, the surge period is half of the sway and yaw period, which is typical for a fishtailing behaviour of a single-point moored system.

In the 30m/s high wind situation, the dynamic motion of the new design has a smaller motion period and yaw amplitude. The new design has around $10^{\circ}$ smaller yaw amplitude when comparing with the 90 yaw motion of the initial design. As a result of long mooring line length and larger fairlead-tower distance, the sway motion of optimised design is 40m larger than when $L_F = 75m$, sway motion is around 140m. Also, the mean value of the sway and yaw motion are negligible and the mean offsets are around 0. Lowest surge motion when the turbine is fishtailing is around 30m, 260m away from the anchor position.

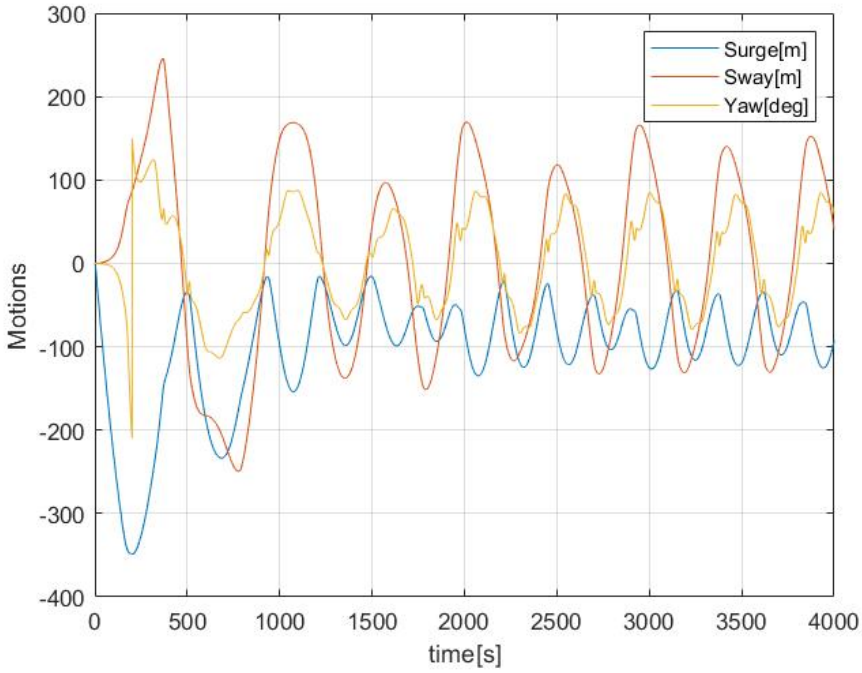


**Figure 8.1:** Fishtailing motion of optimised design-parked

The time-domain operating turbine dynamic motions are shown in Figure 8.2. From the

results, it can be seen that the linearised 3-DOF model provides a close estimation of the stable position of the motions but underestimates the sway and yaw motion period. Comparing with the 30m/s high wind result, a significant increase in the oscillation period can be seen from the turbine. The parked turbine oscillation period is 470s but the operating period is around 1400s, about three times larger. To compare with, the sway and yaw period for initial design is around 520s at 30m/s high wind and 1010s at 25m/s, about twice.

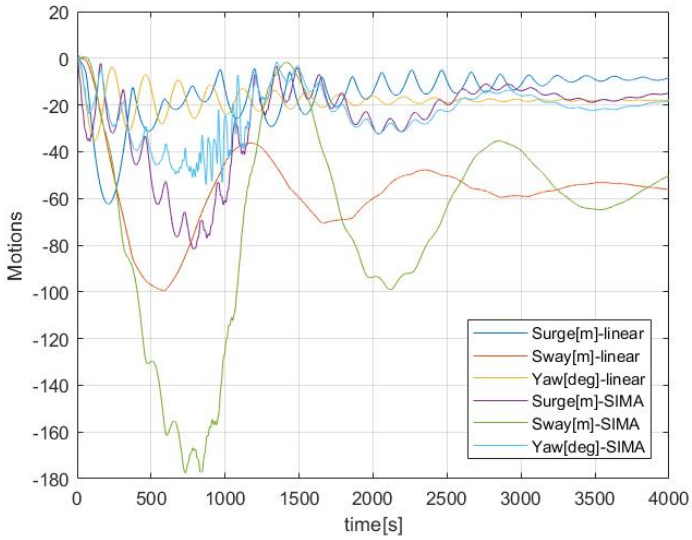


**Figure 8.2:** Motion of optimised design-operating

**Table 8.1:** Fishtailng result of initial and optimised design

| | Initial design | Optimised design |
|---|---|---|
| Anchor position[m,m,m] | (-170,0,-100) | (-290,0,-100) |
| $L_m$[m] | 125 | 200 |
| $L_F$[m] | 75 | 100 |
| Sway amplitude [m] | 101.5 | 140.6 |
| Mean sway motion [m] | -13 | -10 |
| Measured sway period [s] | 530.92 | 474.56 |
| Yaw amplitude [deg] | 89.54 | 80.85 |
| Mean yaw motion [deg] | -5.15 | 3.47 |
| Measured yaw period [s] | 515.03 | 464.32 |
| Operating sway period [s] | 1011.06 | 1407.17 |
| Operating yaw period [s] | 1002.58 | 1393.76 |
| Stable yaw misalignment [deg] | -47.3 | -18.7 |

Table 8.1 compares the motion amplitude and period of sway and yaw motion under cut-out and high wind speed. Either case is oscillating around the x-axis of the coordinate system and the mean motion is close to zero. Even though the yaw motion of the updated design is smaller than initial, but the sway motion is larger. When the turbine is operating, the sway and yaw offsets are much smaller the original design. Also the cost is relatively small with 18 degree steady yaw misalignment when comparing with further increasing $L_F$.

## 8.3 Shaft System Loads Comparison

One importing reason for avoiding a huge yaw angle is to reduce the mean value and fluctuation amplitude to the loads acting on the wind turbine blade, shaft and tower sturctures. As presented previously, the static yaw misalignment aerodynamic load study shows that the side-ways aerodynamic force is similar between -20 degree and -50 degree, the peak value is at -30 degree. Yaw moment result shows a similar result. However, significant growth can be seen when yaw angle exceeds -30 degrees thus aerodynamic thrust force is considerable larger with a high yaw angle.

Figure 8.3 shows the shaft system forth-aft force, it shows that the time consumed by improved design to reach steady state is shorter that the initial design. It suggests that when the wind condition changes, the improved design takes shorter time to reach a new stable point. In Appendix C, zoom in figures of aerodynamic loads are presented. From the result, force for the improved design fluctuates between 480kN and 550kN, the mean value is 515kN. The initial design steady thrust force oscillates between 550kN to 670kN, with a mean thrust of 610kN. The mean thrust is reduced by 16.39% by an increased $L_F$.

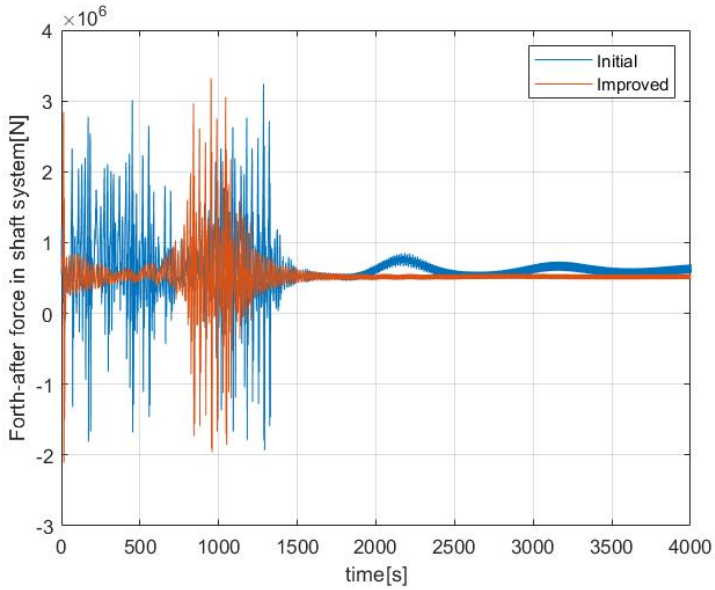


**Figure 8.3:** FA force in shaft system

Side to side aerodynamic load of initial and improved design are shown in Figure 8.4. The improved design side to side force oscillates between 75kN and 125kN, the mean value is around 100kN. Both the fluctuation amplitude and the mean value is more significant in the initial design, of which the lowest steady side way load is also 75kN but the highest is 168kN. with a mean value of 125kN, 25% higher than the improved design. The fluctuation amplitude of the initial design is 43kN, 92% higher than the 25kN optimised design result.

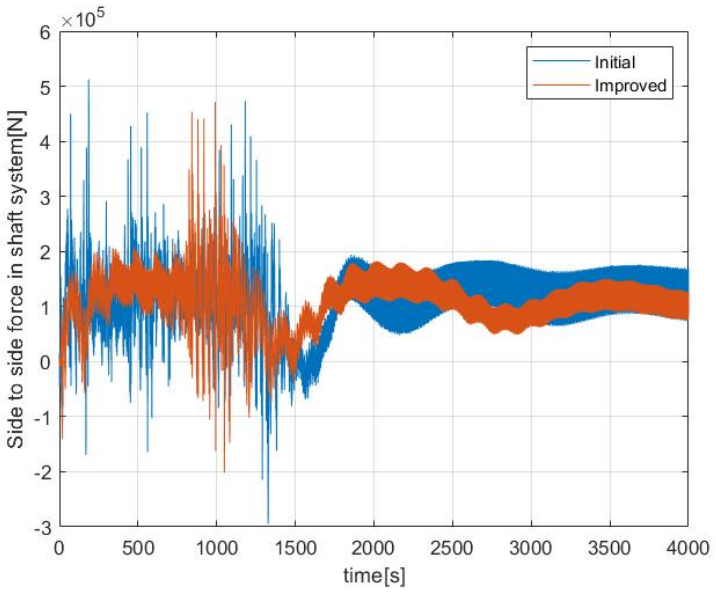


**Figure 8.4:** SS force in shaft system

Figure 8.5 is the torsion around the z-axis in the shaft system. Significant oscillation can be seen from the initial design result. The mean torsion of improved design is $-9.5 \times 10^3 kN \cdot m$ and the oscillation amplitude is about $1000kN \cdot m$. To compare with, the initial design torsion oscillates from $-2.5 \times 10^3 kN \cdot m$ to $-1.2 \times 10^4 kN \cdot m$. Oscillation period for both cases follows the 3p blades tower passing frequency.

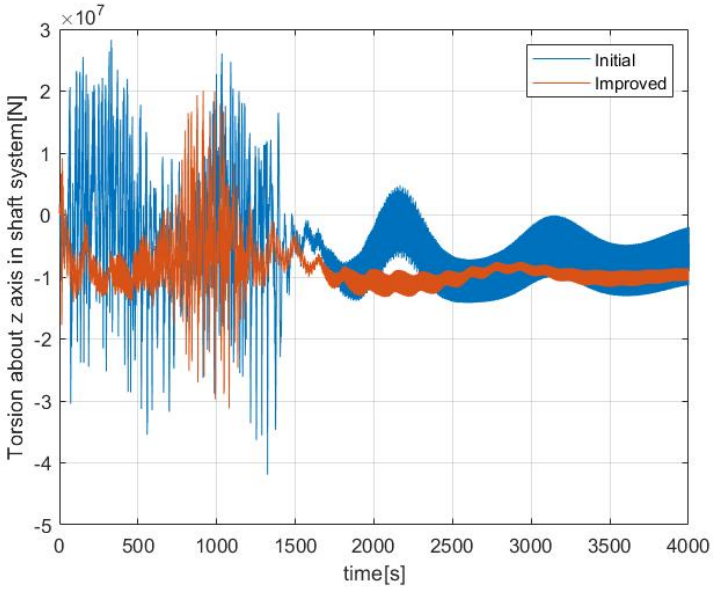


**Figure 8.5:** Shaft system torsion around Z axis

Chapter 9

# Conclusions and Recommendation for Future Works

## 9.1 Conclusions

This master thesis presents the study result of the fishtailing behaviour of single-point moored floating wind turbines. The idea is to use a single point moored barge as the supporting structure of the DTU 10MW RWT, so the FWTs can free weathervaning. However, the turbine tends to have severe side-ways motions when the wind speed is decent. This thesis is down to have a better understanding of this phenomenon, especially around a 30m/s wind speed when the turbine is parked and at cut-out wind speed on an operating turbine. The operating water depth is 100m depth.

A $50m \times 50m \times 10m$ box shape barge finite element model is built in GeniE, hydrostatic and hydrodynamic properties are obtained from HydroD. Hydrostatic stability of the barge is checked by the barge GZ curve and validated by revisiting the operating turbine platform pitch, roll, and heave motion. The mooring line properties are defined based on relevant literature and selection of values of other catenary line moored floating wind turbines.

Simulations are carried out on fixed turbines to obtain the static wind forces. The simulations are done in SIMA and OpenFAST for a parked turbine. For a parked turbine, significant aerodynamic loads can be seen at around $\pm 45^{\circ}$ yaw angle. Good coherence can be seen between among two software in thrust and side-ways load, the aerodynamic moment shares the same trend. However, difference can still be observed at each individual yaw angle. SIMA simulation is done for operating turbine, the result shows that thrust force is more significant than aerodynamic side-ways forces, as a result, the total aerodynamic load is relatively low when the yaw angle is smaller than $\pm 30^{\circ}$.

By implementing the rigid body dynamics theory, a simplified model is developed to study the yaw fishtailing behaviour and yaw misalignment. The model simplified the problem to be a 3-DOF and only surge, sway, and yaw motion are considered. Wind forces are considered to be quasi-static and fixed turbine results are used. The mooring line is considered as a hawser floating above the water surface. The problem itself is non-linear thus an artificial stiffness basing on the 1st order Taylor expansion is used to improve numerical stability and to estimate the period of fishtailing behaviour. The linear damping ratio is chosen as 5% of critical damping and infinite frequency added mass is used.

When the wind speed is at 30m/s, chaotic behaviour shows up when a long mooring line is used. In this case, the mooring system failed to provide enough restoring force and moment thus the turbine travels all over the area with a yaw motion larger than $360^{\circ}$. When a shorter catenary mooring line is used, the fishtailing behaviour shows up. In the initial design, a 75m fairlead-tower distance is selected and the mooring line length is 125m. Fishtailing motions from SIMA and linearised model are compared and the result shows that the models can predict similar period but linearised model will underestimate the motion amplitude. Then a variety of wind speeds above cut-out are discussed, the increasing wind speed means a higher stiffness, thus the motions' amplitude and period decrease. Static aerodynamic wind loads and dynamic time-domain simulation results are compared, which suggests that it is a reasonable assumption to use the static result as wind force input in the simple model but the limitation of the simple model is about the dynamic influence on aerodynamic yaw moment.

The study is then extended on an operating turbine at cut-out wind speed. When the mooring line is long, the turbine shows an asymmetric fishtailing behaviour in the negative y-axis. As for the initial design, a stable point is found at $-50^{\circ}$ yaw angle, SIMA and lineardised model have a good agreement on steady yaw misalignment. To propose a more optimal design, simple linearised model is used to identify the stable yaw misalignment as a function of fairlead-tower distance, some of the critical results are also done and compared in SIMA. The stable region for maximum mooring line is also identified in SIMA by assuming the mooring system as a hawser.

Based on the finding on stable yaw misalignment, an improved design with 200m mooring line and 100m fairlead-tower distance, which is a reasonable value concerning the increased cost regards to reduced yaw angle. The improved design's fishtailing period at high wind speed is smaller and the yaw amplitude also decreased. When the turbine is operating at cut-out, the improved design becomes stable faster than the initial design. Also, a significant alleviation can be seen in the shaft system loads when compared with the initial design because of the yaw misalignment.

As a conclusion, this thesis studies the fixed turbine aerodynamic loads with yaw misalignment, fishtailing behaviour of parked turbine and yaw misalignment on operating turbine in SIMA. To reduce the calculation cost, a simpler 3-DOF linearised model is developed and results are validated by SIMA numerical results. Finally, a more optimal design is identified basing on the linearised model result.

## 9.2 Recommendations for Future Work

This thesis presents some results of fishtailing behaviour and stability study of a single point moored floating wind turbine, the topic itself is broad and there are still many things to be explored, here are some recommendations for future study on the topic:

- The major calculations in this thesis are done in SIMA. Some of the yaw misalignment results are done in OpenFAST but disagreements show up with parked turbine yaw moment, operating turbine side-ways force and yaw moment and some dynamic motions of the platforms. The OpenFAST results need to be validated in the future work and differences are waiting to be discussed.
- This thesis mainly discussed the effect of mooring line length and fairlead-tower distance. Some simulation results suggest that the selection of mooring line damping and added mass coefficient, chain weight and mooring line stiffness also matters, this study needs to be considered.
- The linearized model can be further optimised to provide better estimation about fishtailing amplitude of parked SPM FWTs. A more optimal model can be proposed to provide a better estimation of operating turbine yaw period.
- The current studies are based on constant steady wind, the study can be further extended to a variety of wind speed or more complicated wind field.
- Apart from wind, wave and current also play an important role in fishtailing behaviour of ships and towing operation. These effects on the single-point moored floating wind turbine are to be discussed.
- Although a more optimal design is proposed, the detailed design to achieve such a long fairlead-tower distance is to be studied.
- Wind turbine dynamic motion and stable point below cut-out wind speed is to be investigated.
- Eigen-value analysis is to be done with the linearised model.

# Bibliography


[1] Joao Cruz and Mairead Atcheson. *Floating offshore wind energy: the next generation of wind energy*. Springer, 2016.

[2] Wind Europe. Windeurope annual offshore statistics 2019, February 2020.

[3] Sandy Butterfield, Walt Musial, Jason Jonkman, and Paul Sclavounos. Engineering challenges for floating offshore wind turbines. Technical report, National Renewable Energy Lab.(NREL), Golden, CO (United States), 2007.

[4] Anja Eide Onstad, Marit Stokke, and Lars Sætran. Site assessment of the floating wind turbine hywind demo. *Energy Procedia*, 94:409–416, 2016.

[5] World's first floating wind farm begins operations. *Power Engineering*, 121(12):44, 2017.

[6] Laura Castro-Santos and Vicente Diaz-Casas. *Floating offshore wind farms*. Springer, Switzerland, 2016.

[7] Anne Lene Haukanes Hopstad, Kimon Argyriadis, Andreas Manjock, Jarett Goldsmith, and Knut O Ronold. Dnv gl standard for floating wind turbines. In *ASME 2018 1st International Offshore Wind Technical Conference*. American Society of Mechanical Engineers Digital Collection, 2018.

[8] Barber Wind Turbines. Barge mounted turbine.

[9] Barber Wind Turbines. Barge advantages.

[10] EolMed. Eolmed innovation, Jul 2018.

[11] Ideol Offshore. Floatgen demonstrator, Mar 2020.

[12] Wikipedia. Fishtailing, Jan 2020.

[13] A Fitriadhy, H Yasukawa, and KK Koh. Course stability of a ship towing system in wind. *Ocean engineering*, 64:135–145, 2013.

[14] MM Bernitsas and NS Kekridis. Simulation and stability of ship towing. *International Shipbuilding Progress*, 32(369):112–123, 1985.

[15] Michael M Bernitsas and Nikos S Kekridis. Nonlinear stability analysis of ship towed by elastic rope. *Journal of ship research*, 30(2), 1986.

[16] Fotis A Papoulias and Michael M Bernitsas. Autonomous oscillations, bifurcations, and chaotic response of moored vessels. *Journal of Ship Research*, 32(3), 1988.

[17] Ming-Ling Lee. Dynamic stability of nonlinear barge-towing system. *Applied mathematical modelling*, 13(12):693–701, 1989.

[18] Ming-Chung Fang and Jiun-Han Ju. The dynamic simulations of the ship towing system in random waves. *Marine Technology*, 46(2):107–115, 2009.

[19] Ahmad Fitriadhy and Hironori Yasukawa. Course stability of a ship towing system. *Ship Technology Research*, 58(1):4–23, 2011.

[20] Marco Sinibaldi and Gabriele Bulian. Towing simulation in wind through a nonlinear 4-dof model: Bifurcation analysis and occurrence of fishtailing. *Ocean engineering*, 88:366–392, 2014.

[21] Kamlesh S Varyani, Nigel DP Barltrop, Xuan P Pham, et al. Fishtailing instabilities in emergency towing of disabled tankers. In *The Fifteenth International Offshore and Polar Engineering Conference*. International Society of Offshore and Polar Engineers, 2005.

[22] Alexandre JP Leite, José Augusto Penteado Aranha, C Umeda, and MB De Conti. Current forces in tankers and bifurcation of equilibrium of turret systems: hydrodynamic model and experiments. *Applied Ocean Research*, 20(3):145–156, 1998.

[23] Alexandre Nicolaos Simos, Eduardo Aoun Tannuri, Celso Pupo Pesce, and José Augusto Penteado Aranha. A quasi-explicit hydrodynamic model for the dynamic analysis of a moored fpso under current action. *Journal of Ship Research*, 45(4):289–301, 2001.

[24] Eduardo Aoun Tannuri, Alexandre Nicolaos Simos, AJ de P Leite, and José Augusto Penteado Aranha. Experimental validation of a quasi-explicit hydrodynamic model: fishtailing instability of a single-point moored tanker in rigid-hawser configuration. *Journal of ship research*, 45(4):302–314, 2001.

[25] Knud A Kragh and Morten H Hansen. Load alleviation of wind turbines by yaw misalignment. *Wind Energy*, 17(7):971–982, 2014.

[26] Synne Hoggen Nybø. Windbarge-initial design and preliminary assessment of fatigue damage. Master's thesis, NTNU, 2017.

[27] Stian Hegh Srum. Dynamic stability of weathervaning offshore wind turbines, Nov 2018.

[28] Jason M Jonkman, A Robertson, and Greg J Hayman. Hydrodyn users guide and theory manual.

[29] Kristiansen K Bachynski E. Lecture notes for tmr 4182 marine dynamics, January 2019.

[30] AH Techet. Potential flow theory.

[31] Bachynski E. Lecture notes: Basic aerodynamics for wind turbines, September 2019.

[32] Dale M Pitt and David A Peters. Theoretical prediction of dynamic-inflow derivatives. 1980.

[33] David A Peters and Cheng Jian He. Correlation of measured induced velocities with a finite-state wake model. *Journal of the American Helicopter Society*, 36(3):59–70, 1991.

[34] Erin E Bachynski, Harald Ormberg, et al. Comparison of engineering models for the aerodynamic load distribution along a wind turbine blade. In *The Twenty-fifth International Ocean and Polar Engineering Conference*. International Society of Offshore and Polar Engineers, 2015.

[35] Harald Ormberg, Erin E Bachynski, et al. Global analysis of floating wind turbines: Code development, model sensitivity and benchmark study. In *The Twenty-second International Offshore and Polar Engineering Conference*. International Society of Offshore and Polar Engineers, 2012.

[36] James F Manwell, Jon G McGowan, and Anthony L Rogers. *Wind energy explained: theory, design and application*. John Wiley & Sons, 2010.

[37] Patrick J Moriarty and A Craig Hansen. Aerodyn theory manual. Technical report, National Renewable Energy Lab., Golden, CO (US), 2005.

[38] Bachynski E. Lecture slides: Basic aerodynamics for wind turbines, September 2019.

[39] Hermann Glauert. *The analysis of experimental results in the windmill brake and vortex ring states of an airscrew*. HM Stationery Office, 1926.

[40] Odd Faltinsen. *Sea loads on ships and offshore structures*, volume 1. Cambridge university press, 1993.

[41] Tiril Stenlund. Mooring system design for a large floating wind turbine in shallow water. Master's thesis, NTNU, 2018.

[42] Tony Burton, Nick Jenkins, David Sharpe, and Ervin Bossanyi. *Wind energy handbook*. John Wiley & Sons, 2011.

[43] Jason Jonkman, Sandy Butterfield, Walter Musial, and George Scott. Definition of a 5-mw reference wind turbine for offshore system development. Technical report, National Renewable Energy Lab.(NREL), Golden, CO (United States), 2009.

[44] Morten Hartvig Hansen and Lars Christian Henriksen. Basic dtu wind energy controller. 2013.

[45] Matthew J Benacquista and Joseph D Romano. Rigid body dynamics. In *Classical Mechanics*, pages 225–259. Springer, 2018.

[46] Christian Bak, Frederik Zahle, Robert Bitsche, Taeseong Kim, Anders Yde, Lars Christian Henriksen, Morten Hartvig Hansen, Jose Pedro Albergaria Amaral Blasques, Mac Gaunaa, and Anand Natarajan. The dtu 10-mw reference wind turbine. In *Danish Wind Power Research 2013*, 2013.

[47] DNV GL AS. Dnvgl-st-0119: Floating wind turbine structures. 2018.

[48] GJ Lyons, DT Brown, HM Lin, et al. Drag coefficients for mooring line hydrodynamic damping. In *The Seventh International Offshore and Polar Engineering Conference*. International Society of Offshore and Polar Engineers, 1997.

[49] Bonnie Jonkman and Jason Jonkman. Fast v8. 16.00 a-bjj. *National Renewable Energy Laboratory*, 2016.

[50] H Max Irvine. *Cable structures*. Number Sirsi) i9780486671277. 1992.

Appendix A

# Time domain turbine operating results

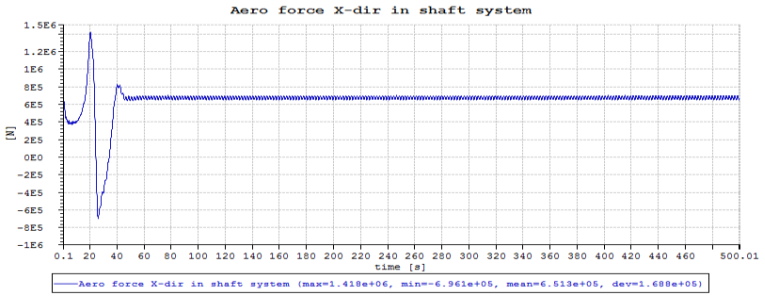


**Figure A.1:** Fixed turbine thrust force, $-50°$ yaw angle, SIMA

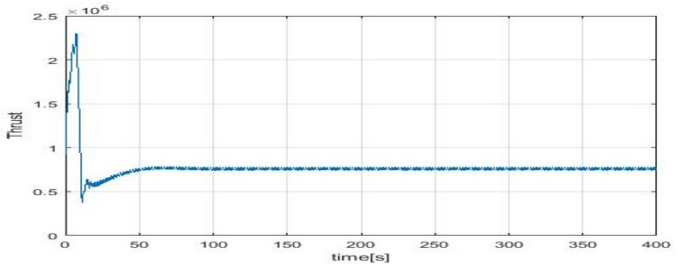


**Figure A.2:** Fixed turbine thrust force, $-50°$ yaw angle, FAST

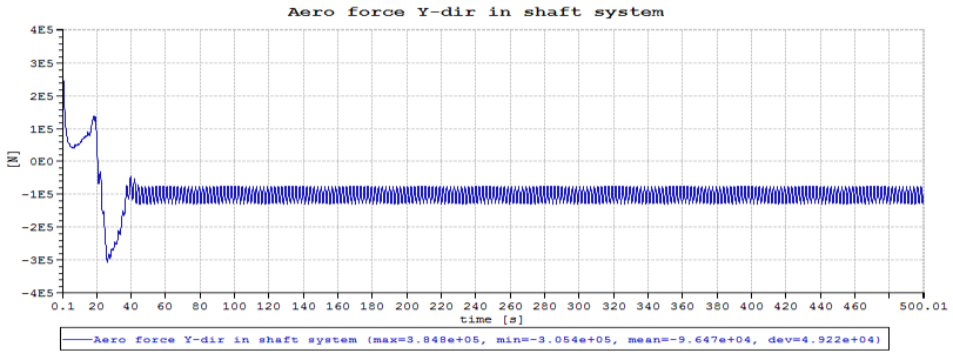


**Figure A.3:** Fixed turbine side-ways force, $-50^\circ$ yaw angle, SIMA

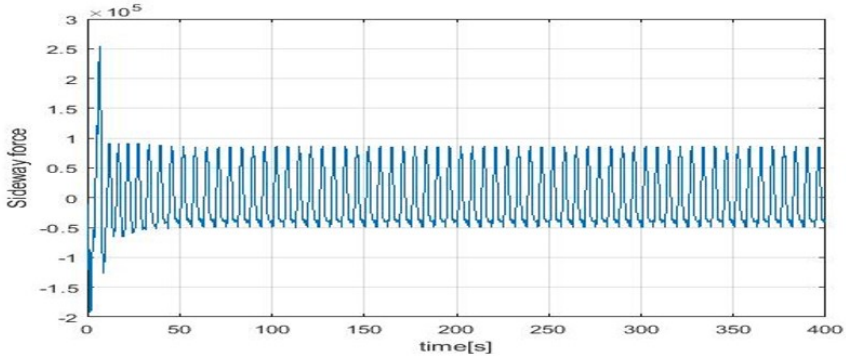


**Figure A.4:** Fixed turbine side-ways force, $-50^\circ$ yaw angle, FAST

Appendix B

# Linearised Model with Various Damping

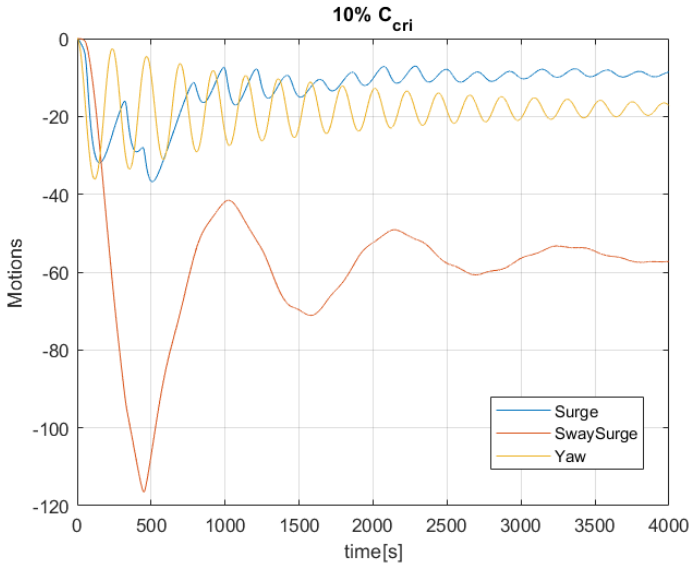


**Figure B.1:** Motions-initial design, 10% critical damping

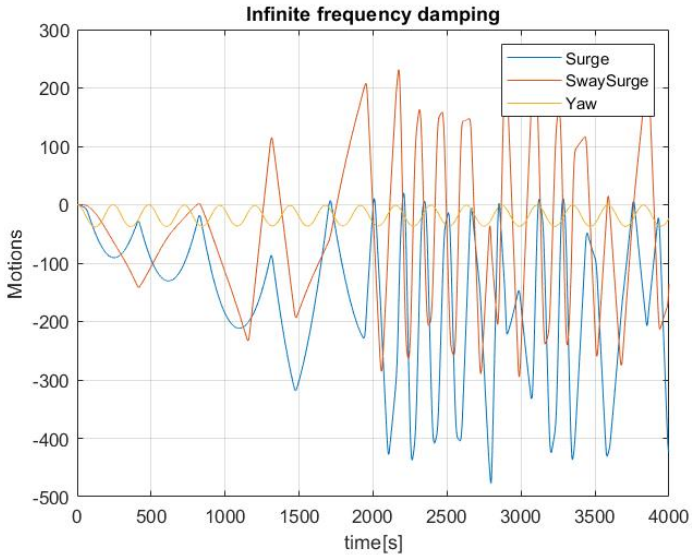


**Figure B.2:** Motions-initial design, Infinite frequency potential damping

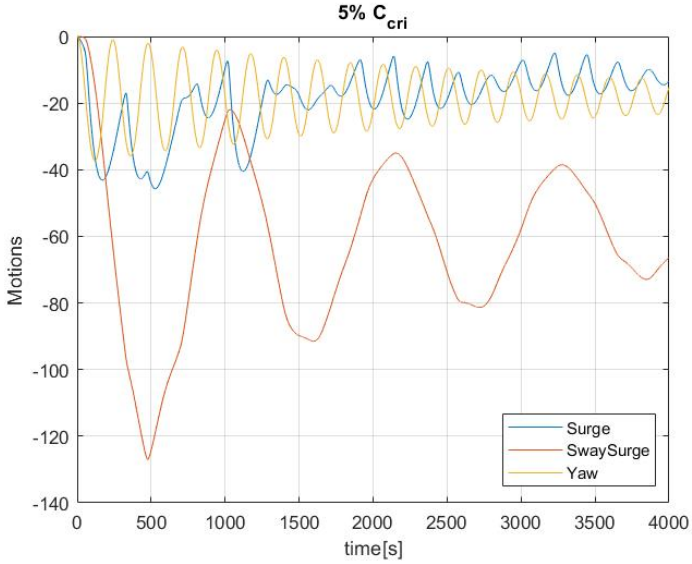


**Figure B.3:** Motions-initial design, 5% critical damping

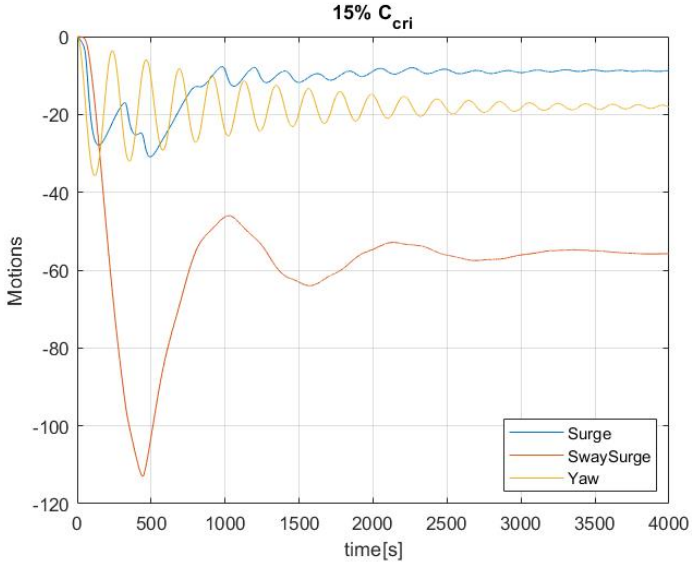


**Figure B.4:** Motions-initial design, 15% critical damping

Appendix C

# Improved design aerodynamic loads

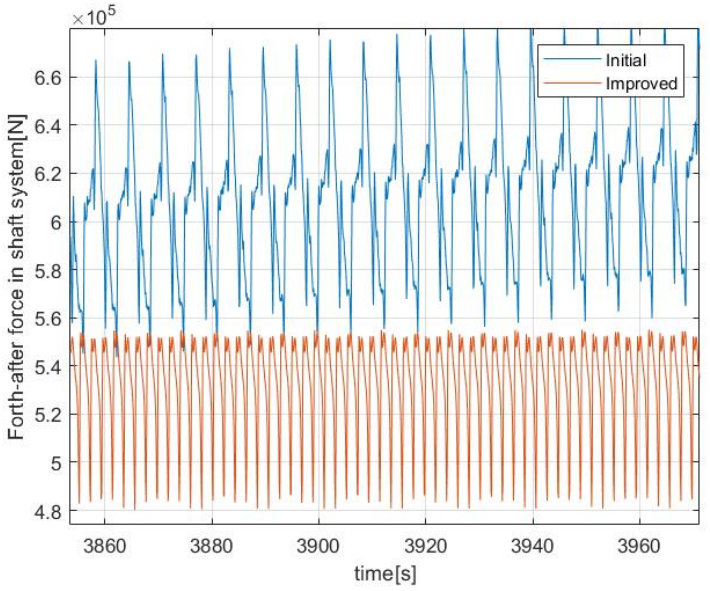


**Figure C.1:** FA aerodynamic load zoom in at 25m/s

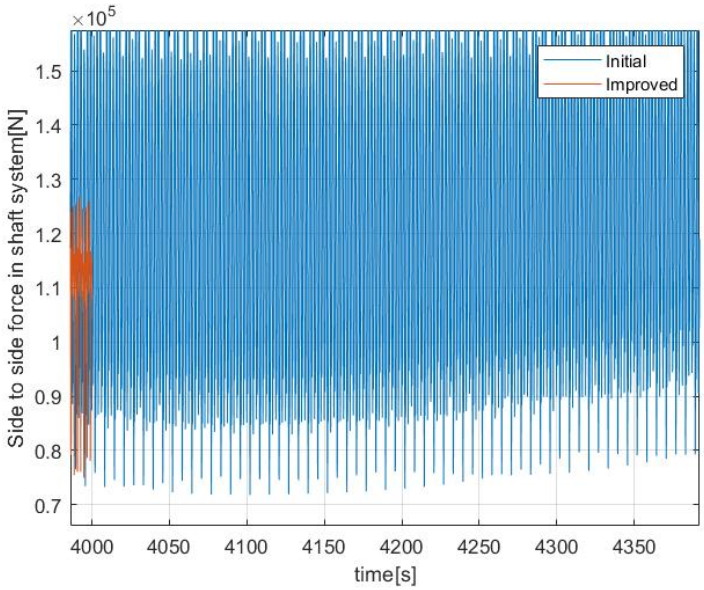


**Figure C.2:** SS aerodynamic load zoom in at 25m/s-1

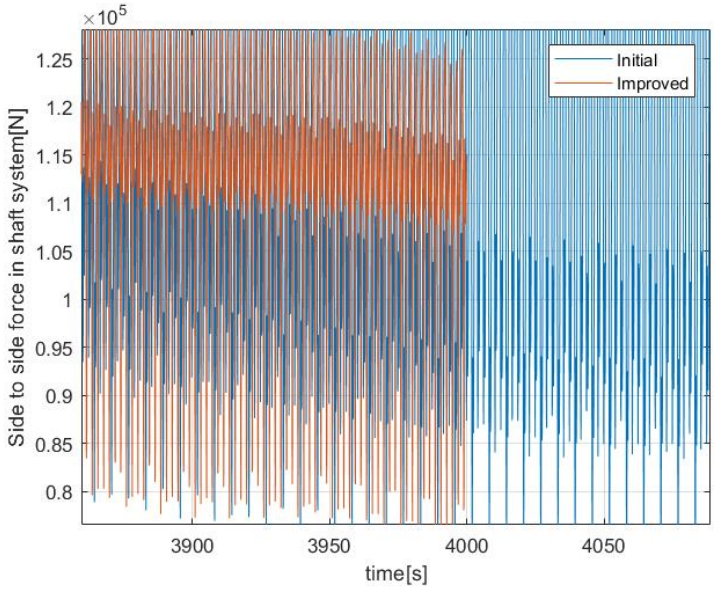


**Figure C.3:** SS aerodynamic load zoom in at 25m/s-2

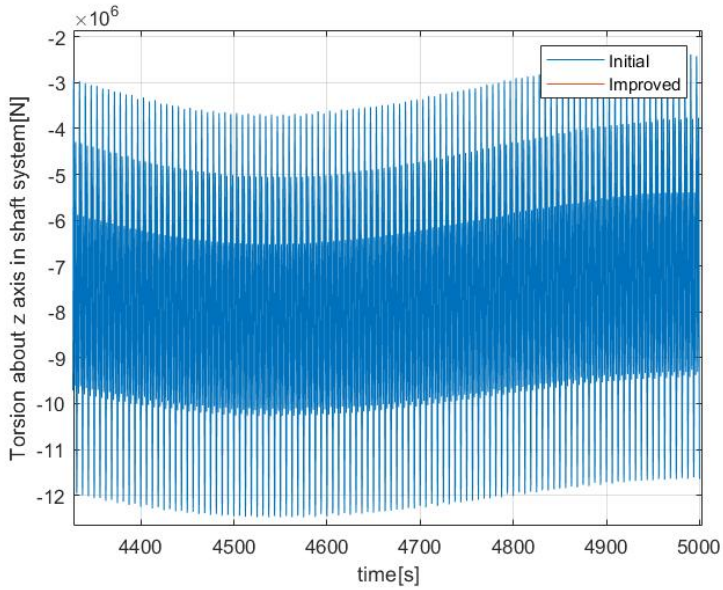


**Figure C.4:** Shaft torsion zoom in at 25m/s-1

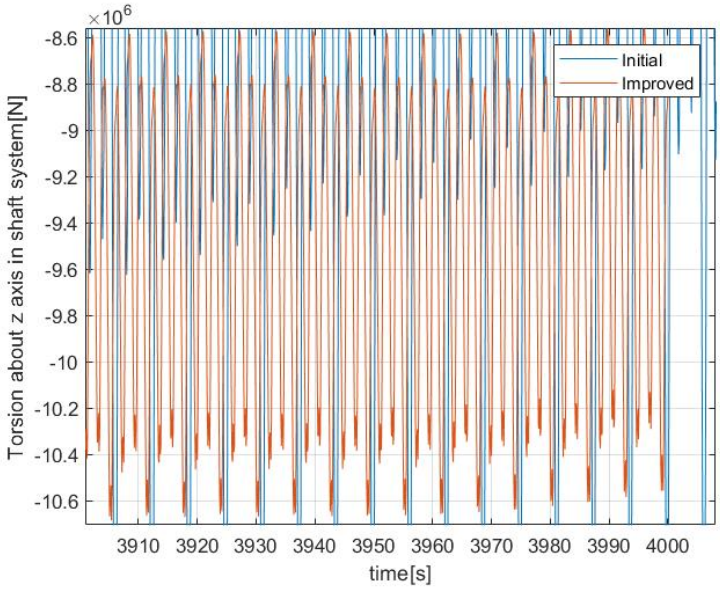


**Figure C.5:** Shaft torsion zoom in at 25m/s-2